MINIATURIZATION OF MICROWAVE BANDPASS FILTERS USING NANOSTRUCTURED AND BULK $YBa_2Cu_3O_{7-\delta}$ SUPERCONDUCTOR FILMS

SALEH EESAA JASIM

Doctor of Philosophy

UNIVERSITI MALAYSIA PAHANG

UNIVERSITI MALAYSIA PAHANG

DECLARATION OF THESIS AND COPYRIGHT

Author's Full Name : Saleh Eesaa Jasim

Date of Birth : 01_07_1971

Title : Miniaturization of Microwave Bandpass Filters using Nanostructured and Bulk $YBa_2Cu_3O_{7-\delta}$ Superconductor Films

Academic Session: PhD

I declare that this thesis is classified as:

☐	CONFIDENTIAL	(Contains confidential information under the Official Secret Act 1997)*
☐	RESTRICTED	(Contains restricted information as specified by the organization where research was done)*
☑	OPEN ACCESS	I agree that my thesis to be published as online open access (Full Text)

I acknowledge that Universiti Malaysia Pahang reserves the following rights:

1. The Thesis is the Property of Universiti Malaysia Pahang
2. The Library of Universiti Malaysia Pahang has the right to make copies of the thesis for the purpose of research only.
3. The Library has the right to make copies of the thesis for academic exchange.

Certified by:

_____	_____
(Student's Signature)	(Supervisor's Signature)
_____	_____
New IC/Passport Number: A2786460	Name of Supervisor
Date:	Date:

NOTE : * If the thesis is CONFIDENTIAL or RESTRICTED, please attach a thesis declaration letter.

THESIS DECLARATION LETTER (OPTIONAL)

Librarian,
Perpustakaan Universiti Malaysia Pahang,
Universiti Malaysia Pahang,
Lebuhraya Tun Razak,
26300, Gambang, Kuantan.

Dear Sir,

CLASSIFICATION OF THESIS AS RESTRICTED

Please be informed that the following thesis is classified as RESTRICTED for a period of three (3) years from the date of this letter. The reasons for this classification are as listed below.

Author's Name
Thesis Title

Reasons (i)

(ii)

(iii)

Thank you.

Yours faithfully,

_____
(Supervisor's Signature)

Date:

Stamp:

Note: This letter should be written by the supervisor, addressed to the Librarian, *Perpustakaan Universiti Malaysia Pahang* with its copy attached to the thesis.

SUPERVISOR'S DECLARATION

We hereby declare that we have checked this thesis and, in our opinion, this thesis is adequate in terms of scope and quality for the award of the degree of Doctor of Philosophy.

_____

(Supervisor's Signature)

Full Name :

Position :

Date :

_____

(Co-supervisor's Signature)

Full Name :

Position :

Date :

STUDENT'S DECLARATION

I hereby declare that the work in this thesis is based on my original work except for quotations and citations which have been duly acknowledged. I also declare that it has not been previously or concurrently submitted for any other degree at Universiti Malaysia Pahang or any other institutions.

_____

(Student's Signature)

Full Name : SALEH EESAA JASIM

ID Number : PSP14001

Date :

MINIATURIZATION OF MICROWAVE BANDPASS FILTERS USING NANOSTRUCTURED AND BULK $YBa_2Cu_3O_{7-\delta}$ SUPERCONDUCTOR FILMS

SALEH EESAA JASIM

Thesis submitted in fulfillment of the requirements
for the award of the degree of
Doctor of Philosophy

Faculty of Industrial Sciences & Technology

UNIVERSITI MALAYSIA PAHANG

MARCH 2018

ACKNOWLEDGEMENTS

Firstly, I acknowledge and admit that Allah is the Almighty who has assisted me during of my Ph.D. course. study. Also, I would like to express my deep appreciation and sincere thanks to my prominent supervisor Dr Mohamad Ashry bin Jusoh and my co-supervisor Prof. Jose Rajan for your supervisions, guidance and encouragements. Special thanks to all staffs and my friends in Faculty of Industrial Sciences & Technology, Universiti Malaysia Pahang for your advices and scientific assistances.

Special thanks to my friends: Suhail Najm Shahab, Ali Mahmood and Qamar Wali for your supports. Also, I appreciate the helps offered by all international postgraduate students who have supported my research work. Also, I would like to thank Dr Azhan and M. Suazlina for your continuous supports.

To all the technical Lab staff, especially Mr Abd Latip, Mr Muhammad Halim, Mr Mohd Farid, Mr Muhamad Husaini, Mr Khairul Affendi and Mr Shaharunizam bin Omar. please accept my sincere thanks for your professional assistances offered in the laboratory.

Finally, thanks a lot to my parents, my brothers, my sisters, my children and my wife who are so sincere and have provided a lot of moral supports during my study.

ABSTRAK

Dalam era objek rantaian internet (IoT), komunikasi tanpa wayar adalah teknologi penting untuk membolehkan sambungan antara peranti-peranti elektronik. Penapis lintasan jalur gelombang mikro adalah komponen penting dalam sistem komunikasi tanpa wayar dan litar gelombang mikro untuk membolehkan pemilihan isyarat fideliti-tinggi dalam siaran frekuensi radio (RF). Penapis gelombang mikro konvensional mengambil ruang yang besar kerana ia terdiri daripada beberapa komponen litar; saiz yang lebih besar menambahkan kerugian tidak dapat dielakkan. Oleh itu, pendekatan inovatif diperlukan untuk membuat penapis gelombang mikro berprestasi tinggi. Penapis yang ideal dicirikan oleh kehilangan pulangan yang tinggi (> -10 dB), tiada kehilangan masukan (~ 0 dB), dan jalur lebar yang luas (> 1.5 GHz). Tesis ini memperihalkan tentang rekabentuk dan pembangunan penapis gelombang mikro lintasan jalur dengan kehilangan pulangan yang tinggi (-30 dB), kehilangan masukan yang kecil (sehingga -2 dB), bersaiz kecil (100 mm^2) dan jalur lebar yang luas (1.5 GHz) dengan menggunakan superkonduktor suhu tinggi $YBa_2Cu_3O_{7-\delta}$ (HTS YBCO). HTS YBCO disintesis dengan kaedah reaksi keadaan pepejal dan proses elektrospinning. Litar penapis lintasan jalur gelombang mikro direka menggunakan perisian rekabentuk berbantu komputer (CAD) menggunakan pemodelan unsur terhingga dikenali sebagai perisian simulator struktur frekuensi tinggi (HFSS). Satu lata dari 4 garisan selari diterimapakai untuk direalisasikan supaya penapis lintasan jalur gelombang mikro bersaiz mini yang beroperasi pada frekuensi yang lebih tinggi menggunakan pemalar dielektrik yang tinggi (ε = 24) seperti $LaAlO_3$. YBCO bahan nano dalam lima morfologi seperti nanorods (NRs), nanogarlands (NGs), nanopartikel (NPs), nanohierarki (NH) dan nanopartikel agglomerat (ANPs) disediakan menggunakan polimer polivinilpyrrolidone (PVP) daripada pelbagai berat molekul dan nisbah berat (perbandingan kepada prekursor). Sampel HTS YBCO yang disintesis dicirikan dengan menggunakan Analisis Termogravimetrik (TGA/DSC), Pembelauan Sinar-X (XRD), Pengimbas Elektron Emisi Medan (FESEM), dan Brunauer-Emmett-Teller (BET) Teknik Permukaan Kawasan Spesifik). Pencirian struktur sampel YBCO menunjukkan struktur kristal ortorombik dengan parameter kekisi yang dilaporkan. Sifat superconduktor bahan ditentukan oleh ukuran kerentanan magnet. Sampel pukal YBCO yang disediakan dengan reaksi keadaan pepejal menunjukkan T_c yang lebih tinggi (iaitu 92 K). Sebaliknya, nilai T_c sampel elektrospun adalah antara 82 K dan 90 K ditentukan dari kaedah kerentanan semasa (ACS). Pengukuran BET sampel YBCO (ANPs) menunjukkan 6.8 m^2/g dengan T_c = 84 K. Sementara itu, NGs menunjukkan kawasan permukaan tertinggi (7.06 m^2/g) dan T_c pertengahan (88 K). Kawasan permukaan sampel pukal memberikan 1.0 m^2/g dengan T_c yang tinggi (iaitu 92 K). Berdasarkan simulasi, penapis lintasan turas gelombang mikro dibangunkan menggunakan filem nipis bersalut-berputar pada substrat $LaAlO_3$. Sifat gelombang mikro litar penapis telah ditentukan secara eksperimen menggunakan penganalisis rangkaian vektor (VNA) pada suhu bilik (300 K) dan kehadiran nitrogen cecair (77 K). Penapis keadaan pepejal menunjukkan kehilangan pulangan yang lebih tinggi (iaitu -22 dB) pada operasi frekuensi 9.7 GHz dan lebar jalur lebar 1.5 GHz, yang konsisten dengan keputusan simulasi. Walau bagaimanapun, hasil terbaik telah dicapai dengan menggunakan tindakbalas keadaan pepejal terhadap YBCO dan rekabentuk novel. Hasilnya yang terkandung dalam tesis ini memberikan petunjuk yang menggalakkan untuk membangunkan gelombang mikro generasi akan datang.

ABSTRACT

In Internet of Things (IoT) era, wireless communication is an essential technology to enable connection between electronic time devices. Microwave bandpass filters are essential components in the wireless communication systems and microwave circuits to enable selection of high-fidelity signals within the broadcast radio frequency (RF). The conventional microwave filters occupy large space due to consisting of several circuit components and larger sizes inevitably add up losses. Innovative approaches are therefore required to fabricate high performing microwave filters. An ideal filter is characterized by high return loss (> -10 dB), no insertion loss (~0 dB), and broad bandwidth (>1.5 GHz). This thesis describes the design and development of microwave bandpass filters characterized by high return loss (-30 dB), small insertion loss (up to -2 dB), small size (100 mm^2) and broad bandwidth (1.5 GHz) using high-temperature superconducting $YBa_2Cu_3O_{7-\delta}$ (HTS YBCO). The microwave bandpass filter circuit is designed using the computer-aided design (CAD) software using finite element modelling employing known as High Frequency Structural Simulator (HFSS) software. A cascaded of 4 parallel-coupled lines is adopted to realize so that the miniaturized microwave bandpass filter operating at higher frequency using a substrate of high dielectric constant (ε = 24) such as $LaAlO_3$ substrate. The HTS YBCO is synthesized by electrospinning process and solid-state reaction method. Using electrospinning, YBCO nanomaterials in five morphologies, i.e. nanorods (NRs), nanogarlands (NGs), nanoparticles (NPs), nanohierarchical (NH) and agglomerated nanoparticles (ANPs) are prepared using polyvinylpyrrolidone polymer (PVP) of different molecular weights and weight ratios (relative to the precursors). The synthesized HTS YBCO samples are characterized using Thermogravimetric Analysis (TGA/DSC), X-ray Diffraction (XRD), Field Emission Scanning Electron Microscopy (FESEM), and Brunauer–Emmett–Teller (BET) specific surface area techniques. The structural characterizations of YBCO samples have demonstrated the orthorhombic crystal structure with reported lattice parameters. The superconducting properties of the materials are determined by alternating current susceptibility (ACS) measurements. The YBCO bulk sample prepared by solid-state reaction shows the higher T_c (i.e. 92 K). On the other hand, the T_c values of electrospun samples are ranging between 82K and 90K. The BET measurements of YBCO sample (ANPs) showed 6.8 m^2/g with T_c = 84 K. Meanwhile, NGs shows the highest surface area (7.06 m^2/g) and intermediate T_c (88 K). The surface area of bulk sample presents 1.0 m^2/g with high (T_c 92 K). Based on the simulated design, the microwave bandpass filters are developed using spun-coated thin films on $LaAlO_3$ substrate. The microwave properties of filter circuits were experimentally determined by the Vector Network Analyser (VNA) at room temperature (300 K) and in liquid nitrogen (77 K). The solid-state filter showed higher return loss (i.e. -22 dB) at operating frequency of 9.7 GHz and bandwidth of 1.5 GHz, which is consistent with the simulation results. However, the electrospun YBCO filters have exhibited lower performance than conventional powders derived through solid state reaction due to the nano-structural properties of the former which leads to high surface resistance. Nevertheless, the best result has been achieved using the solid state reacted YBCO and the novel design. The results embodied in this thesis is therefore giving promising directions to develop next generation microwave filters.

TABLE OF CONTENT

LIST OF TABLES

LIST OF FIGURES

LIST OF SYMBOLS/UNIT

A	Ampere
Å	Angstrom (10^{-10} meter)
˚C	Celsius degree
cm	Centimetre
cP	Centipoise
eV	Electron Volt
J_c	Critical current density
Oe	Oersted (unit of the auxiliary magnetic field H)
f_s	Femtosecond (10^{-15} second)
GHz	Gigahertz
g	Gram
K	Kelvin
kV	Kilovolts
µS	Micro Siemens
ml	Millilitre
mm	Millimetre
Mw	Molecular weight
nm	Nanometre
Ω	Ohm
rpm	Rotation per minute
T	Tesla
T_c	Critical transition temperature

LIST OF ABBREVIATIONS

1-D	One-dimensional
2-D	Two-dimensional
3-D	Three-dimensional
AAO	Anodic Aluminium Oxide
Ac	Acetate
ANPs	Agglomerated nanoparticles
BBW	Broad Band Width
BET	Brunauer-Emmett-Teller
CAD	Computer-Aided Design
CPU	Central Processing Unit
CVD	Chemical Vapor Deposition
DSC	Differential Scanning Calorimeter
EM	Electromagnetic
E6	Engineering Version 6
Fc	Frequency center
FEM	Finite Element Method
FESEM	Field Emission Scanning Electron Microscopy
FM	Frequency Modulation
FR4	Flame Retardant created from four material
HFSS	High- Frequency Structural Simulator
HTS	High-Temperature Superconductors
IL	Insertion Loss
IE3D	Integrated Electromagnetic Three-Dimensional Software
LTS	Lower Temperature Superconductors
NFs	Nanofibers

NGs	Nanogarlands
NH	Nanohierarchical
NPs	Nanoparticles
NRs	Nanorods
NS	Normal Structure
NTs	Nanotubes
NWs	Nanowires
PAAc	Polyacrylic Acid
PLD	Pulsed Laser Deposition
PVA	Polyvinyl Alcohol
PVP	Polyvinyl Pyrrolidone
RF	Radio Frequency
RL	Return Loss
SBPWM	Simple Boost Pulse Width Modulation
TGA	Thermogravimetric Analyser
VNA	Vector Network Analyser

CHAPTER 1

INTRODUCTION

1.1 Background

Microwave bandpass filters are the essential part in the wireless communication and microwave circuits. It is implemented to achieve a unique and selective radiation frequency in RF for several applications such as broadcasting radio and wireless communication systems. Filters were found with several designing and dimensions such as cavity filters, electronic filters, planer filters etc. Development of superconducting microwave passive circuit components with low loss and broad bandwidth bandpass filters is an active research area nowadays. The outcome would enable selection of high-fidelity signals within the broadcast radio in radio frequency (RF) and microwave communication systems (Mansour, 2002; Nisenoff, 2011; Ribadeneira-Ramírez et al., 2016). Generally, the electrical performances of the filters are described in terms of return loss, insertion loss and high frequency-selectivity (i.e. attenuation at rejection band) (Davidson, 2010). Good filters should have small insertion loss, large return loss (for good impedance matching with interconnecting components), high frequency-selectivity (prevent the interference) and broad bandwidth. Many works related to the developments of high performance and low cost superconducting microwave circuits such as antenna, filter, phase shifter, multiplexer, coupler and delay lines have been published (Newman & Lyons, 1993; Weigel et al., 1993).

High-temperature superconductor (HTS) $YBa_2Cu_3O_{7-\delta}$ (YBCO) is characterized by several unique properties to be used as a microwave filter material, such as lower RF losses in comparison with the conventional conductors (Newman & Lyons, 1993; van Delft, 2012; Weigel et al., 1993). HTS YBCO is more popular than other ceramic superconductors due to its high critical temperature (T_c ~92 K), high current density (J_c ~10^6 A/cm^2, 77 K), high critical magnetic field (B ~16 T), and good chemical stability (Luo et al., 2014; Uslu et al., 2010). Besides, YBCO can be synthesized easily into single-phase material using relatively

low-cost precursors such as metal oxides, acetates, nitrates, etc. (Nawaz et al., 2013; Shen et al., 2013). High performance microwave circuits of bandpass filters based on HTS YBCO thin films have been reported with superior performances (Bai et al., 2013; Chung, 2000; Shivhare, 2008). These films were prepared on $LaAlO_3$ substrate with size > 2 cm^2 using several techniques such as pulsed laser deposition (PLD), chemical vapor deposition (CVD), electron-beam lithography (E-beam) and anodic aluminium oxide (AAO) templates (Arpaia et al., 2015; Golubev et al., 2014).

At higher microwave frequencies, the surface resistance of HTS YBCO is an order of magnitude smaller than that of the normal conductors. This is because, for microwave applications, the surface resistance is directly proportional to the square root of frequency in normal conductors, whereas it is directly proportional to the square of frequency in superconductors (Luo et al., 2014). The HTS YBCO filters have better frequency selectivity, low insertion loss, small size and light weight as compared to devices developed from the normal conductors (Zhang et al., 2015). Besides, due to the low losses of the HTS YBCO at high microwave frequencies, it is possible to reduce the size of the bandpass filter while still having excellent performance (i.e. lower losses and broad bandwidth) (Lancaster et al., 1996).

Nowadays, nanoscale superconductivity is gaining popularity because of many underlying fundamental and technological advantages at such length scales such as high surface to volume ratio, size induced modification in optical and electronic properties, high mechanical strength, and light weight. Owing to the guided transport in one-dimensional structures such as nanowires (NWs), nanotube (NTs), and nanofiber (NFs), their properties and practical applications have been extensively studied (Duarte et al., 2014; Shen et al., 2013). Many techniques have been proposed for the synthesis of HTS YBCO as NWs, NTs and NFs, e.g. template method, sol-gel, anodization, etc. Among them, the polymeric solution based continuous nanofiber production method such as the electrospinning technique offers scalable production (Cui et al., 2006; Duarte et al., 2014; Greenberg et al., 2008; Shen et al., 2013; Uslu et al., 2010).

1.2 Problem Statement

Conventional microwave filters in the electronic and communication devices occupy a large space because they consist of several resonators, whose dimensions are similar to the guided wavelength (≥ 1 mm). Because of these large dimensions design, filters have much power losses. Therefore, many efforts have been adopted to develop the miniaturized microwave filters (Lee, 2009), i.e. an ideal filter that offers high frequency selection, low losses and broad bandwidth. Miniaturization of filters can be achieved by changing the filter geometry from the 3-dimensional waveguide (e.g. cavity filter) filter to the 2-dimensional planar waveguide (e.g. microstrip lines) filter. Several microwave microstrip lines based bandpass filters, such as parallel edge line, strip line, pole, parallel edge, network, compact loop, linear phase and etcetera were designed with surface area greater than 2 cm^2 have been developed. Cascade design (or parallel coupled strip lines) is the most common method adopted to realize high performance and miniaturized microwave circuits (Marimuthu, 2004).

A parallel arrangement of the filter components gives relatively large coupling for a given space between the resonators. Its performance can be further improved by increasing the number of the lumped elements (i.e. couple lines) (Sun, 2011). Hence, this parallel lumped element structure is particularly convenient for construction of filters with a broad bandwidth compared to end-couple structures (Marimuthu, 2004). The broadband bandpass filters have been designed by different methods and structures in recent years. Methods such as multilayer coupled structure, stub-loaded resonators, and multi-mode resonators have been shown to produce high performing bandpass filters (Liu et al., 2017). However, a wider bandwidth filter requires very closely spaced coupled lines; its fabrication is rather cumbersome (Sharma et al., 2013). Parallel coupled microstrip lines with an equal ripple could support the broad bandwidth better than the half-wavelength line resonators (Zhang, 2006). While the strip lines are much smaller than the wavelength (λ, λ/2, λ/4, etc.) at high operating frequencies. The filters based on the short line elements could be physically small (Ghosh et al., 2014; Lancaster et al., 1996). Thus, it turns out that as the line width is limited by the fabrication process, the center frequency of the filter approaches tens of gigahertz. Hence, the amount of losses is reduced due to lower surface resistance (i.e. using superconducting material).

Many efforts have been devoted to find the physical dimensions of the microwave bandpass filter circuits employing the design equations (Zhang, 2006). Nowadays, microwave filter circuits can be designed and simulated using the computer-aided design (CAD) software based on the insertion and return losses method. Many versatile CAD tools have been developed and used to design various microwave circuit components. The main purpose of the CAD is to obtain the physical dimensions of a circuit component with the prescribed specifications promptly. This process could reduce or even avoid the experimental debugging and tuning period after the manufacturing process (Zhang, 2006). Therefore, CAD is a powerful design tool with high accuracy (Sun, 2011). However, CAD is computationally costly and requires long processing time. On the other hand, High Frequency Simulation Software (HFSS) that is based on finite element method offers capability of modelling circuits with broad bandwidth and low losses.

Therefore, an innovative approach will be proposed in the current work to fabricate high performance microwave circuits. The current work aims to develop a high performing microwave filter using YBCO nanostructures. These structures are developed by a scalable nanofabrication process in a new device designed based on finite element modelling. A conventional YBCO film and a normal design can be adopted as control device to validate the performance obtained.

1.3 Research Objectives

The main objectives of this work are:

1. To design a microwave filter circuit with low loss and broad bandwidth using finite element modelling employing HFSS.

2. To optimize the formation conditions of superconducting $YBa_2Cu_3O_{7-\delta}$ nanostructures by using electrospinning technique.

3. To develop a newly designed microwave filter circuits employing nanostructured and bulk HTS $YBa_2Cu_3O_{7-\delta}$ thin films.

4. To test the performance of the HTS YBCO microwave bandpass filters using vector network analyser and explore the electromagnetic properties for both YBCO prepared by electrospinning and solid-state techniques.

1.4 Research Scope

The broad scope of this study is to design the high-performing microwave bandpass filters using a cascade design of four parallel coupled lines by finite element modelling employing HFSS software. The proposed filters are developed from the high-temperature superconductor YBCO nanostructures and conventional YBCO films to compare the performance obtained. The specific research plans adopted to achieve the first research objective are:

i. Design the microwave bandpass filter circuit employing a cascade design (four parallel couple lines) using HFSS software.

ii. Finding the physical dimensions of the parallel coupled lines i.e. the length, width (space between the couple lines) and the thickness using HFSS software employing the return loss method.

iii. Achieving broad bandwidth and high performing of high return loss microwave bandpass filter using the small dimension substrate (10×10 mm^2) ($LaAlO_3$).

As for the second objective:

i. Fabricate the HTS YBCO nanostructures via employing the so-gel solutions of different precursor to polymer concentration ratios and different polymer molecular weight using electrospinning technique.

ii. Synthesis of bulk YBCO samples with $T_c > 90$ K using solid-state reaction method.

iii. Deposits the thin films from the prepared YBCO powder on Lanthanum alumina substrate ($LaAlO_3$) using electrospinning and spin coating techniques.

iv. Analyse and characterize the superconducting properties and the structure (i.e. XRD, FESEM, T_c and BET surface area) for YBCO samples.

As for the third objective:

i. Preparing the thin films of HTS YBCO prepared by electrospinning technique and solid-state reaction method

ii. Fabricating the microwave bandpass filter using heat transfer paper and etching process.

As for the fourth objective:

i. Testing the performance of microwave bandpass filter using Vector Network Analyzer (VNA).

ii. Comparison the responses of the filters and find the answer of research question on how the superconducting electromagnetic properties for YBCO in one-dimensional morphology differ from those of the three-dimensional counterpart.

1.5 Novelty of The Work

Up on using the HFSS software, the physical dimensions of the filter circuit have been obtained. A new morphology obtained for YBCO via optimization the electrospinning process. A new microwave bandpass filter has been designed using the finite element modelling protocols and fabricated using electrospun HTS YBCO.

1.6 Thesis Layout

This thesis consists of five chapters, Chapter 1 presents the research backgrounds, problem statements, objectives, research scopes, thesis contributions and thesis layout. Chapter 2 highlights the literature reviews on the backgrounds of design the microwave bandpass filter devices and their fabrication based on high temperature superconducting (HTS) $YBa_2Cu_3O_{7-\delta}$ (YBCO) thin films, the brief histories of the superconducting YBCO, structure properties, applications of superconductors, microwave and superconductivity, superconductivity in nanoscale, synthesize process and its properties, and some practical applications. Reviews on electrospinning technique, main parameters used to control and manipulate the nanostructures, YBCO morphologies in nanostructure by electrospinning, spin coating technique and etching process are reviewed as well. Chapter 3 describes the characterization, analysis and techniques used to study the properties and the crystal structures of HTS YBCO nanostructured samples. The designed and simulated microwave devices, the fabrication process used to yield the thin films of YBCO nanostructured samples, the etching process and the analysis performed using microwave devices are also described in this chapter. Chapter 4 presents the results and discussions, followed by the conclusions and recommendations as highlighted in Chapter 5.

CHAPTER 2

LITERATURE REVIEW

2.1 Introduction

This chapter presents the backgrounds of design the microwave bandpass filter devices using computer aid design (CAD) software's based on high temperature superconducting (HTS) $YBa_2Cu_3O_{7-\delta}$ (YBCO) thin films, the superconductivity, nanostructured material as well as the structure, property and application of HTS YBCO. The microwave and superconductivity, the properties of YBCO thin films and nanosized morphologies of YBCO samples will be presented as well. The Fabrication process, process parameters, morphology of YBCO and scalable process will be reviewed. The one-dimensional (1-D) nanostructures and the configurations of HTS YBCO produced via the electrospinning process will be explained. Finally, the synthesis procedure used to produce the thin films and the etching process used to prepare the HTS YBCO microwave devices will be illustrated.

2.2 Microwave Bandpass Filter

Microwave bandpass filter is the essential part in the input and output of wireless communication and microwave circuits. It is implemented to achieve a unique and selective radiation frequency (Marimuthu, 2004). The circuits of the microwave bandpass filters are found in two types (i.e. active and passive circuits). Microwave bandpass filter passive circuit is adopted in this work. Microwave bandpass filters having the properties such as broad bandwidth, miniaturized size, low-power losses, easy to fabricate and low cost are desirable for broadcasting applications (Liu et al., 2006). At higher microwave frequencies, the surface resistance of HTS YBCO is an order of magnitude smaller than that of the normal conductors ($R_s < R_n$) see Figure 2.1. This is because, for microwave applications, the surface resistance is directly proportional to the square root of frequency in normal

conductors, whereas it is directly proportional to the square of frequency in superconductors (Luo et al., 2014; Romanenko & Grassellino, 2013). The above requirements can be achieved with the using the HTS YBCO films and the 2-dimensional planar waveguide (e.g. microstrip lines) i.e., the design of lumped element (strip lines) as explained in Chapter 1. Therefore, YBCO filter will has better frequency selectivity, low insertion loss and high return loss, small size and light weight as compared to devices developed from the normal conductors, which are desirable for microwave devices.

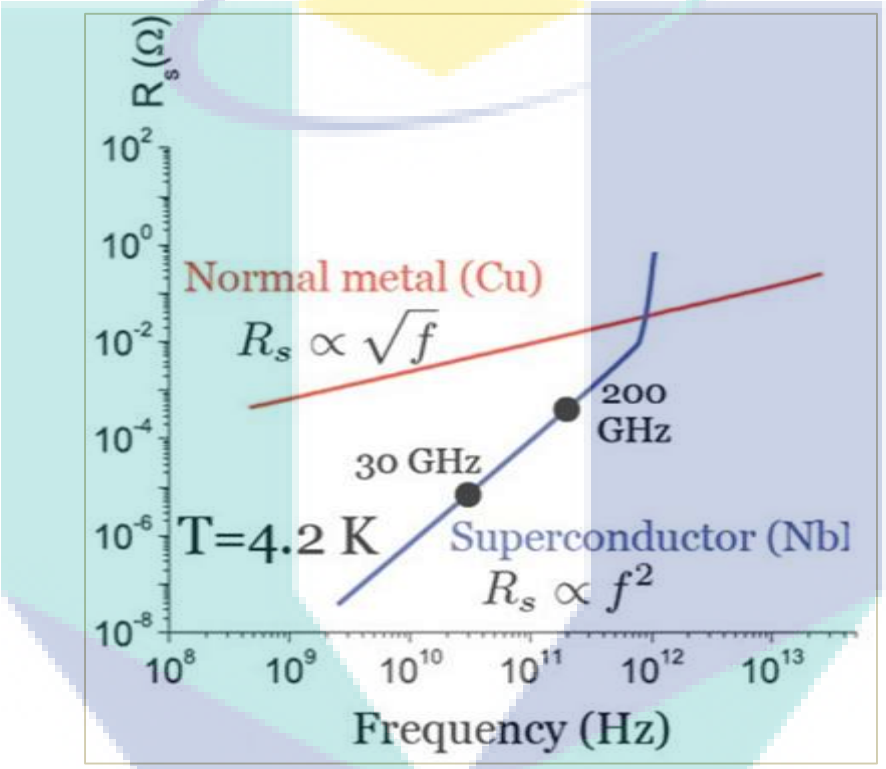

Figure 2.1 The relation between the surface resistance and frequency for normal metal (Cu) and superconductor (Nb)

Source: (Romanenko & Grassellino, 2013)

Many microwave bandpass filters were designed using HTS YBCO thin films with several types of lumped elements such as four-pole cross-coupled (Wang et al., 2005), compact eight-pole (Bai et al., 2013), parallel-connected network (Zhang et al., 2015), parallel coupled poles, coupled line edge, compact connected and not connected network (Zhang et al., 2015). Using high-temperature superconductor (HTS) $YBa_2Cu_3O_{7-\delta}$ (YBCO) as a microwave filter material is interesting and has more advantages as it exhibits lower RF losses as compared to conventional conductors (Newman & Lyons, 1993; Van Delft, 2012; Weigel et al., 1993).

2.3 Filter Design

Table 2.1 shows the designed, simulated and measured microwave bandpass filters using several types of CAD software's, models, material substrates and dimensions. Chung, (Chung, 2000) have deposited the YBCO thin film onto MgO substrate with small dimensions of 30 mm^2 and center of frequency of 16.6 GHz with narrow bandwidth of 1 GHz. Wang. *et al.* (Wang et al., 2005) have designed microwave filter from the YBCO thin film deposited on $LaAlO_3$ substrate with dimension of 225 mm^2, operation frequency at 2.152 GHz with narrow bandwidth of 12 MHz and return loss of - 23.3 dB. Most bandpass filters were prepared based on the thin films of YBCO deposited onto MgO substrate and $LaAlO_3$ substrates (Chung, 2000; Shivhare, 2008).

YBCO thin films were mostly deposited on Lanthanum aluminate $LaAlO_3$ using several techniques. Because $LaAlO_3$ is a popular substrate and used widely for artificial thin films growth in the high-temperature superconductor materials and electronic applications. $LaAlO_3$ is a type of perovskite-structure and targeted material as a common substrate, which characterized with several properties such as high melting temperature ~2130 °C (Ushakov & Navrotsky, 2014), good thermal stability, high dielectric constant (ε ~ 24) (Mansour, 2002), extensive physical, mechanical and low losses RF spatially for microwave application (Suzuki, 2012). For these properties $LaAlO_3$ is used for the epitaxial growth of YBCO thin films and applied extensively in microwave bandpass filters research for a long time (Jing et al., 1994; Wang et al., 2005).

The other works were adopted to reduce the size of filter circuit and power consumption was the designed and integrated microwave bandpass filter based on YBCO thin films, which has been reported by (Zhang et al., 2012). The authors aimed to improve the coupling efficiency between the filter passive and active circuits and achieve the low loss (-0.5 dB), small size (200 mm^2) and high efficiency. The YBCO thin films were deposited on a single chip MgO for the first time to realise a monolithic HTS downconverter. The passband filter designed to allow for the signals to pass from 7.2 to 8.5 GHz (i.e. operation frequency at 8 GHz, bandwidth of 2 GHz). The measured insertion loss ~ 0.5 dB and return loss ~-45 dB were consistent with simulation results, see Figure 2.2 (a).

However, most of the reported bandpass filters were required large area (~225 – 5900 mm^2). These filters were designed and simulated using different CAD software's

such as EM, IE3D, E6, and HFSS. The experimental results of these bandpass filters showed bandwidths between 10 MHz and 3.6 GHz. The insertion losses from 0.2 to 3.5 (see Table 2.1).

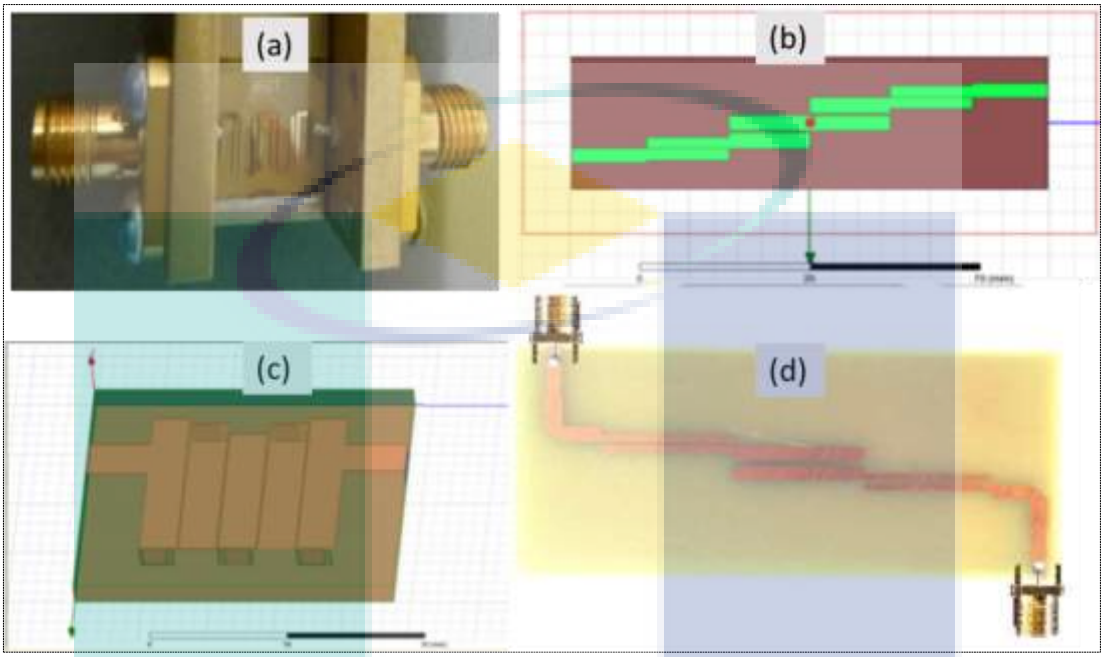

Figure 2.2 The designed and fabricated microwave bandpass filters using parallel couple line elements and simulated employing HFSS

Source: Reproduced from (Zhang et al., 2012; Kumar et al., 2014; Gupta et al., 2015; Gunjal et al., 2016)

Microwave bandpass filter has been designed and simulated using the HFSS software employing 5-parallel coupled lines. The design of the device was based on apart spacing < 1 mm between the parallel lines and small dimensions (71 mm^2) (Kumar et al., 2014). The filter was designed on FR4 substrate (i.e. a composite material consisting of flame resistant woven fiberglass cloth with an epoxy resin binder) of dielectric constant (ε = 4.2) and thickness (1.58 mm). The simulated filter result was, the operating frequency at 2.48 GHz, bandwidth 0.6 GHz, higher insertion loss -2.2 dB, and low return loss -12 dB. In the same manner, microwave bandpass filter of dimensions (480 mm^2) has been designed based on 5- parallel coupled lines on FR4 substrate using HFSS (Gupta et al., 2015). In order to achieve the broad bandwidth filter, the authors have been optimized the dimensions obtained by the design equation using HFSS simulator (i.e. the authors modified the dimensions using HFSS). The result was the bandpass filter has operation frequency centre at 3 GHz and bandwidth of 66% (2 GHz). The insertion loss less was -1.8 dB and the return loss ~ -8 dB (see Table 2.1, Figure 2.2 (b) and (c)). However, the filter showed broad

bandwidth due to the large area used for the design and the smallest spacing < 0.1 mm compared to the first design by (Kumar et al., 2014).

On the other hand, a microwave bandpass filter of large area (2627 mm^2), designed using 4-parallel coupled lines based on FR4 substrate with ($\varepsilon = 4.4$), the spacing between the parallel lines was (1.0 and 0.5 mm), the filter was simulated using HFSS. The testing and measurement of the printed filter presented the operating frequency at 2.4 GHz, 10% bandwidth (140 MHz), the insertion loss was -4.0 dB and the return loss ~ -8 dB. The simulated and measured results of the bandpass filter are consistent with each other (Gunjal et al., 2016) (see Table 2.1, Figure 2.2 (d)).

To summarize, these filters were designed and simulated using the design equations and simulated using HFSS software, and therefore, as the filters have different dimensions, they are having different performance. The fact stands behind is the relation between the frequency wavelengths and the filter components dimension by this time the performance parameters such as return losses and broad bandwidth are affected by the dimension of the design, while the insertion losses related with the impedance of the filter which controlled the passed signals (Zhang, 2006). Table 2.1 shows the sum of last microwave bandpass filters designed upon parallel coupled lines and simulated using HFSS.

The researchers have calculated the physical dimensions of the microwave bandpass filter (i.e. circuit components) depending on the design equations and found the finalized general structure for the filter (Gunjal et al., 2016; Gupta et al., 2015). The parallel lines were designed in adjacent parallel to each other along half of their length to achieve a relatively large coupling for the given spacing between the lines. This design is particularly convenient for a wider bandwidth as compared to the end couple constructing filters. The microwave bandpass filter has been designed depending on the following the specific considerations:

1. Number of the parallel coupled lines; (The performance of the filter can be further improved by increasing the number of lines. It was found the increase in orders of the filters can improve the selectivity of frequency, while the dimensions, return loss and insertion loss so on increased).

2. The frequency center; (High frequency required smallest dimension filter circuits because they are having short wavelength approaches to 1 mm, so that as the frequency is lower the wave length will be longer).

3. The bandwidth; (for example 10%, 30%, 50% ..etc of center frequency). As the coupled line area approached more than the half of the wavelengths, the bandwidth will be increased.

4. The symmetric design; (i.e. an equal ripple for a given 0.5 or 1.0 dB). The symmetric design is important to increase the selectivity and improve the resonance between the couple lines.

5. The substrate dielectric constant, thickness and dimensions; (As the substrate material having the ability for more charge storage as well as its properties of mechanical strength (i.e. can be prepared with the thickness of small dimension) the efficiency of the microwave circuit will be increased).

According to these requirements (Zhang et al., 2015), the physical dimensions of the designed parameters (i.e. parallel coupled lines) of the filter circuit were found upon using the design equations. The full design equations were commonly used to find the physical dimensions of the microwave bandpass filter using parallel coupled lines design are found in (Gunjal et al., 2016; Gupta et al., 2015).

Table 2.1 Summary of the designed microwave bandpass filters, the simulation and measured results with different software, types, substrate, and size using YBCO superconductor

Reference	**Characterization**				**Performance Evolution**							
					Simulation				**Experiment**			
	Platform for simulation	**Filter Design**	**Substrate**	**Dimensions (mm^2)**	**Fc (GHz)**	**BW**	**RL (dB)**	**IL (dB)**	**Fc (GHz)**	**BW**	**RL (dB)**	**IL (dB)**
(Chung, 2000)	EM Sonnet	Three parallel coupled H-type	MgO	30	16.65	1.0 GHz	-22.0	0	16.5	1.35 GHz	-22.0	-0.5
(Wang et al., 2005)	IE3D	Four-pole cross-coupled	$LaAlO_3$	225	2.152	12.0 MHz	-23.3	0	2.18	9.8 MHz	-5.0	-1.48
(Shivhare et al., 2008)	E6	Four parallel-coupled poles	$LaAlO_3$	254	4.035	80.0 MHz	-20.0	-0.5	3.7	3.6 GHz	-5.8	-3.5
(Zhang et al., 2012)	HFSS	Five-parallel pole hairpin	MgO	200	8.0	2.0 GHz	-45.0	-0.5	7.8	2.0 GHz	-20.0	-1.2
(Shang et al., 2013)	EM Sonnet	Ten poles	MgO	218	10.0	4.0 GHz	-20.0	0	10.0	2.5 GHz	-14.0	-0.31
(Bai et al., 2013)	EM Sonnet	Ten poles	$LaAlO_3$	5898	2.15	0.1 GHz	-20.0	0	2.15	0.1 GHz	-15.0	-3.0
(Bai et al., 2013)	EM Sonnet	compact eight-pole	MgO	200	11.0	2.0 GHz	-40.0	0	11.0	2.0 GHz	-40.0	-0.8
(Kumar et al., 2014)	HFSS	Five parallel-coupled lines	FR4	71	2.48	0.6 GHz	-12.5	-2.2	…..	…..	…	….
(Zhang et al., 2015)	EM Sonnet	Parallel-connected network	$LaAlO_3$	666	2.0	30.0 MHz	-25.0	0	2.0	30.0 MHz	-12.5	-0.3

Continue

(Gupta et al., 2015)	HFSS	Five parallel-coupled lines	FR4	480	3.0	2.0 GHz	-8.0	-1.8	…..	…..	….	……
(Zhang et al., 2015)	EM Sonnet	linear phase filter.	$LaAlO_3$	425	0.83	10.0 MHz	-20.0	0	0.83	10.0 MHz	-13.0	-0.3
(Gunjal et al., 2016)	HFSS	4- parallel line coupled	FR4	2627	2.4	140 MHz	-10.0	-4.0	2.35	140 MHz	-10.0	-5.0
(Liu et al., 2017)	EM Sonnet	multi-loop resonators	MgO	335	1.8	1GHz	-20.0	0	1.5	1.0 GHz	-19.0	-0.2

Where,

Fc, Centre of frequency

BW, Bandwidth

RL, Return loss

IL, Insertion loss

Nowadays, after two decades of continues developments in CPU (central processing unit) and the clock speeds in personal computers. Therefore, multi-physics capability have been increased, for example, in radio-frequency and microwave applications several computational engineering for designing microwave components using computers are dominating the conventional modelling design using design equations (Davidson, 2010). Hence, microwave bandpass filter circuits could be designed and simulated using the computer-aided design (CAD) software's based on their performance such as, insertion and return loss methods. Therefore, CAD is a powerful tool, by which researchers can design and find the physical dimensions of any microwave component with high performance and accuracy (Sun, 2011; Toossi et al., 2015).

Many developed and versatile CAD tools have been used to design various microwave filter circuit components. However, some of CAD are computationally costly and requires long processing time. On the other hand, High Frequency Simulation Software (HFSS) that is based on finite element method offers capability of modelling circuits with broad bandwidth and low losses. The HFSS software has been developed to design several kinds of the microwave components such as, antennas, filters, etc. Upon using HFSS the physical dimensions of any microwave component can be obtained for the specific performance. By HFSS, researchers can reduce the number of trying and errors, avoid the experimental debugging and could tune period time used to produce the microwave circuit components (Davidson, 2010; Zhang, 2006).

Lastly, numerous studies have been reported on designing and simulating the microwave bandpass filters using HFSS software. The researches tried to design and fabricate the microwave devices based on the thin films to study the potential applications of different material and substrates (Lu et al., 2015; Zhang et al., 2013). A compact bandpass filter has been proposed and designed by (Sun, 2011) using HFSS. The filter results found that, the fabricated filter has a good matching and consistent with the simulated results.

2.4 Superconductivity

Superconductivity is an active field of research, which takes in an account of some popular topics include reduction of transition power losses, producing new superconductors and finding new applications (Huebener, 2015). Superconductivity is a phenomenon, in which some materials seem to have transitioned from a normal state to a superconductor state (i.e. zero resistance to the flow of current). These materials are common conductors or insulators. Superconductivity was firstly found on mercury by a Dutch physicist, Heike Kamerlingh Onnes in 1911 (Nisenoff, 2011). The phenomenon was found while the mercury resistance was measured at different temperatures. At temperature below 4.2 K, interestingly, the resistance of mercury dropped to zero. After this discovery, attentions have been paid on reproducing this important phenomenon in diverse materials. The phenomenon is called superconductivity, whereby the material exhibits zero electrical resistance. Moreover, it is also characterized by removing the magnetic flux lines outside its body when it is cooled down to a specific temperature. The temperature at which the transition takes place from the usual state to the superconducting state is known as the transition temperature or the critical temperature (T_c).

Superconductivity is a powerful phenomenon standing at the forefront of scaling-up the commercial manufacturing development. Superconductors can be classified into two types. The first type can be found at low temperature (> 4 K) on several metals and alloys (cooling via liquid helium). These superconductors are known as low temperature superconductors (LTS). The LTS era had several exciting scientific events, most of them have awarded Nobel prize (Poole, et al., 1999). Below the summary of these events and their years awarded Nobel prize:

1. Discovery of superconductivity H. Kamerlingh Onnes (1911), 1913 Nobel prize.
2. Perfect diamagnetism (Meissner effect): Meissner and Ochsenfeld (1933).
3. London equation: F. and H. London (1933).
4. Ginzburg-Landau theory: 1950s, 2003 Nobel prize (with Abrikosov).
5. Isotope effect: H. Frohlich (1950).
6. BCS theory: J. Bardeen, L. Cooper and J.R. Schrieffer (1957), 1972 Nobel prize.

7. Tunneling: Josephson effect (1957), 1973 Nobel prize.

The second type was explored in 1986 on ceramic materials which have high transition temperature of above 77 K (boiling temperature of liquid nitrogen). Thus, it is called high-temperature superconductors (HTS) (Huebener, 2015), and it will be discussed in detail.

2.5 Superconductivity in YBCO

Superconductivity has gained a considerable attention due to its intrinsic properties and its potential applications versus normal conductors. Superconductivity in YBCO was firstly observed by Chu and his group in 1987 (Nisenoff, 2011; Zhao et al., 1987). Thereafter, numerous research works on HTS have been published. In the last decade, YBCO was prepared via solid-state reaction method with transition temperature of ~92 K (Alikhanzadeh-Arani et al., 2013). Solid-state reaction method is a relatively long process. Meanwhile, the sol-gel method appears to be the first technique used to prepare YBCO after combining with several other techniques. Sol-gel method has been used to mix the metallic oxide at atomic level and form a precursor of similar solution within a short time (Kullberg et al., 1991). Furthermore, sol-gel method has been commonly used to fabricate YBCO from metal oxides, acetate and nitrate (Duarte et al., 2014; Shen et al., 2013; Uslu et al., 2010; Zhao et al., 1987).

Amongst the highest transition temperature superconductors, YBCO has been applied commercially in several application because of owning their properties such as, high transition temperature (T_c ~92 K) (Shen, 1994), high critical current density (J_c ~10^6 A/cm^2, 77 K) (Papari et al., 2012), high critical magnetic field (B ~16 T), and good chemical stability (Luo et al., 2014). Its components are non-volatile, less anisotropic, capable of having single phase and comparatively low cost (Emeakaroha, 2016). In point of fact, HTS YBCO has been used in applications such as, power transmission (Paranthaman & Izumi, 2004), transformers (Schlosser et al., 2003; Zueger, 1998), motors, generators and high frequency electronic applications (Barnes et al., 2005; Izumi & Shiohara, 2010).

2.6 Structure of YBCO

As proven before, YBCO has perovskite structure, which is consists of three cubic cells. The big yttrium atom occupies the centres the of cubic cells and the remaining two

cells, which are holding the barium atoms located at the top and bottom of the center of cubic cell. Copper and oxygen atoms occupied the corner and the middle edge positions, respectively. The dimensions of these three-unit cells are (a = 3.82 Å, b = 3.89 Å, and c = 11.69 Å). The crystal structure of YBCO is known as orthorhombic (i.e. a ≠ b ≠ c) and it has a two-dimensional copper-oxygen layer and plane structures (Zaleski & Kopeć, 2006). The superconductivity phenomenon is critically depending on the layers and chains of Cu-O, which is located mainly along of the crystal structure of YBCO. These layers are represented as chains for charge reservoirs, which keeps the charge neutrality and the solidity of the lattice structure. The highlighted regions represent the copper-oxygen layers, which are oriented along the b-axis (Arpaia, 2016a; Walliman, 2010) (see Figure 2.3).

Benzi *et al*. (Benzi et al., 2004) have proposed the procedure to determine the non-stoichiometric oxygen in YBCO superconductors based on the relationship between oxygen content and the structure parameter size c-axis for YBCO unit cell. The test proposed, the oxygen content of YBCO samples prepared from different precursors and tested by X-ray diffraction analysis then compared with those oxygen content has been obtained via iodometric titration method correspondence. The resulting oxygen content was found by the two procedures are consistent with. Moreover, the experimental values of T_c measured for YBCO agree with that calculated oxygen content values obtained from iodometric titration and the XRD method and indicating that the reliable oxygen content obtained from the proposed method is overestimates.

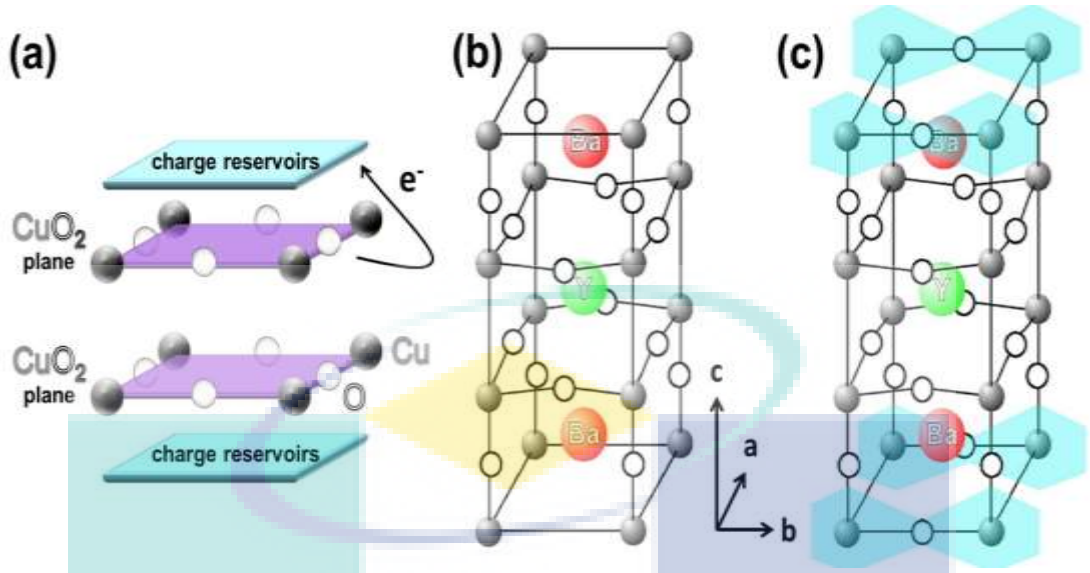

Figure 2.3 (a) The stacking of copper-oxygen planes and the charge reservoir, (b) YBCO unit cell, (c) Cu-O chains.

Source: Reproduced from (Arpaia, 2016a; Walliman, 2010)

2.7 YBCO at Nanoscale

In general, materials with diameter of less than 100 nm are defined as nanostructure materials. Meanwhile, there is no limitation on how long they are can grow (Bezryadin et al., 2000; Singh et al., 2012). Fabrication of nanostructured materials will be explained in the next sections. Materials such as nanofibers (NFs), nanowires (NWs), nanorods (NRs) and nanotubes (NTs) have been gaining popularity nowadays (Duarte et al., 2014; Shen et al., 2013). Owing to the guided transport in one-dimensional structures, intensive research works focusing on their properties and practical applications have been widely undertaken. The optimal fabrication of the nanostructures depends strongly on the synthesis procedure and the process parameters.

Nanoscale-YBCO structure (e.g. single crystal structure, pure, uniform and high performance) has fabricated by employing various techniques (Barnes et al., 2012). Techniques such as pulsed laser deposition (PLD), chemical vapor deposition (CVD), electron-beam lithography (E-beam) and anodic aluminium oxide (AAO) template have been used to synthesize YBCO at nanoscales. However, most of the proposed techniques are complex and expensive (Barnes et al., 2002; Cui et al., 2006; Duarte et al., 2014; Shen et al., 2015). In contrast, amongst various methods used to fabricate YBCO structures at nanoscale, electrospinning technique is relatively simple, effective, cheap, controllable and

versatile. It allows further manipulation on the scales of atomic structure. Also, it can change the atomic structure to an amazing nanoscale construction (Ramaseshan et al, 2007).

HTS YBCO nanowires have intrinsic transport properties that are not found in conventional bulk, thick and thin films (Shen et al., 2013; Uslu et al., 2010). Therefore, it has promoted the related studies and examining the essential properties of superconductivity at nanoscale (i.e. quantum phase slip and thermal dynamics for HTS YBCO NWs) that lead to low resistant when the working temperature is below the transition temperature of superconductor (Montemurro et al., 2015). Certainly, as the length scale of these structures decreased (to nanoscale), the grain boundaries are reduced as well (Duarte et al., 2014). Consequently, the transport properties (i.e. current density, magnetic field) are more prominent (Eom et al., 1992; Ma et al., 2004). For example, the critical current density (J_c) of YBCO superconductor increases from 10^4 A/cm^2 for bulk samples to 10^6 A/cm^2 for thin films at 77 K (Higuchi et al., 1995; Salama et al., 1989). For HTS YBCO nanowires, the critical current density is three order of magnitude larger than those of thin film and bulk samples, respectively (Nawaz et al., 2013).

Figure 2.4 shows the critical current density of the superconducting YBCO. It decreases as the tilt-angle of grain boundaries increases (Durrell & Rutter, 2008). Clearly, the superconductivity of HTS YBCO nanowires is beneficial for the developments of quantum sensor devices and photon detectors due to its stability, short coherence length (~2 Å) (Arpaia et al., 2014; Walliman, 2010), short quasiparticle coalescence time (150 fs) (Pashkin et al., 2010), affordability, ease of production and high transition temperature (Arpaia et al., 2014).

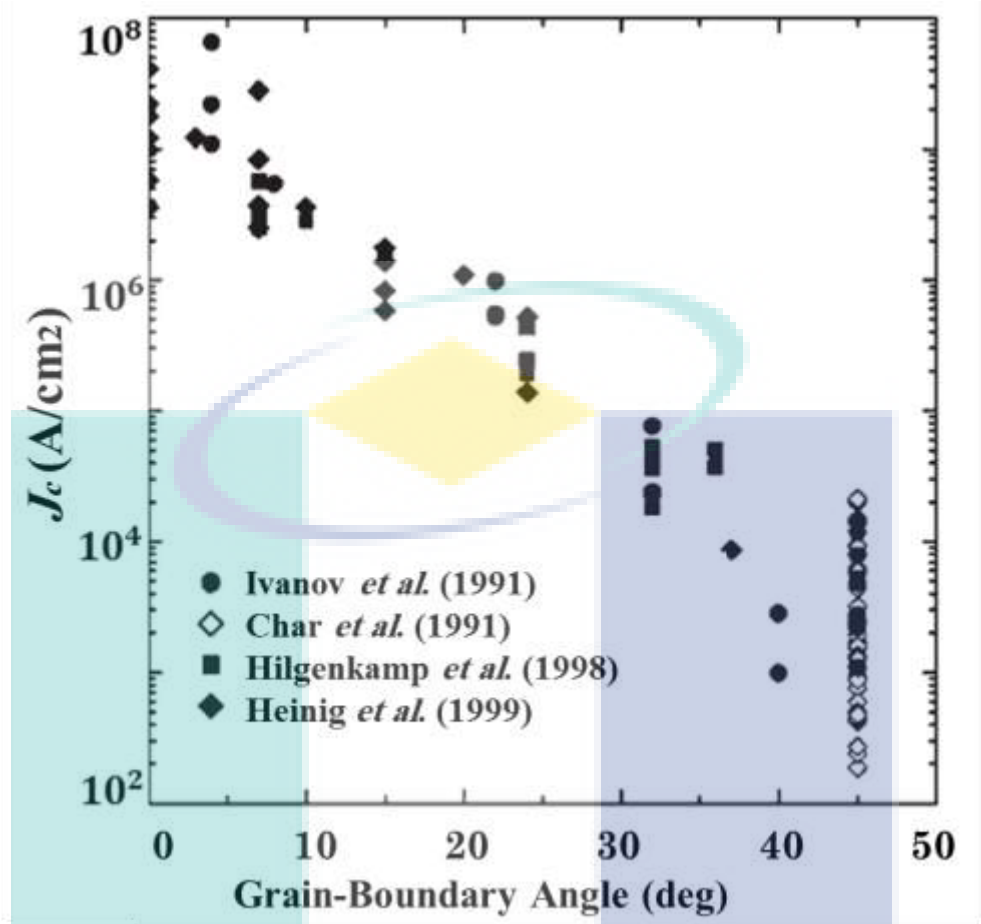

Figure 2.4 Grain boundaries angle of YBCO relation with their critical current density (J_c).

Source: Reproduced from (Durrell & Rutter, 2008)

2.8 Microwave and Superconductivity

Coated superconductors have been studied extensively as well as used in many microwave practical applications, due to their better performance than the conventional conductors. Implementing superconductors could decrease the power losses, which is an industrial requirement. The advantages of using superconducting material with high transition temperature including the higher critical field, higher critical current density (J_c) and lower cryogen costs (Huebener, 2015). The applications of coated nanostructures such as YBCO superconductors in microwave passive circuits such as filters are still not reported in open literature. Therefore, this question will be addressed in this work.

One of the earliest reports in microwave superconductivity applications was published in 1971 by DiNardo *et al*. (DiNardo et al., 1971; Nisenoff, 2011) that is revolved around the fabrication of thin film superconducting microwave filter. The researchers have reported the first design of the microwave filter fabricated using the thin ring of lead with half wave length operating frequency at 14 GHz. The results have showed that the Q-values of are ~ 200,000 at 4 K and about ~500,000 at 1.8 K, which are extremely difficult to be achieved via conventional conductors even with large structures. Weigel *et al*. (Weigel et al., 1993) have highlighted the practicability of HTS YBCO microwave device in industry. Most microwave researchers have concentrated on HTS YBCO due to their lower losses at high frequencies (Newman & Lyons, 1993; van Delft, 2012; Weigel et al., 1993).

In microwave applications, superconductivity offers a significant breakthrough in the performance of many components and subsystems. Properties such as lightweight, zero resistance, small volume, high current density and high performance, are desirable for microwave devices (Mansour, 2002; Nisenoff, 2011). The feasibility of employing the superconductivity to design the microwave circuits such as the antenna, filters, phase shifters multiplexers, couplers and delay lines with high performance and low cost has been demonstrated (Newman & Lyons, 1993; Weigel et al., 1993). Superconductivity is possessing several unique properties, which differ from those of normal state of conductors, because, it presenting much lower RF losses as compared to the conventional conductors (Baquero, 2005; Weinstock & Nisenoff, 2012). At higher microwave frequencies, the surface resistance of the superconducting materials is smaller than of normal conductors by one order of magnitude. Experimentally, the surface resistance of normal conductors is directly proportional to the square root of frequency, while it varies directly proportional with square of frequency magnitude in superconductors (Arpaia (Arpaia, 2016a; Hein, 2011; Weinstock & Nisenoff, 2012).

On the other hand, nanoscale superconductivity is gaining popularity as interesting properties such as high surface to volume ratio, size induced modification in optical and electronic properties, high mechanical strength and light weight can be realized. Usually, wet-chemical methods such as template method, sol-gel, anodization etc. are used for preparing nanoscale superconducting YBCO. However, its scalability is poor, hence, this issue can be addressed by employing a new technique that offers highly scalable manufacture. In this context, nanomaterials fabrication using a polymeric solution and

electric fields based continuous nanofiber production method, called electrospinning process that offers scalable production (Cui et al., 2006; Duarte et al., 2014; Greenberg et al., 2008; Shen et al., 2013; Uslu et al., 2010). Therefore, the current work deals with the development of broadband bandpass filters with small size (100 mm^2) and low losses and using nanostructured thin films prepared via electrospinning process as well as using finite element modeling via HFSS software.

2.9 Electrospinning Technique

Electrospinning process is one of the renowned techniques used to prepare the nanopattern structures, which was observed by formulas in 1934 (Li & Xia, 2004; Valizadeh & Farkhani, 2014). The method had been forgotten and did not claimed as an electrospinning technique and exploited as nanotechnology (Frenot & Chronakis, 2003; Li & Xia, 2004; Shen et al., 2013). More than 80-year electrospinning appear the first technique to use overall the nanostructure researches. Electrospinning process consists of four setups, i.e. the high voltage power supplier, spinneret, syringe pump and collector. The electrospinning relies on an electric field applied between the tip nozzle and the collector.

Nowadays, electrospinning technique is used to fabricate continuous nanostructures with diameters close to few nanometres. Electrospinning is a powerful technique, generally used in combination with sol-gel technique followed by calcination at high temperature (Cui et al., 2006; Greenberg et al., 2008). The typical sol-gel method used with electrospinning technique consists of the precursor of the desired material plus polymer and a relatively volatile solvent. Solvent utilized to control the solution viscosity, conductivity, and morphology. The typical solvents are used water, methanol, isopropanol, and ethanol (Bhardwaj & Kundu, 2010; Cui et al., 2006; Duarte et al., 2014; Shen et al., 2013; Uslu et al., 2010).

Electrospinning process has been employed to synthesize different morphologies of HTS YBCO, which has attracted much attention by researchers and widely developed to produce nanowires as well as nanofibers (Duarte et al., 2014; Greenberg et al., 2008). The detailed research works employing electrospinning and sol-gel method to prepare different nanostructures morphologies will be discussed in the next sections. The electrospinning process depends basically on the applied electric field between the tip nozzle and the rotated collector. In electrospinning technique, a polymeric solution containing metal ions of

specific stoichiometric ratio is injected into a strong electric field (~10^7 V/m). The solution undergoes spinning due to various instabilities and finally the solid random fibres are collected from the collector surface placed at ~10 – 15 cm away from the injector. Inorganic nanofibers are obtained from the polymeric fibres through appropriate heat treatment (Shen et al., 2013; Wu et al., 2012). Furthermore, electrospinning has been used extensively in industry to produce several nanostructure and different morphologies (Li & Xia, 2004; Nirmala et al., 2014).

With electrospinning technique, it is now possible to explore some additional intriguing physical properties of superconductivity at nanoscale. Electrospinning technique is relatively simple, cheap, inexpensive, scalable and versatile bottom-up approach, and controlled parameters, which plays a vital role in the fabrication of different nanostructured materials (Li & Xia, 2004; Sigmund et al., 2006). Figure 2.5 shows the components and schematic diagram of the electrospinning process. Normally the high voltage is used to generate a gaunt charged jet solution from the droplet at the tip of the needle. The drop begins to stretch to form a monofilament. The monofilament leaves the drop when the electric field strength increases and the electrostatic repulsive force overcomes the surface tension (Lee et al., 2014; Li & Xia, 2004).

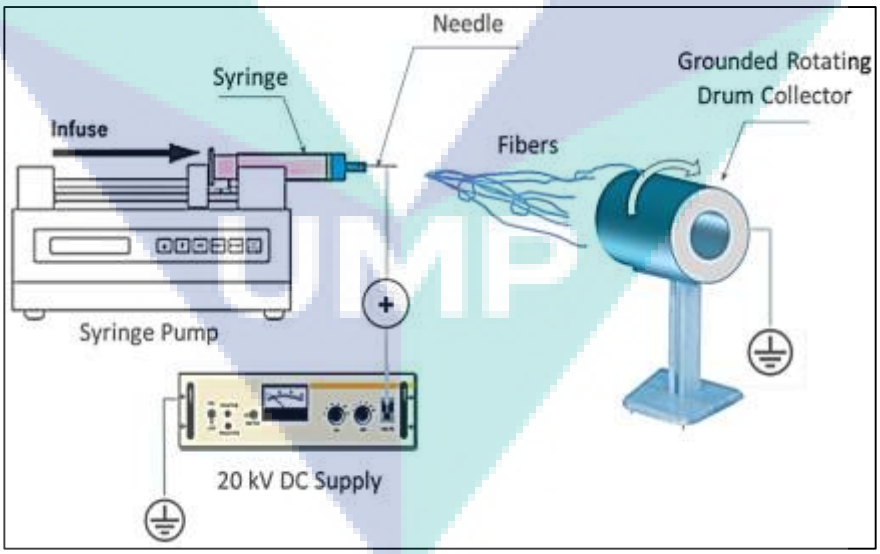

Figure 2.5 A schematic diagram of the electrospinning process parameters.
Source: Reproduced from (Khalil et al., 2016)

The polymers with sol-gel composite solutions are used as a solution aid to adjust the viscosity, to support formation of nanostructure, to control the diameter of nanostructures, and to verify collections of nanostructures at the initial time (Duarte et al., 2014). Commonly, HTS YBCO nanostructures are made from the electrospinning of sol-gel metallic acetate precursors in the presence of a specific ratio of polymer followed by calcination at higher temperatures to burn out the polymer. Finally, the pure structure of HTS YBCO can be collected (Greenberg et al., 2008).

Generally, in electrospinning process the nanostructure of HTS YBCO can be obtained from the using of three controlled parameters. First of all, the solution properties (e.g. conductivity, viscosity and surface tension) which play an important role in the forming of the nanostructures via electrospinning technique (Sigmund et al., 2006; Tan, et al., 2013). The polymer concentration ratio, molecular weight of polymers, the solvent quality, precursor concentration and polymer ratio are some examples of the basic solution parameters (Li & Xia, 2004). Secondly, the electrospinning parameters such as, the applied voltage, tip collector distance, (motion and size) of the collector, needle gauge, and flow rate injection are essential electrospinning parameters. Thirdly, the ambient circumstances such as temperature, humidity and air velocity inside the chamber of the electrospinning unit will affected on the fabrication process and the quality of the product. These parameters can be used to control and manipulate morphologies of nanostructured materials (Li & Xia, 2004; Tan et al., 2013; Yao et al., 2015).

2.9.1 Solution Parameter

Doshi *et al*. (Doshi & Reneker, 1993) was the first group who reported the fabrication of polymer fibres via electrospinning. The polymer fibres have been produced with different shapes, cross sections and morphologies were produced. The fibres diameter is dependent heavily on the polymer concentration. In general, it has been reported when the polyvinyl acetate (PVAc) concentration increases in the spinning solution, the diameter of the electrospun fibres increases as well due to increased viscosity (Doshi & Reneker, 1993; Park et al., 2008; Tekmen et al., 2008). The electrospun solution is influenced by the several parameters, such as the polymer molecular weight, solvent quality, solution viscosity, solution conductivity and surface tension (Li & Xia, 2004; Park et al., 2008; Sawicka & Gouma, 2006; Tekmen et al., 2008). The polymer concentration ratio plays a significant role in the solution properties. Thus, it can be used to control the solution

viscosity and tune the diameter of nanostructure shapes (Li & Xia, 2004; Sigmund et al., 2006; Tan et al., 2013; Tekmen et al., 2008).

Table 2.2 summarizes the synthesizing procedures of HTS YBCO with different morphologies using electrospinning process. The average polymer concentration ratio ranges from 4 – 10%. The propionic acid solution has been utilized to dissolve metallic acetates of Y, Ba and Cu (Cui et al., 2006; Duarte et al., 2014). The acetic acid can prevent any hydrolysis of polymers (Cui et al., 2006; Duarte et al., 2014; Shen et al., 2013). Moreover, the acid medium was suitable to prevent the hydrolysis of the sol–gel precursor. Finally, the methanol solution can be used as a polymer solvent to tune the viscosity (Duarte et al., 2014). The high concentration ratio of polymers in the spinning solution increases the viscosity and results in thicker nanostructure (Cui et al., 2006), as described in Table 2.3.

In contrast, the low concentration ratio of polymers leads to decreased viscosity and results in thinner nanostructure diameter (Duarte et al., 2014). The relation between precursor and polymer is complex and it is normally determined by trial and error process. Jin *et al*. (Jin, 2009) studied the effect of weight ratio of poly (vinyl alcohol) (PVA) on the composite concentration. The authors studied the applied voltage and the relative content of polymer and composite as well. The fabricated nanostructures were somewhat similar to the necklace structure. The structure was obtained by controlling the volumes of polymer, composite and solvent. The composite concentration was affected by the amount of polymer and solvent. Thus, the electrospun nanostructure was dependent on three parameters mentioned earlier (Baji et al., 2010; Jin, 2009; Park et al., 2008; Sawicka & Gouma, 2006).

Table 2.3 shows the polymer to YBCO precursor ratio; it is evident from the first row that the high ratio of the precursor YBCO to polymer PVA results in high viscosity and thick fibres diameter (Cui et al., 2006). Greenberg *et al.* (Greenberg et al., 2008), reported experimentally that the ratio of polymer to YBCO precursor solution of 2:1, this means that the result of the spinning precursor was made by adding one part of YBCO precursor to two parts of polymer PAAc. The result was indicated with would generate lower viscosity and thinner fibres diameter (Greenberg et al., 2008). A typical YBCO precursor concentration ratio relative to polymer was adopted by Uslu *et al*. (Uslu et al., 2010). The HTS YBCO nanotube structure with small cross section was produced. Lastly,

Duarte *et al.* (Duarte et al., 2014) prepared two spinning precursor solutions by adding two different precursors to the same ratio of polymer, see Table 2.3. The solvent was adjusted to lower the viscosities of two solutions (~75 cP and 50 cP). Different nanostructure diameters were obtained by electrospun various solutions of different viscosities and their results were consistent with other report (Jin, 2009; Sawicka & Gouma, 2006; Tekmen et al., 2008).

Table 2.2 Summary of the synthesis procedures of HTS YBCO with different morphologies using electrospinning process.

Polymer	Polymer Ratio	Solvent	Precursor	Calcination Temperature	Structure	Viscosity (cP)	Diameter (nm)	Ref.
PVA	5%	Propionic acid, 2-hydroxy isobutyric acid	Y, Ba, and Cu acetate	450 °C	$YBa_2Cu_3O_{7-\delta}$ NFs	300-500	540	(Cui et al., 2006)
PAAc	10%	deionized water	Y, Ba, and Cu nitrate	450 °C	$YBa_2Cu_3O_{7-\delta}$ NFs	52	50-100	(Greenberg et al., 2008)
PVA	10%	Deionized water	Y, Ba, and Cu acetate	500 °C	$YBa_2Cu_3O_{7-\delta}$ NFs	Not given	300-800	(Uslu et al., 2010)
PVA	10%	Deionized water	Y, Ba, and Cu acetate doped boron	600 °C	$YBa_2Cu_3O_{7-\delta}$ + Bo NFs	Not given	200-500	(Uslu et al., 2010)
PVP	18%	ethanol and acetic acid	Y, Ba, and Cu acetate	450 °C	$YBa_2Cu_3O_{7-\delta}$ NTs	Not given	110-150	(Shen et al., 2013)
PVP	4%	Methanol, propionic acid, and acetic acid	Y, Ba, and Cu acetate	450 °C	$YBa_2Cu_3O_{7-\delta}$ NWs	75	120-550 50-80	(Duarte et al., 2014)

Table 2.3 The polymer to the precursor ratio, nanostructure diameter of the HTS YBCO and its concentration with polymer

Polymer	Polymer Ratio	Polymer: Precursor Ratio	Structure	Viscosity (cP)	Diameter (nm)	Ref.
PVA	5%	1:5	$YBa_2Cu_3O_{7-\delta}$ NFs	300-500	540	(Cui et al., 2006)
PAAc	10%	2:1	$YBa_2Cu_3O_{7-\delta}$ NFs	52	50-100	(Greenberg et al., 2008)
PVA	10%	Not given	$YBa_2Cu_3O_{7-\delta}$ NFs	Not given	300-800	(Uslu et al., 2010)
PVA	10%	Not given	$YBa_2Cu_3O_{7-\delta}$ + Bo NFs	Not given	200-500	(Uslu et al., 2010)
PVP	18%	8:5	$YBa_2Cu_3O_{7-\delta}$ NTs	Not given	110-150	(Shen et al., 2013)
PVP	4%	1:1 1:5	$YBa_2Cu_3O_{7-\delta}$ NWs	75 50	120-550 50-80	(Duarte et al., 2014)

2.9.2 Electrospinning Parameter

Table 2.4 shows the electrospinning parameters were employed to synthesize different nanostructured morphologies from YBCO. The electric field strength is ranging from 15 – 28 kV. Appling the high electric field between the tip nozzle and the collector, the so-called Taylor cone is then formed, and the molecules of the solution are elongated and stretched. Upon separating from the top of the cone, the charged jet goes to the collector directly (Garg & Bowlin, 2011; Lee et al., 2004; Sawicka & Gouma, 2006; Yao et al., 2015). The tip collector distance is ranging from 10 to 18 cm. The increasing in the distance play a critical role for manufacturing small size structure and vice versa. The injected solution flow rate is adjusted accordingly (1 – 3 ml/h). Slow injected solutions are desirable for a smooth, uniform and scalable structure. The needle inner diameter ranges from 0.3 to 0.8 mm, big needle diameter is slightly affects the production at nanoscale and it required for viscous solutions.

Table 2.4 Electrospinning parameters were used to fabricate different morphologies from the HTS YBCO

Polymer	**Applied voltage (KV)**	**Tip collector distance (cm)**	**Flow rate (ml/h)**	**Needle diameter (mm)**	**Structure**	**Diameter (nm)**	**Ref**
PVA	24-28	10-18	1-3	0.83	$YBa_2Cu_3O_{7-\delta}$ NFs	540	(Cui et al., 2006)
PAAc	~20	18	1-3	0.5	$YBa_2Cu_3O_{7-\delta}$ NFs	50-100	(Greenberg et al., 2008)
PVA	15	15	1	0.8	$YBa_2Cu_3O_{7-\delta}$ NFs	300-800	(Uslu et al., 2010)
PVA	15	15	1	0.8	$YBa_2Cu_3O_{7-\delta}$ +Bo NFs	200-500	(Uslu et al., 2010)
PVP	19.2	12	3	0.5	$YBa_2Cu_3O_{7-\delta}$ NTs	110-150	(Shen et al., 2013)
PVP	21	16	0.8	0.3	$YBa_2Cu_3O_{7-\delta}$ NWs	120-550 50-80	(Duarte et al., 2014)

The strength electric field is required to generate the jets and form the nanofilaments depending on several conditions and solution properties such as conductivity, viscosity and surface tension of the solution (i.e. solvent properties) (Li & Xia, 2004; Tan et al., 2013). Higher electric field strength and viscosity would increase the average diameters of nanostructures such as nanofibers and nanowires (Duarte et al., 2014; Greenberg et al., 2008; Park et al., 2008). The diameter of the nanostructures versus the year of their fabrication is presented in Figure 2.6, which shows the high applied voltage results in large fibre diameter as reported by Cui *et al.* (Cui et al., 2006).

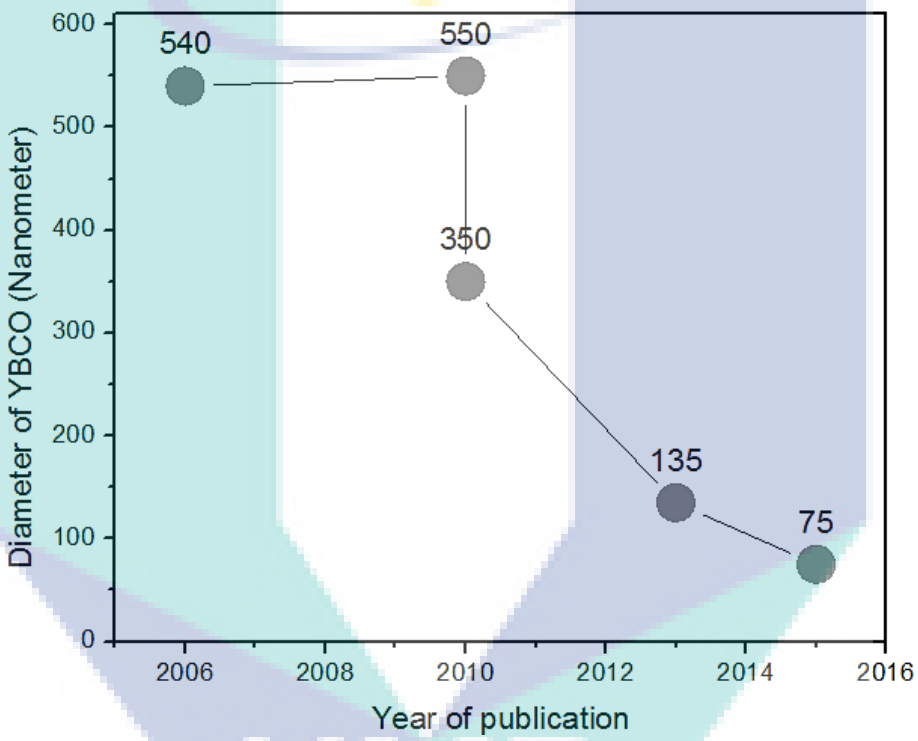

Figure 2.6 The nanostructure diameter of HTS YBCO vs. the years of publication, the data was taken from Scopus, December 2017, keywords "electrospinning and YBCO''.

2.9.3 Ambient Circumstances

Ambient circumstances such as humidity temperature and air velocity inside the electrospinning unit chamber affect the properties of nanostructures as well. These parameters can be used to manipulate the size and morphologies of nanostructures (Li & Xia, 2004; Tan et al., 2013; Yao et al., 2015). For example, low humidity and high temperature could damage the nanostructure as well as the induce air motion within the unit thus preventing the charged jet from reaching the collector. Therefore, modernize

electrospinning process is accomplished by adding full electronic control in order to reduce the sensitivity of ambient condition (Garg & Bowlin, 2011). Table 2.5 shows some information about the variations of fibre diameter subjected to the changes of solutions parameters, electrospinning process parameters and ambient circumstances.

Table 2.5 The variation of fiber diameter with many parameters

Parameters		The influence	fibre diameter description
Solution parameters	Viscosity	High	Increase
		Low	Decrease
	Conductivity	High	Increase
		Low	Decrease
	Surface tension	High	Decrease
		Low	Increase
	Polymer concentration	High	Increase
		Low	Decrease
	Molecular weight	High	Decrease
		Low	Increase
Electrospinning parameters	Electric potential	High	Increase
		Low	Decrease
	Tip collector distance	High	Decrease
		Low	Increase
	Flow rate	High	Increase
		Low	Decrease
	Needle diameter (jet size)	Big	Increase
		Small	Decrease
	Motion and size collector	Fast	Decrease
		Slow	Increase
Ambient circumstances	Humidity	High	Increase
		Low	Decrease
	Temperature	High	Increase
		Low	Decrease
	Air velocity	Fast	Increase
		Slow	Decrease

2.10 Morphology of HTS YBCO Nanostructures

Fabrication of HTS YBCO nanostructures via electrospinning process has been performed since the past ten years. Several constructions morphologies of HTS YBCO have been obtained. This section summarizes the research procedures followed to fabricate HTS YBCO nanostructures such as nanofibers (NFs), nanorods (NRs), nanotubes (NTs) and nanowires (NWs) (see Figure 2.7).

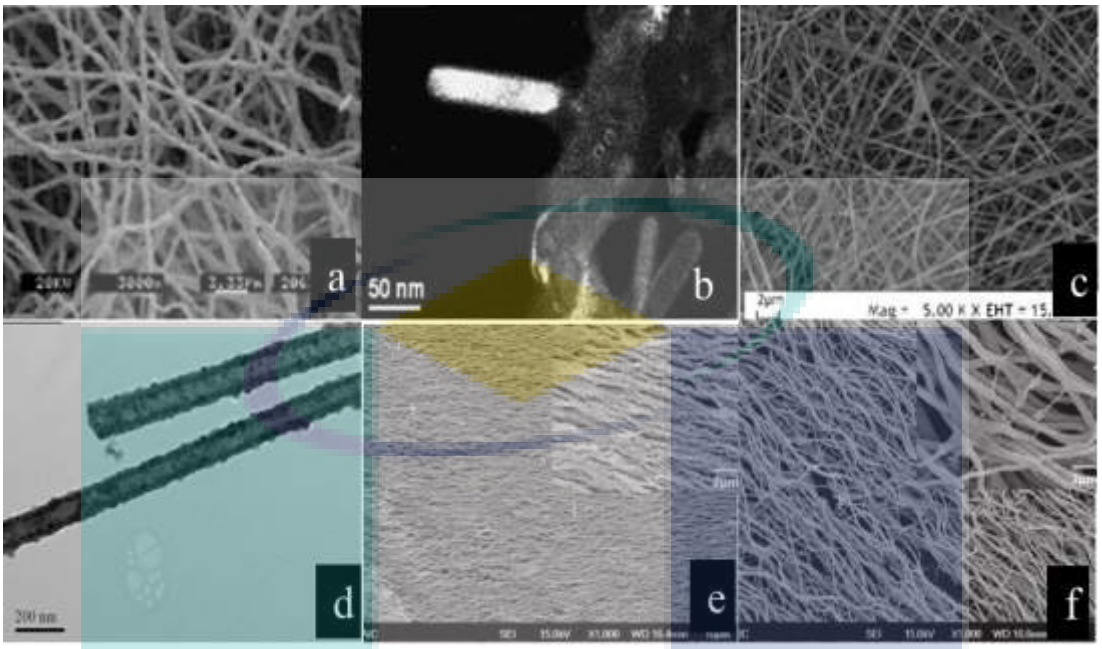

Figure 2.7 Morphologies of YBCO nanostructures fabricated by electrospinning process;(a) Nanofiber, (b) Nanorod, (c) Nanofiber contains Boron, (d) Nanotube, (e) Nanowire (Ratio, 5:1), (f) Nanowire (Ratio, 1:1).

Source: (Cui et al., 2006; Duarte et al., 2014; Greenberg et al., 2008; Shen et al., 2013; Uslu et al., 2010).

2.10.1 YBCO Nanofibers

Cui *et al.* have reported the early work to prepare and characterize the HTS YBCO nanofibers (Cui et al., 2006), see Figure 2.7 (a). The nanofibers were prepared from the metal acetate of Y, Ba, and Cu with stoichiometric ratio of 1:2:3, by combination sol-gel aqueous solution of Polyvinyl Alcohol (PVA) (Mw = 78000) with electrospinning process. The solution viscosity was controlled by evaporating/condensing the solvent during the electrospinning process. The reported optimum viscosity used for electrospinning was ranging from 300 to 500 cP. The nanofiber diameter increased rapidly upon increasing the applied voltage, viscosity, and the flow rate. The reported optimal ratio between the metal acetate Ac and PVA was 5.0, and the electrospinning parameters setup is tabulated in Table 2.2. The obtained nanofiber diameter was ~ 870 nm and decreased to 540 nm due to the decomposition of polymer after the heat treatment. Nanofibers of long length and large diameter were obtained due to several factors such as high voltage, flow rate, short distance and large inner needle diameter. However, the nanofibers of YBCO consisted of single-

phase structure and its transition temperature was high, i.e. 92 K. The phase structure and morphology of YBCO nanofibers is generally dependent on the heat treatment process.

2.10.2 YBCO Nanorod

Greenberg *et al.* (Greenberg et al., 2008) have synthesized the YBCO nanorods using metallic nitrate salts of Y, Ba, and Cu under the stoichiometric composition of 1:2:3 with poly (acrylic acid) (PAAc) (Mw = 450,000) using electrospinning process. The precursor solution was controlled by the mass ratio of 2:1 between 5% of (PAAc) aqueous solutions and 5% of (Y, Ba, and Cu)-nitrite. The viscosity of the aqueous polymer solution was 52 cP and its ion concentration increased upon adding metal nitrites. Therefore, the conductivity and the partial charge of aqueous solution increased. More information can be found in Table 2.2 and Table 2.3. The electrospun solutions was pyrolyzed using the tube furnace with complex heat treatments and the single nanorod was collected with small diameter ranging between 50 nm and 100 nm (ten micrometres in length) (see Figure 2.7 (b)). The small aspect ratio of nanorods is due to the thermal decomposition of PAAc during the heat treatment process and the small quantities of (Y, Ba, Cu)-nitrite in the precursor solution. The authors investigated the fabrication of shareable of YBCO and studied the structures of nanorods produced by electrospinning of PAAc/metal nitrate precursor solution followed by heat treatments.

2.10.3 YBCO Nanofibers Contains Boron

Uslu *et al*. (Uslu et al., 2010) have synthesized and characterized the nanofibers of YBCO doped Boron from mixing the components of Y, Ba, and Cu acetates according to the stoichiometric ratio of 1:2:3 (see Figure 2.7 (c)). The aqueous solution of Polyvinyl Alcohol (PVA) (Mw = 720,000) with weight ratio of 10% was used. The YBCO nanofiber was prepared with free boron solution first time and 1% of boric acid was added to prepare the second set boron doped solution. Then, the electrospun fibres results with two nanofiber types were subjected to heat treatment to burn out the polymer. The YBCO free boron and doped boron fibres were then collected. The results showed that the free boron fibre diameter was ranging between 300 nm and 800 nm, while the doped boron fibre diameter was between 200 nm and 500 nm. The results were consistent with those of Cui *et al.* (Cui et al., 2006). In general, the fibres doped boron are usually more stable, more conductive, smaller and exhibiting higher transition temperature. Table 2.2 and Table 2.3, show the

solution and electrospinning parameters, the process was used with a higher flow rate as well as a slightly large diameter jet solution. As a result, the fibre diameter is larger as compared to those of Greenberg *et al.* (Greenberg et al., 2008) and Duarte *et al*. (Duarte et al., 2014). The fibre diameter decreases to 50 nm. Thus, the fibre diameter can be decreased by using relatively higher applied voltage, lower injection flow rate, smaller needle diameter and higher polymer molecular weight such as PVP poly (vinyl pyrrolidone) (Mw = 1300000).

2.10.4 YBCO Nanotubes

Shen *et al.* (Shen et al., 2013) have prepared the HTS YBCO nanotubes by electrospinning process. As shown in Figure 2.7 (d), the precursor solution is made from polymer PVP (Mw = 1300000; 18% weight ratio) and Y, Ba, and Cu acetates according to the stoichiometric ratio 1:2:3. The polymer PVP of high concentration ratio was used, thus increasing the viscosity of precursor solution. The authors worked with high viscosity solution, high applied voltage, small inner diameter (i.e. small jet solution) and high flow rate. A new morphology called nanotube of HTS YBCO with relatively small inner diameter and thin wall was then formed as described in Table 2.2 and Table 2.3. The nanotubes of HTS YBCO were annealed in oxygen atmosphere at elevated temperature, i.e. 900 °C. The obtained diameters were between 110 nm to 150 nm (wall thickness ranged from 30 nm to 40 nm). As compared to the standard bulk YBCO, HTS YBCO nanotubes show higher critical temperature with broader transition, unlike the standard bulk YBCO.

2.10.5 YBCO Nanowires

Duarte *et al.* (Duarte et al., 2014) have reported a new progress by preparing YBCO nanowires with high transition temperature T_c ~92 K using sol-gel and electrospinning techniques. The nanowires were obtained via manipulating the concentration ratio of the precursor and polymer solutions. The precursor solution was consisted of Y, Ba and Cu acetates. These acetates were mixed with polymer PVP (Mw = 1300000) according to the chemical atomic ratio 1:2:3. The HTS YBCO nanowires were prepared through using two concentration ratios (metal acetate to polymer). The first one mixed the metal acetate to polymer with ratio 5:1, while the second one, mixed according to ratio 1:1. However, the experiment was used with different polymer ratio relative to metal acetate mainly to control the viscosity. By this procedure the viscosity of the first solution was 75 cP and the second

solution was 50 cP. Therefore, two kinds of nanowires, i.e. random and alignment nanowires were obtained (see Figure 2.7 (e) and (f)). The diameters of nanowires prepared by using 75 cP and 50 cP solutions ranged from 300 nm to 600 nm and 150 nm to 350 nm, respectively, as described in Table 2.2 and Table 2.3. This result was consistent with those reported in the literature, whereby higher viscosity would lead to large diameter nanostructures (Sigmund et al., 2006; Zhan et al., 2006).

2.11 Hierarchical and Garland Shaped Nanostructures

The morphologies of YBCO nanostructures have been prepared by electrospinning process have been presented in the last sections (2.10.1 - 2.10.5). This section presents the fabrication technique used to prepare the hierarchical and garland shaped nanostructures from ZnO and CuTCNQ, respectively. Lao *et al.* (Lao et al., 2002) have produced various symmetrical hierarchical nanostructures by vapor transport and condensation techniques. The ZnO hierarchical nanostructures were deposited on 3-dimensional backbone of In_2O_3 nanowires by vapor transport and condensation processes. The hierarchical nanostructures were grown parallel or perpendicular to the In_2O_3 nanowires backbone with symmetrical number of fold (2, 4, 6, etc.) as shown in Figure 2.8, (a) and (b).

Pal *et al.* (Pal et al., 2014) have synthesized Cu nanowires as thick sheets using hydrothermal technique. The nanowires were prepared by dissolving 0.53 g of octadecylamine and 0.13 g of anhydrous copper(II) chloride in 80 ml of D.I. water. The solution was then stirred overnight by ultrasonication to generate a smooth, light blue emulsion. It was transferred to a 100-ml autoclave and the solution was heated at 160 oC for 72 h. The thick sheet of Cu nanowires formed at the autoclave bottom was then washed by using D.I. water and dried at room temperature. The collected Cu nanowires were immersed in the acetonitrile solution and the reddish Cu nanowires turned bluish. After 2 minutes, the sample was washed by using D.I. water and dried in vacuum overnight. The gradual consumption of Cu nanowires in acetonitrile solution at different time intervals was responsible for triggering various structures. As shown in Figure 2.8, (c) and (d), the 3-dimensional backbone of Cu nanowire is used to materialize a garland shape of hierarchical forms.

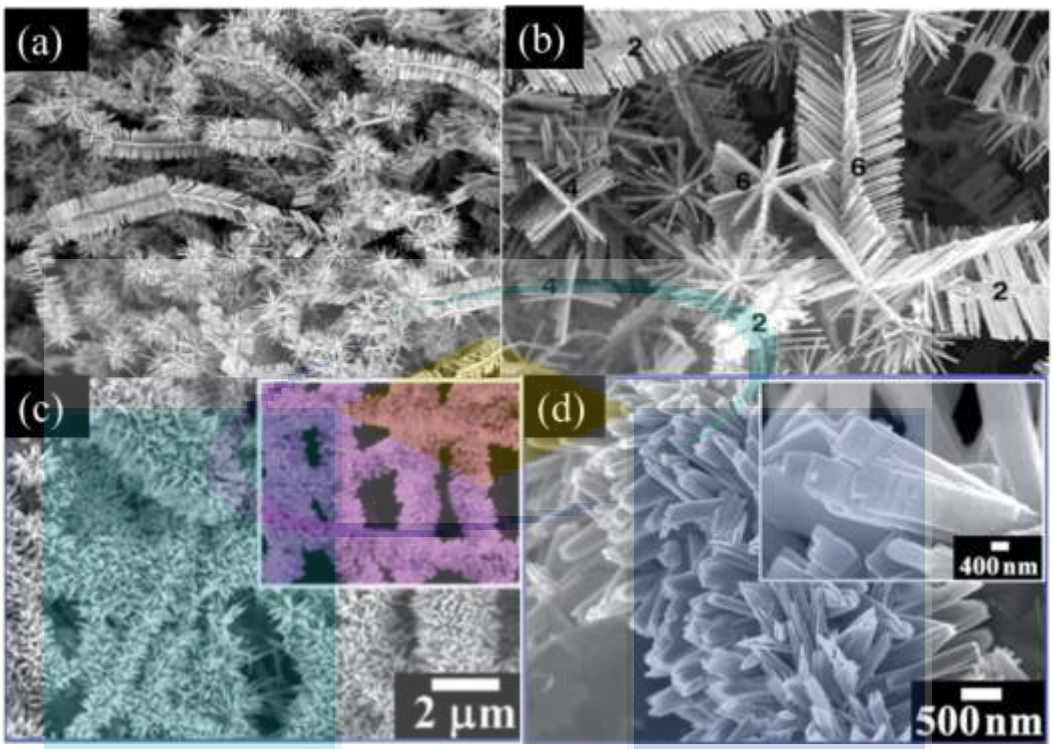

Figure 2.8 Hierarchical and garland shaped nanostructure morphologies
Source: (Lao et al., 2002; Pal et al., 2014).

2.12 Spin Coating Technique

Several techniques have been used to deposit the thick and thin films of YBCO superconductor on various substrates ($LaAlO_3$ in particular). Spin coating is one of the common methods used to deposit a uniform thin film on a flat substrate. Usually, the spin coating applies a small amount of dissolved material (paste) on a substrate, while it is rotating at high or low speed or not rotating at all. Spin coating has the ability for quickly and efficiently to produce high-quality thin film of thickness ranging from a few nanometres up to a submicron using high quality paste (Zayer, 2016). The paste produced from the milled precursor of the desired material could be dispersed in solvents such as water, α-terpinol, ethyl cellulose (E.C, 10 wt. %), aqueous and non-aqueous solutions (Choi et al., 1989). These solutions were stirred in an ultrasonic bath to produce a homogenous solution. Spin coating is an effective and controllable technique. It is versatile and able to produce solar cell (Wali et al., 2014). The dense paste has been used to deposit YBCO superconductor with three dimensions successfully. The product can be used to construct high superconducting YBCO hollow cylinder with long levitation time than others and it could be used for potential applications (Wei et al., 2017).

2.13 Etching Process

Numerous etching methods have been employed to produce nanostructured patterns from YBCO thin films such as electron-beam lithography, ion beam, ion irradiation, photolithography and selected epitaxial growth (Arpaia, et al., 2013). Specific study shows that the nano-patterning procedure of the superconducting YBCO nanowire limits the lateral size of an array of sub-micron length to 10 nm (Xu & Heath, 2008). On the other hand, most of the expenses used to produce the limited nanowires are affected the superconductivity from the etching procedure. In general, etching processes are performed for the thin films of thickness d greater than 20 nm (Curtz et al., 2010). An electron-beam lithography technique is a versatile tool used to fabricate materials with nanostructure patterns by electron irradiation. It is maskless based on the chemical modulation of the thin film polymer resist (Arpaia, 2016a, 2016b; Kolodziej & Maynard, 2012; Rius Suñé et al., 2008).

2.14 Summary

This chapter presented a brief introduction of superconductivity, the properties of HTS YBCO as well as its structure, the nanoscale property of YBCO and applications. The background of microwave and superconductivity, the applications of coated YBCO superconductors in microwave passive circuits. The microwave properties of thin films and their properties at high frequency. The kinds of the microwave bandpass filters designed, simulated and manufactured using different CAD software's, models, substrates and dimensions are discussed. The fabrication process parameters, used to produce different morphologies of YBCO used in electrospinning process. The one-dimensional (1-D) nanostructures and the configurations of HTS YBCO produced via the electrospinning process are addressed. This chapter highlights the extensive efforts in preparing and fabricating HTS YBCO nanostructures such as nanofibers (NFs), nanorods (NRs), nanotubes (NTs) and nanowires (NWs) using electrospinning and sol-gel techniques. This review has been found that the diameter of nanostructures depends strongly on the solution properties such as viscosity, conductivity and electrospinning parameters including applied voltage and injection flow rate. The preparation of other nanostructures materials has been reviewed as well as presented the fabrication technique used to prepare the hierarchical and garland shaped nanostructures. The reported effects of controlling parameters on the diameter of the nanostructures are consistent. In general, the morphology is dependent on

electrospinning parameters and solution properties. The spin coating has been explained, it is one of the common methods used to deposit a uniform thin film on a flat substrate ($LaAlO_3$ in particular). Usually, the spin coating applies a small amount of dissolved material (paste) on a rotated substrate. Finally, the synthesis procedure used to prepare the HTS YBCO microwave devices from the thin films was presented. The etching method has been employed to produce nanostructured patterns from YBCO thin films prepared by several techniques.

CHAPTER 3

METHODOLOGY

3.1 Introduction

This chapter describes the research methodology adopted to design and simulate the microwave bandpass filter using CAD software. The development of the microwave bandpass filter circuits based on YBCO thin films. The filter circuits were fabricated from the thin films of the superconducting YBCO prepared by two different techniques (i.e. electrospinning and solid-state techniques). The measurements, structures and characteristic of the prepared YBCO samples were studied. The HTS YBCO thin films were deposited on $LaAlO_3$ substrates using electrospinning and spin coating techniques. The etching process was employed on the superconducting YBCO thin films to fabricate the microwave filter circuits.

3.2 Research Methodology

Figure 3.1 shows the flow chart of the current research methodology is consisted of three parts to achieve the three objectives. The first part deals with the design and analyses the microwave filter circuits based on the simulation parameters (i.e. length, space and thickness) employing Ansoft HFSS software. The second part started with the preparing HTS YBCO by electrospinning process and solid-state reaction method. The structural characterizations were examined via XRD, FESEM and the BET surface area measurements. The transition temperature (T_c) of the superconducting YBCO samples was measured via a closed cycle of liquid helium refrigeration systems using the AC susceptibility. The third objective is to fabricate the microwave device via etching process of the prepared thin films of the superconducting YBCO powder prepared in the second research methodology part.

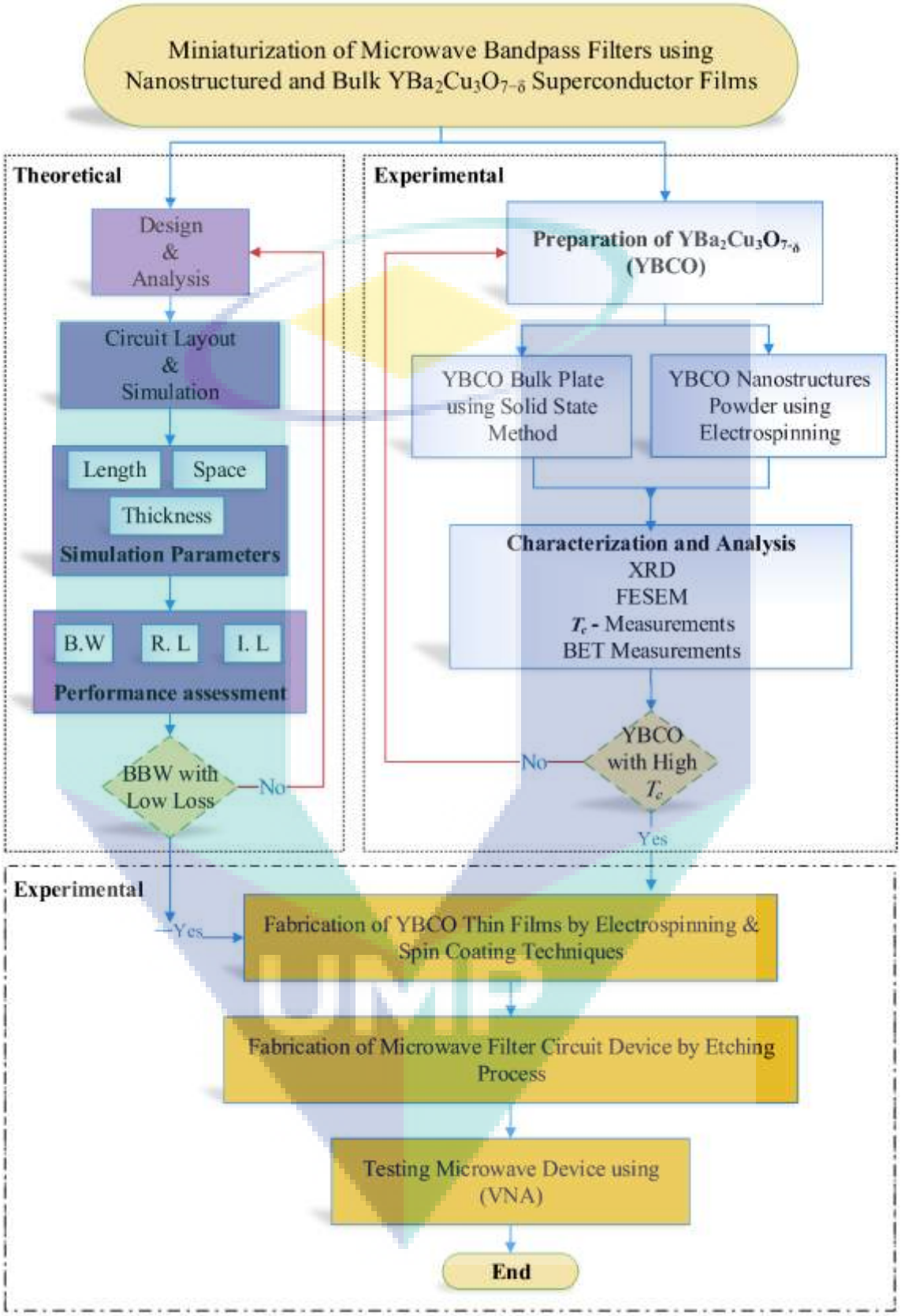

Figure 3.1 Flow chart of the research methodology.

The deposition of the superconducting YBCO thin films was performed using the electrospinning process and spin coating technique. The thin films were deposited on a single crystal (10 ×10 mm^2) $LaAlO_3$ substrate. The YBCO microwave filter circuits were realized from thin films of YBCO superconductor prepared by electrospinning and solid-state reaction techniques using the etching process. Finally, the microwave filters were tested using the Vector Network Analyser (VNA).

3.3 Design and Simulation of Microwave Bandpass Filter

Microwave bandpass filter is the essential part in the input and output of the microwave wireless circuits in the communication systems. It is implemented to achieve a unique and accurate radiation frequency (Marimuthu, 2004). A cascade of parallel-coupled four lines has been adopted to design the planar microwave filter. The microwave filter components were designed readily utilizing CAD computer software. Many methods, as well as versatile CAD apparatus have been progressing to use for planning the microwave components for several types. By using the CAD many advantages could be realized, mainly save the time, gain the high performance, obtaining the right physical dimension of the component, reduce the try and errors cases, and avoid the experimental treatment and manufacturing an optimum component. Upon using CAD, the research objectives can be achieved easily through the designing and developing the microwave circuit components. The advantages will shorten the time of research and reducing the total costs of the experiments (Sun, 2011; Zhang, 2006).

In this work, the CAD tool called high-frequency structural simulator (HFSS) software, it is a commercial finite element method (FEM) solver used for electromagnetic structures. Ansoft HFSS software is a high-performance designer developed by Professor Zoltan Cendes and his group in 1989 at Carnegie Mellon University (Chowdhury & Chowdhury, 2014). The HFSS is standard software working for full three-dimensional (3-D), electromagnetic field, and full-wave. The CAD HFSS is a commercial from Ansys, uses integral equation and meshing for calculating the electromagnetic structures. It is offering the art of an engineering task, which is used to create and simulate the microwave circuits for the desired frequency (Zhang, 2006).

3.4 Filter Design

This section describes an efficient method used to design the microwave strip line filter. It is including the 3-D full-wave field solver combining with the circuit simulator. Microwave bandpass filter was designed via high-frequency structural simulator HFSS Ansoft software which is an industrial standard software used widely for simulating the microwave passive circuit. In this work, a microwave filter is designed to allow for the central frequency 10.0 GHz to pass through and attenuated other frequencies outside. The microwave filter is designed with parallel coupling line model. There are several ways to create coupling resonator between the microstrip lines. The basic principle to design the coupled lines is the two microstrip lines must be parallel at least sub-sections of their lengths. The coupled lines of the microwave filter were designed with four parallel tapes which were assigned as a perfect conductor. The microwave filter is designed using $LaAlO_3$ substrate of ($10 \times 10 \times 0.5\ mm^3$) dimension, which is assigned as dielectric material with dielectric constant 23.5 (Mansour, 2002).

The microwave filter is proposed to be in symmetrical geometry using the duplicate mode. The device was designed using the drawing technique followed by editing the characteristics from the command tab windows. The HFSS software has been developed to design several kinds of the microwave components, which is able to obtain the physical dimensions of any microwave component with the specifications of high performance (i.e. high return loss method). However, using the insertion loss method would allow for high control over the bandpass amplitude (i.e. broad bandwidth) and phase characteristics. In addition, the insertion loss method in all cases, permits for high-performance device and improve a straightforward manner for systematic design and found the physical dimensions for the filter circuit components (Gunjal et al., 2016; Zhang, 2006). The bandpass filter is consisted of dual number of the geometrical components (i.e. tape), which can be duplicated easily and created the symmetrical microwave filter in HFSS successfully. Figure 3.2 shows the research methodology for filter design and simulation using HFSS to find the optimized physical dimensions using return loss method.

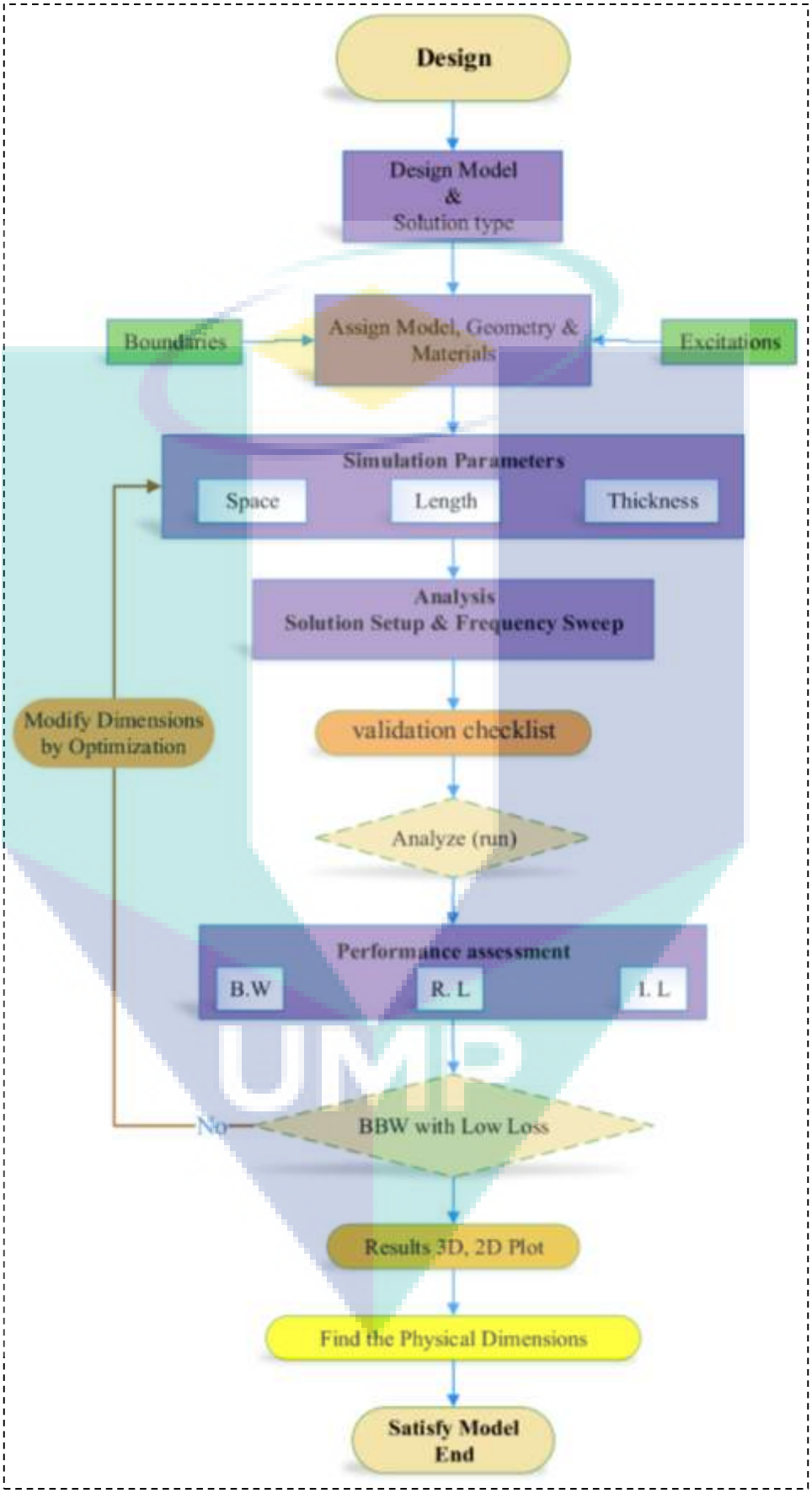

Figure 3.2 Flowchart research methodology for design and simulation.

3.5 The Step by Step the Filter Design Using HFSS Graphical User

The instructional guideline follows to use the HFSS software is (Lawrence, 2012; Lee, 2015). This section presents the bandpass filter design step by step upon using the HFSS graphical. Design the bandpass filter includes two of main steps and each of these steps consisted of several topics as explained below.

Step number (1): The setup required to design any model covers the following basic topics:

3.5.1 Launch HFSS

Firstly, create a copy from the shortcut of the HFSS application on the desktop then store it inside a new folder. The next is to double-click the HFSS icon to launch the application. If the application does not ready, click file, and select new. The project manager window will appear, if not, click view to enable it.

3.5.2 Set Tool Options

This setup is under the tools option menu and started as follows:

Click tools > options > HFSS options. The HFSS options dialogue box will appear. On the general tab confirm all the assignment options are selected then close the dialogue box by click ok. Figure 3.3 shows the section of the HFSS options dialogue box.

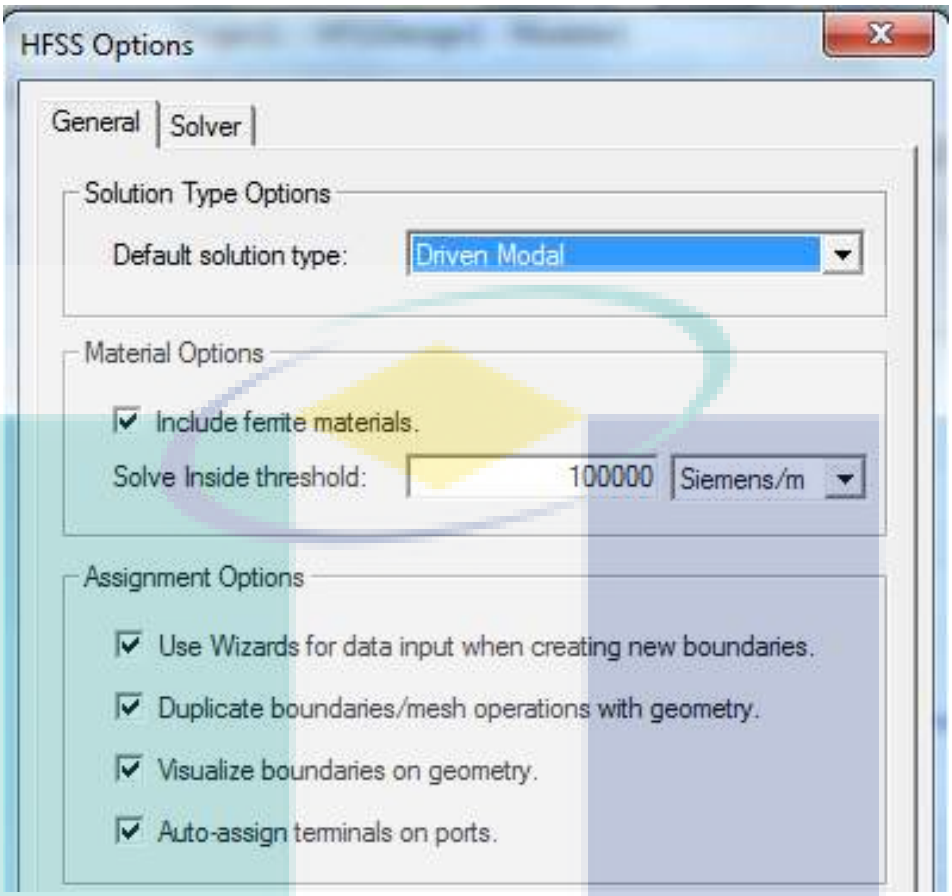

Figure 3.3 The section of the HFSS options dialogue box.

Click tools > options > modeler options. The modeler options dialogue box will appear. On the operation tab, select automatically cover closed polylines. On the drawing, tab checks edit properties of new primitives and click ok.

3.5.3 Insert HFSS design

The icon below represents the insert HFSS design (IHd) option. The next step is to expand the project tree, if (IHd) presents, then rename and save the project, if (IHd) is not there, click the (IHd) icon in the HFSS launch to include it,

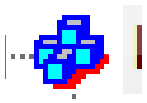

The IHd icon

3.5.4 Set the Model Units

The model units must be defined before starts the design. On the toolbar, click modeler > units. Then the set model units dialogue box will appear, select in (mm) and click ok.

3.5.5 Set the Solution Type

To specify the design solution type; On the toolbar, click the HFSS > solution type. Then, the solution type dialogue box will appear, then select the driven terminal and click ok.

Step number (2): The HFSS design environment has many features and the users can create the desired model upon using the following steps:

1. To create the model, select the 3-D solid modelling action to design the device using the primitive's shapes such as cylinders and boxes.
2. To create the rest of the filter circuit, select boolean operations and duplicate the filter circuit around the z-axis.
3. Create plots in cartesian co-ordinates (i.e. xy, xz, yz).
4. Set the analysis setup and sweep option to analyse the model.
5. Assign the boundary and excitations for all the filter circuit components and assign the wave ports and the terminal lines for the feed pin.
6. Avoid field overlays to plot electromagnetic fields.
7. Check the validates of the model.
8. Analyse the Model
9. Add the 2-D and 3-D field plots for the data results.

3.6 Create of 3-D of the Filter Model

The 3-D model of the microwave bandpass filter circuit is designed to includes some of the individual geometrical components and these components could be duplicated

to achieve the symmetrical design. Then an air body is enclosed all the filter components of the model. The microwave bandpass filter was designed by click on the toolbar and choose the desired shape followed by editing the positions and shapes from the command tab windows (Flanner, 2011; Sun, 2011). Then enter the data of the specific dimensions of the circuit components (e.g. width, height, and radius). Upon using the primitives such as cylinders and boxes to create the model, the filter components are listed in Table 3.1. The dimensions were edited upon the performance of the designed model, it can be edited from the command dialogue windows of the software to realize the desired high-performance for each run need to repair the circuit dimensions.

Table 3.1 The component of the designed microwave bandpass filter system.

NO.	The designed part	The Number	Assigned material
1	Air body (enclosure contains the filter)	1	Vacuum
2	Feed1 (Coax outer diameter)	2	Vacuum
3	Feedpin1 (Coax inner diameter)	2	Perfect conductor
4	Substrate ($LaAlO_3$)	1	Dielectric material
5	Ground plane	1	Perfect conductor
6	Resonators (lines)	4	Perfect conductor

The first part is the enclosure air body which includes the whole filter circuits, while the rest parts designed with duplicate mode as illustrated before. To create rest of the model using duplication mode. The x-y coordinates center of the filter was assigned at the top center of the substrate. However, the duplicate mode can make a symmetrical and uniform circuit, this stage is very important and would save the time and gain the accuracy. The internal components of filter are almost through with the drawing of the model is could be duplicate simply as follows;

Click edit > select > objects. Then HFSS will enter the object-selection mode.

Click edit > select > by name. The select object dialog box will appear. Then select the following objects as illustrated in Table 3.1 (i.e. Feed1, Feedpin1 and Resonators L1, L2) and click ok. To create the rest of the filter circuit, from the toolbar click on edit select Boolean operation to duplicate the filter circuit around the z-axis.

Click edit > duplicate > around axis. Then, the duplicate around axis dialogue box will appear, the select around z-axis, and click ok.

3.7 Analysis Setup of the Model

This section contains the significant topics such as select the solution setup, frequency sweep, analyse (check) the bandpass filter validation, review the solution data, review the profile panel, review the convergence panel, review the matrix data panel, review the mesh statistics panel, create report for the simulation results, create S-Parameter Vs frequency, apply trace to the existing plot, change plot scale, create field overlay, and finally modify plot attributes.

3.7.1 Set the Solution Setup and Frequency Sweep

On the project manager window make the right-click on analysis and select add the solution setup. Then the solution setup dialogue box will appear, and set the fields tab. The setup1 appears under analysis, then set the frequency solution and the adaptive solutions in the solution setup dialogue box and select the parameters and click ok.

On the project manager window make click on analysis to expand and click right on setup 1, then select add frequency sweep. The frequency sweep window will appear, then select fast, then edit the fields of frequency setup, select frequency linear, the start and stop frequencies as shown in Figure 3.4, then save the project by click ok.

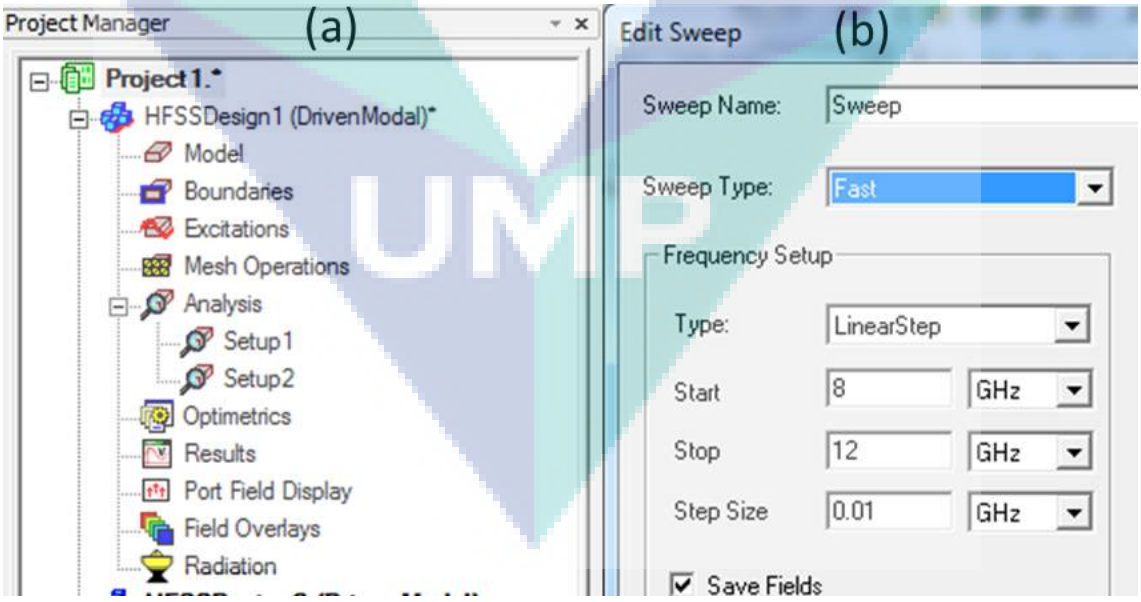

Figure 3.4 (a) The project manager window, (b) Frequency setup dialogue box.

3.7.2 Analyse the Bandpass Filter

The model of the project must pass the validation checklist by the software to confirm the construction is completed and the assignment is perfect before analysing process. On the toolbar click HFSS then select validation check. The validation check dialogue box will appear, if the project is correct the messages will appear with green colours for all the steps and the next step can proceed, if not the massages will warnings and show the specific error is assigned with red colours, the action is come back and solve the problem see Figure 3.5 (a) and (b), then click close. Then click HFSS from the toolbar and select analyse all, the software HFSS will run the simulation and solve the design, from the messages manager the warnings will appear the simulation process is completed. The solutions of data results can explore the for the designed project, from the toolbar click HFSS, then select the results and move to create terminal data report for the simulation results, then select rectangular plot.

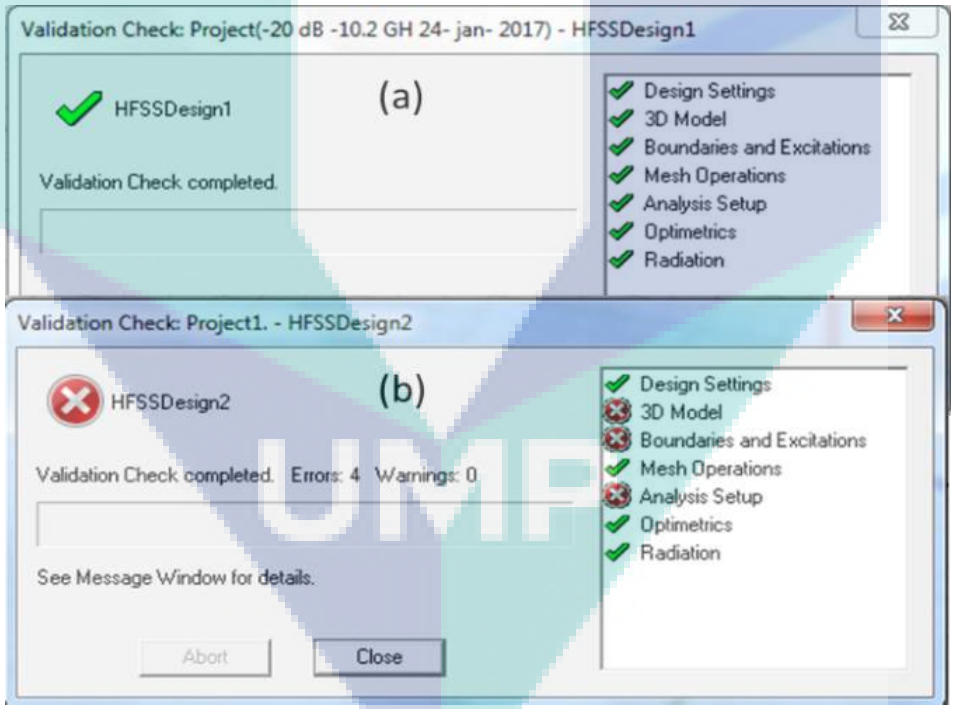

Figure 3.5 The validation checklist by the software, (a) project is correct, (b) project is not correct.

3.8 Preparation of HTS YBCO

In the present work, the materials in their original forms were used completely without any purification process. Materials such as Poly (vinyl pyrrolidone), PVP [Mw = 1,300,000 g/mole], and Poly (vinyl pyrrolidone), PVP [Mw = 160,000 g/mole], were obtained from Aldrich. Yttrium (III) acetate tetrahydrate [powder $Y(OOCCH_3)_3.4H_2O$, 99.9% (REO)], Barium acetate [crystalline $Ba(OOCCH_3)_3$, ACS 99.0%] and Copper(II) acetate monohydrate [powder $C_4H_6CuO_4.H_2O$] were purchased from Alfa Aesar. The commercially supplied solutions, Methanol (CH_4O), Acetic acid ($C_2H_4O_2$) and Propionic acid ($C_3H_6O_2$) of purity (99%) were used. The calculated amount of Ethyl cellulose (E.C, 10 *wt*. %) and α-terpinol (α: T, 18 *wt*. %) solutions were prepared in the laboratory.

3.8.1 Preparation of HTS YBCO by Sol-Gel and Solid-State Method

Figure 3.6 shows the main steps followed to prepare the YBCO samples using solid-state reaction method. The samples were prepared by mixing and dissolving 4.0 g of Y-Ba-Cu acetates powder in 25.0 ml of propionic acid at stoichiometric ratio of 1:2:3. The propionic acid was able to dissolve metallic acetate (Cui et al., 2006; Duarte et al., 2014). The solution was stirred at room temperature in a covered beaker for 12 h. It was then dried in an oven up to 200 °C for 3 h. The dried powder was grinded using a mortar and pestle before it was transferred to the box furnace (Nabertherm, 30-3000 °C) and proceed to the first heat treatment from the room temperature up to 500 °C for 3 h at a heating rate of 50 °C/h. The second heat treatment (sintering) was performed to produce the single pure structure of YBCO. It was performed in a tube furnace (Nabertherm, 30-3000 °C). Upon grinding process, the samples were heated and cooled from the room temperature up to 900 °C for 4 h at a heating rate of 250 °C/h. In the third heat treatment step, the sample powders were then grinded and weighted about one gram using sensitive balance. Then each 1 g of powder was pressed with force of 9 ton to form bulk plate samples of 10 mm in diameter and 1 mm thickness. Then, the samples were annealed at 250 °C/h heating rate from room temperature up to 950 °C for 4 h in the presence of oxygen. Finally, the sample plates of YBCO were subjected to Meissner effect to verify the superconductivity of these prototypes.

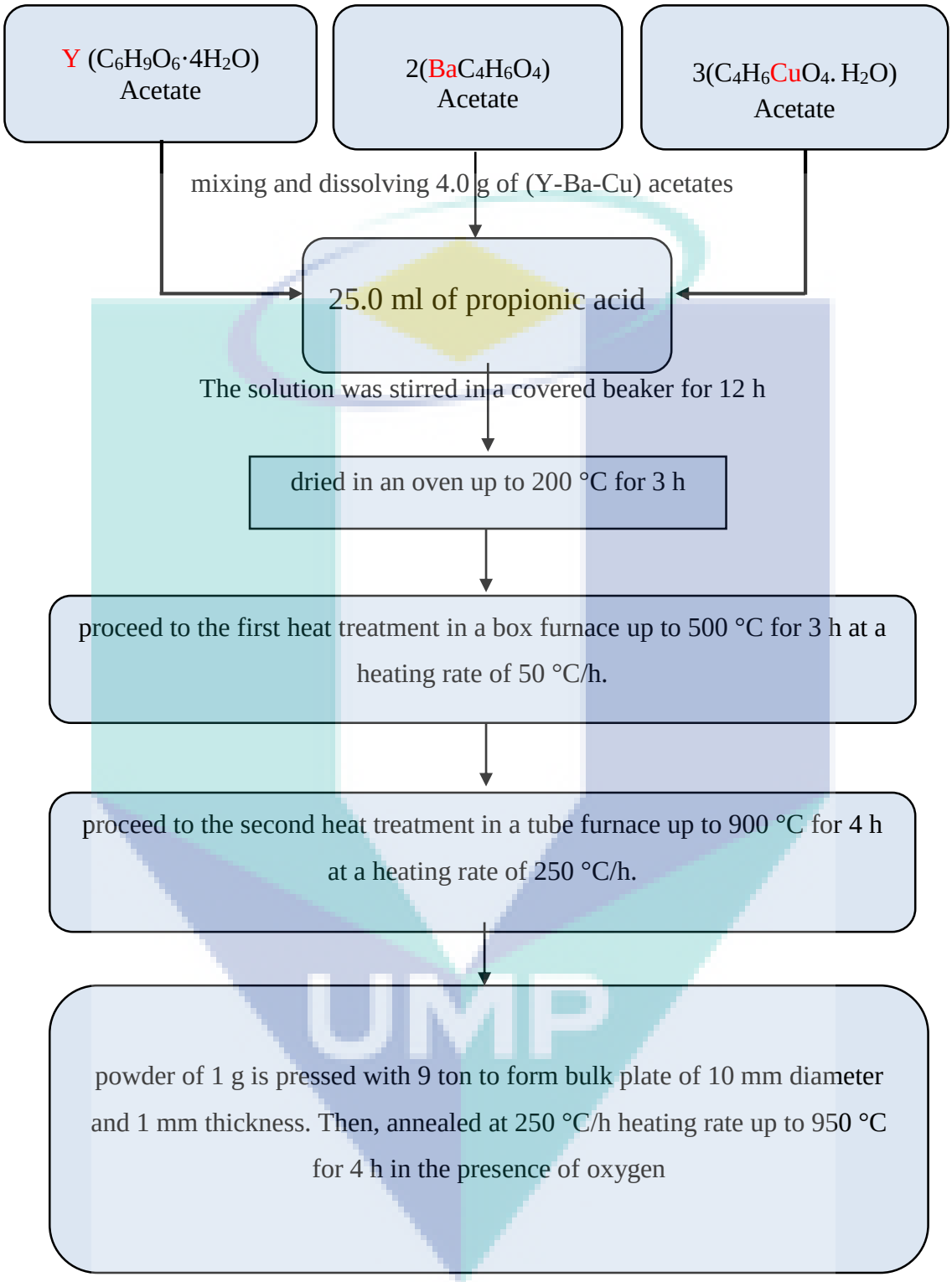

Figure 3.6 The main steps followed to prepare the HTS YBCO samples using sol-gel and solid-state reaction method.

3.8.2 Preparation of HTS YBCO via Electrospinning Technique

Figure 3.7 shows the procedures of sample preparation using, sol-gel method, electrospinning process and heat treatments. The samples were prepared via mixing the components of Y-Ba-Cu acetate with a stoichiometric ratio of 1:2:3 molar mass among acetate. Samples of different weight ratios (between Y-Ba-Cu acetate to polymer concentration solvents) were prepared. In addition, solutions with different molecular weight of PVP polymer (Mw = 1,300,000, 160,000 g/mol) were used to produce the final precursor solution. Propionic acid has been successfully utilized to dissolve the metal acetate (i.e. Y, Ba and Cu) (Cui et al., 2006; Duarte et al., 2014). Acetic acid is extremely important to sidestep hydrolysis of the polymers (Duarte et al., 2014; Shen et al., 2013).

Furthermore, a stable solution can be created from an acidic environment, thus avoiding the hydrolysis of the sol–gel precursor. Methanol has been used to dissolve the polymer as well (Duarte et al., 2014). The precursor solutions were made by dissolving the amounts from 2 g to 4 g of Y-Ba-Cu acetates in 10 ml of propionic acid. The solutions were stirred for 12 h. The polymer solutions were produced by dissolving the weights from 1 g to 5 g of PVP polymer in 10 ml of ethanol. The sol-gel solutions were produced from the mixture of PVP polymer, precursor solution and 5 ml of acetic acid then stirring for 12 h. The polymer was added to maintain the nanostructure shapes and to adjust the viscosity (Cui et al., 2006; Duarte et al., 2014; Li & Xia, 2004). The solution viscosity was controlled by adjusting the amounts of polymer and solvent. Different weight ratio and solvents quantity could change the viscosity and lead to get new results. Both viscosity and conductivity were determined to be consistent during the electrospinning process (Cui et al., 2006).

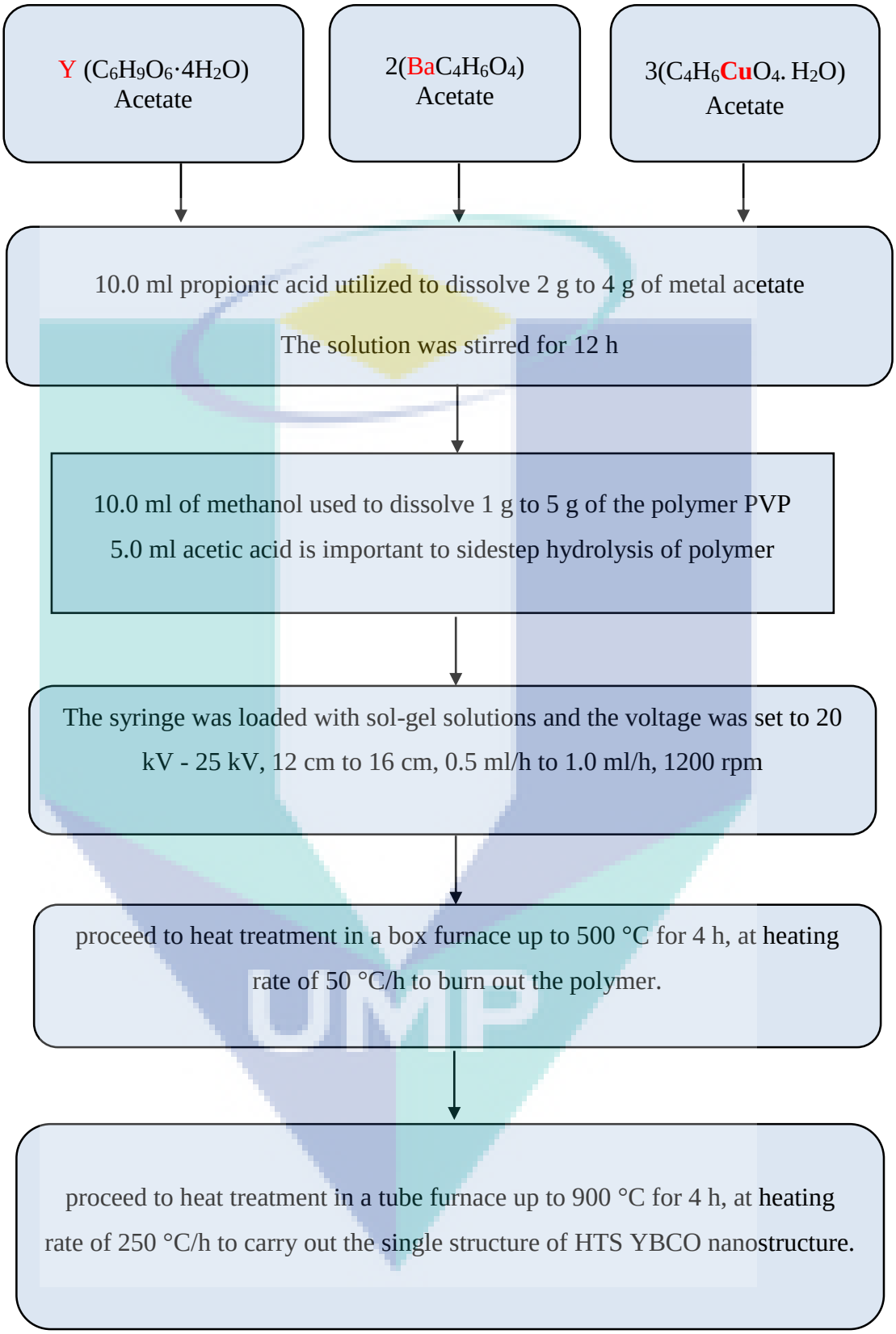

Figure 3.7 The procedures of HTS YBCO samples preparation using sol-gel solution, electrospinning process and heat treatments.

A typical electrospinning process involves the usages of 5 ml syringe with 14 cm diameter, stainless steel needle (20 gauge), 10 cm diameter ground collector (30 cm length, stainless steel, and controlled speed), high voltage power supplier and controlled injection pump (Li & Xia, 2004; Nirmala et al., 2014; Wu et al., 2012). The syringe was loaded with sol-gel solutions and the voltage was set from 20 kV to 25 kV. The tip collector distance was adjusted to range between 12 cm to 16 cm. Also, the flow rate injection was set to vary between 0.5 ml/h to 1.0 ml/h and the collector speed was adjusted to 1200 rpm. The electrospun YBCO samples were deposited on a flat LaAlO3 (100) substrate and an aluminium foil. The electrospinning process was conducted at room temperature in a closed environment. All electrospun samples were placed in a closed desiccator for drying, vaporization of remained gasses and stabilization for 48 h.

The heat treatment process was divided into two steps one to burn out the polymer and the second was to carry out the single structure of HTS YBCO nanostructure. The electrospun samples were firstly transferred to the box furnace (Nabertherm, 30 °C - 3000 °C) and heated from room temperature up to 500 °C for 3 h at a heating rate of 50 °C /h. The second heat treatment was performed in the tube furnace (Nabertherm, 30 °C - 3000 °C) after grinding the powder. The samples were heated from the room temperature up to 900 °C for 4 h at a heating rate of 250 °C /h. The samples were then heated up by 25 °C /h from room temperature to 950 °C for 3 h in the presence of flowing oxygen. The samples powder was undergoing two procedures of heat treatments are followed by grinding the to yield the desired single structure of YBCO.

3.9 Characterization and Analysis of HTS YBCO

The solution viscosity and conductivity were measured by using high-resolution viscometer (Brook Field, model: LVDV -11+P) and digital conductivity meter, respectively, at room temperature. The samples were transformed from the electrospun mats to the final nanostructure could be clarified by the thermal analysis data. The thermogravimetric analyser (Mettler Toledo, TGA/DSC) was used to examine the thermal analysis of the electrospun (Y–Ba–Cu acetates) samples. The data of Thermogravimetric Analyzer (TGA) and the Differential Scanning Calorimeter (DSC) curves versus temperature for YBCO nanostructures mats, were obtained.

3.9.1 XRD Analysis

The crystal structure of the synthesized samples was examined using X-ray diffractometer (Rigaku, model: Miniflex II, Cu Kα radiation, λ = 0.15406 nm) see Figure 3.8. The operating conditions were 30 kV and 15 mA. X-ray is a high energy electromagnetic wave and it has a very short wavelength, by which it can pass through any materials that are opaque to light (Attwood & Sakdinawat, 2017). This property of X-rays due to their wavelength is about few nanometres ranged from 0.01 to 10 nm, which includes most of the crystals lattice spacing. Therefore, it is useful technique and used widely to analyse the crystal lattice structure, strain, phase identification, unit cell dimension, average crystallite size and atomic spacing in the crystal lattice (WALI, 2016).

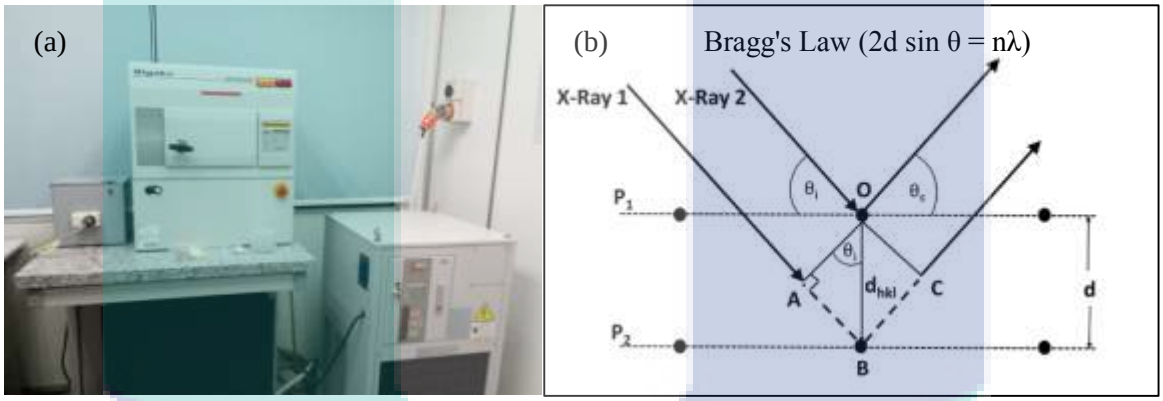

Figure 3.8 (a) The X-ray diffractometer (Rigaku, model: Miniflex II), (b) The diagram for the X-ray diffraction indicating the angle θ and the atomic spacing d.

The diffraction patterns measurements of the samples were analysed at the angle 2θ from 5° to 80° with a count speed of 1° per minute. The sample was grinded to a fine powder and the powder was placed on a glass sample holder (10 × 10 mm^2) inside the diffractometer. The diffraction pattern showed the miller index's peak after the reflection of X-rays and the interference between the scattered radiations emitted from the sample powder. Each indicated peak obtained from the diffraction patterns could be seen under the index that is corresponding to the lattice atomic d-spacing. The d-spacing between the atomic layers of any structures can be determined by Bragg's Law (2d sin θ = nλ), where λ represents the X-ray wavelength and θ is the diffraction angle. This law simply relates the scattering angle with the d-spacing between the parallel miller indices (hkl) of the cubic crystalline sample. Hence, the crystal unit cell dimension can be calculated by substituting the d-spacing and the miller indices in the cubic cell equation $(1/(d_{hkl})^2= h^2/a^2+k^2/b^2+l^2/c^2)$,

where d_{hkl} is the distance between parallel (hkl) and a, b, c are the dimensions of the crystal unit cell (Callister & Rethwisch, 2012).

The average crystallite size L (nm) for the samples were calculated from XRD data using Scherrer formula equation ($L = K \lambda / \beta \cos \theta$) (Salama et al., 2015). Where K ~ 0.9, is the constant depending on the crystallite shapes, $\lambda = 0.15406$ nm, is the wavelength of x-ray, β = (FHWM) in radians unit, is the full width of the dominant diffraction peak at the half of the maximum heights from the XRD data and θ, is equals to the half of Bragg angle 2θ from the diffraction profile must be in degrees.

3.9.2 Field Emission Scanning Electron Microscopy (FESEM) Analysis

The morphology and size of the fabricated nanostructures were observed and investigated by Field Emission Scanning Electron Microscope (FESEM, JEOL, model: JSM–7600) see Figure 3.9. The operating voltages were ranging from 3.0 kV- 10.0 kV. FESEM is a powerful characterization tool. It can be employed to explore the shape and size of the nanostructures as well. The resolution of FESEM is significantly higher as compared to that of optical electron microscope (Wijeyesekera et al., 2016). FESEM operates at high power by which it can focus highly. The highly active electrons emitted from the surface source accelerate in a very strong electric field and pass through the electronic lenses. The electronic lenses are focused in a narrow energetic electron beam, thus exciting the target object.

Upon striking the object of specimen, the secondary electrons will be emitted from the target and this process is captured by a detector (Goldstein et al., 2012). The procedure to investigate the morphologies of the sample surface, shape, size and roughness, was to prepare the samples in a powder form. The samples (in powder form) were coated with a thin layer via sputtering the top side of the double sided adhesive tape. The lower side, however, was connected to the sample holder platform to prevent charge distribution and falling during the FESEM analysis. Finally, the samples were loaded to the chamber of the measurements unit and examined at different operation voltages, multi zooms and directions (i.e. the sample can be rotated inside the FESEM unit).

Figure 3.9 The (FESEM, JEOL, model: JSM–7600) unit used to analyse the morphology of the samples.

3.9.3 Transition Temperature (T_c)

The transition temperatures (T_c) of the samples were determined using an AC Susceptometer, consisting of a closed cycle of liquid helium refrigeration system (Cryo Industry model REF-1808-ACS). Figure 3.10 shows the AC susceptibility technique used elsewhere (Mohajeri, 2016; Nur-Akasyah et al., 2017) to find the transition temperatures of YBCO superconductors. The samples for AC Susceptibility measurements were in the bar-shape dimension of 2×3×6 mm^3. These bars were produced by pressing the materials in a stainless-steel die and subsequently sintering at 950 °C in the presence of oxygen for 6 h. The susceptibility data of the samples were collected at temperature in between 20 and 130 K. The frequency of the AC signal setup was fixed at 295 Hz. The applied magnetic field was H = 5 Oe. The T_c values of YBCO samples were measured after the samples cooled to 20 K in vacuum of 10^{-4} mbar. The measurements were conducted for all the YBCO samples after cooling the samples down to 20 K. The critical temperatures of samples were obtained by heating the samples from 20 K to 130 K at a heating rate 1 K/min.

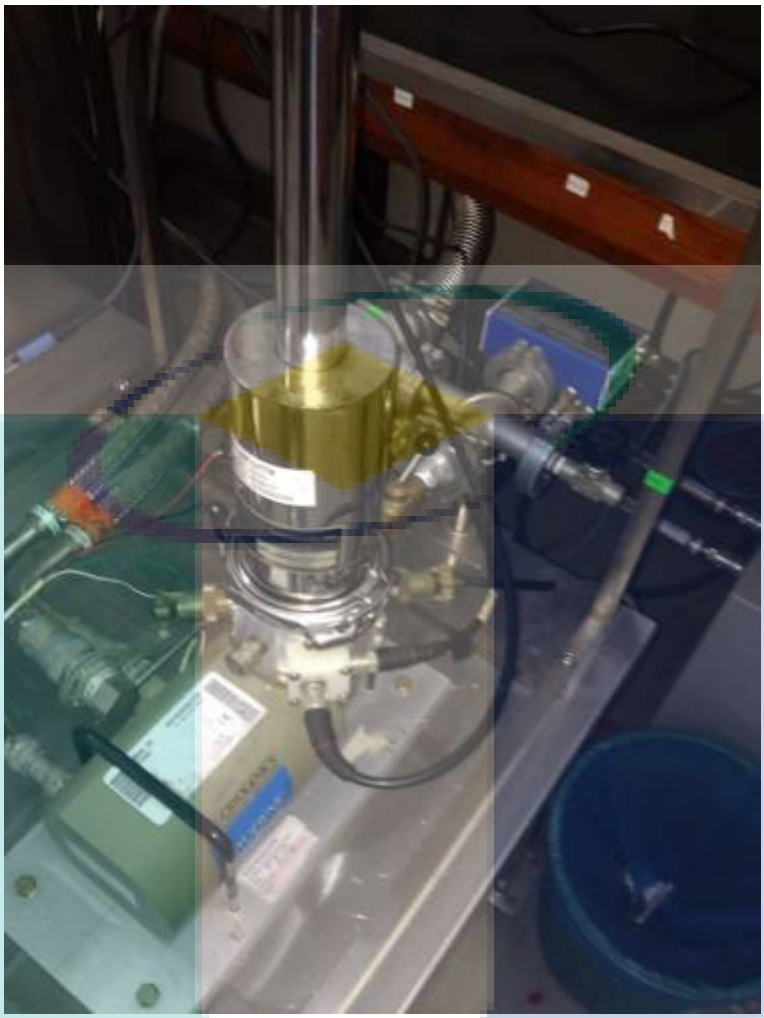

Figure 3.10 The AC Susceptometer, consisting of a closed cycle of liquid helium refrigeration system (Cryo Industry model REF-1808-ACS) used to test the superconductivity transition of the samples .

3.9.4 BET Surface Area Measurements

The surface areas for both bulk and electrospun samples were measured using ASAP 2020 analyser (Micrometrics, USA). The name BET was generated from the names of the inventors, i.e. Brunauer, Emmett and Teller (BET) (Sing, 1985; Thommes et al., 2015). BET is a standard method used to measure internal surface area, pore size and pore volume. The theory assumes that adsorption happens upon forming multilayer spaces that are infinite in number under the saturation pressure. These multilayers expand and adsorb all molecules ultimately (Klobes et al., 2006). The hypothesis of BET surface area measurements can be explained as follows (a) a small amount adsorbed of the gas molecules upon the layers of the powder without interaction between layer and gas (b) then

each adsorption layer has follows Langmuir theory. Then the surface area measurements as well as the pore size, the nitrogen adsorption/de-adsorption isotherms process at 77 K with relative pressure (P/P_o) from 0.05 - 1.0 can be employed.

The International Union of Pure and Applied Chemistry (IUPAC) have been classified the adsorption isotherms depending on the pore types into four; Type I (cylindrical pores), Type II (pore blocking), Type III (plate/slit type pores), Type IV (bottleneck pore type) Type V (is uncommon) and finally Type VI (stepwise multilayer) (Thompson et al., 2006) (see Figure 3.11). The degas temperature of YBCO samples was found at 400 °C. The sample tube was filled with the suitable amount ~ 300 mg of sample powder and firstly degassed for 7 h for purification purpose, then the sample tube was shifted to the testing channel for nitrogen adsorption after immersed into liquid nitrogen for several minutes. The adsorbed nitrogen molecules can be quantified by desorption process. The BET surface area analysers are used widely for the measurements of gas adsorption and desorption into porous and solid material. Nitrogen, carbon dioxide and argon gasses are commonly used as adsorbent gases at absolute temperature (273 K).

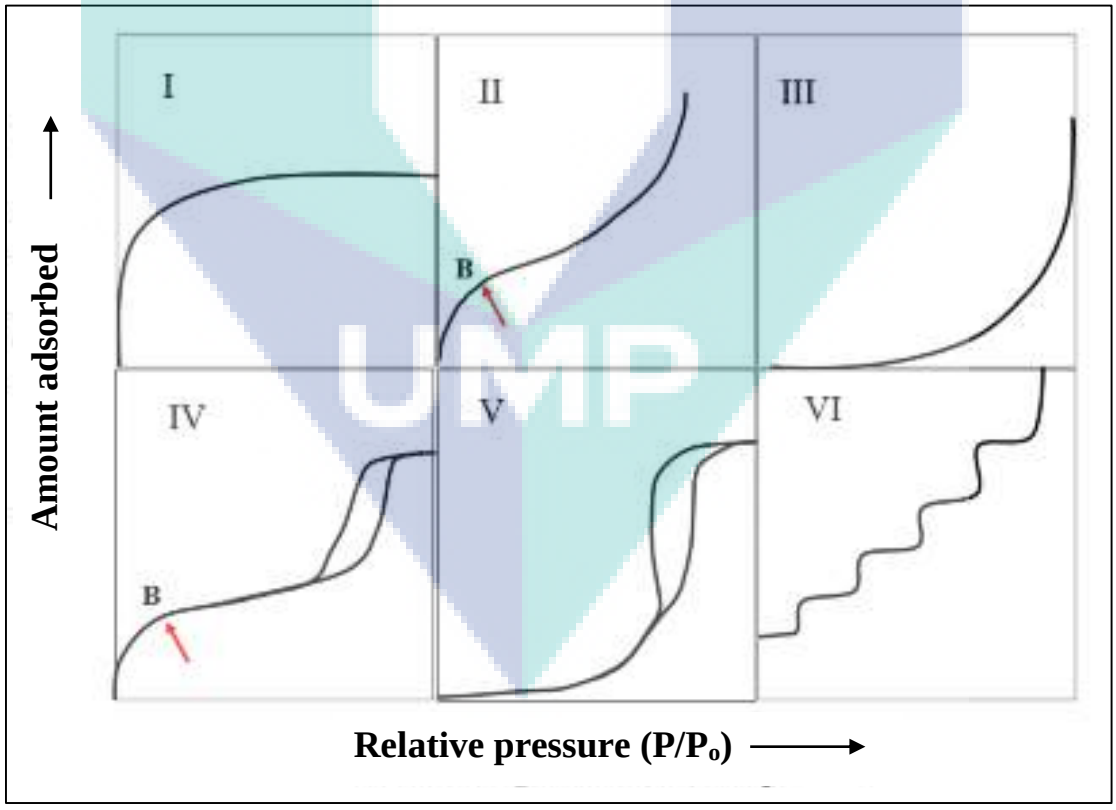

Figure 3.11 IUPAC classification of adsorption isotherms

3.10 Deposition of HTS YBCO Thin Film

The thin films of YBCO nanostructures were deposited on (10×10 mm^2) $LaAlO_3$ substrate via electrospinning process and spin coating procedure.

3.10.1 Electrospinning Deposition

Thin films of YBCO nanostructures were deposited on the roughness side of $LaAlO_3$ substrates (10 × 10 mm^2) by the electrospinning process. The thin films were deposited by fixing the substrates properly on the rotating collector. The electrospinning process was conducted in a closed environment at room temperature with humidity less than 50%. The electrospun thin film samples were dried in the closed desiccator for 48 h. The samples were then heated by using the box furnaces (Nabertherm, 30 - 3000 °C) up to 500 °C for 3 h at a heating rate of 50 °C/h to burn out the polymer. The last procedure was repeated for several times until reaching the desired thickness of thin film was attained. The second heat treatment, i.e. sintering process was performed by using a tube furnace (Nabertherm, 30-3000 °C). Samples were heated from room temperature up to 900 °C for 4 h at a rate of 250 °C/h. Subsequently, they were undergone heating at 25 °C/h up to 950 °C for 3 h in the presence of oxygen.

3.10.2 Spin Coating Technique

The spin coating technique was adopted in this work to produce the desired thin films from the paste of the of YBCO superconductor powder, which have been prepared by solid-state and electrospinning methods. The coated paste is a standard method and it was stated elsewhere (Muralidhar et al., 2007; Wali et al., 2014). A uniform suspension of the YBCO powder was prepared by dissolving ~300 mg of YBCO in α-Terpineol (α: T, 18 wt.%) and ethyl cellulose (E.C, 10 wt.%) solutions in the ratio of YBCO: α-T: E.C (1: 4.05: 0.5) and followed by stirring in an ultrasonic bath. The above suspension was spun coated on $LaAlO_3$ substrate and dried using heated stirrer for several times followed by heating treatment and etching process to prepare the device.

3.11 Fabrication of Microwave Circuit via Etching Process

The designed microwave filter circuit was transferred from the HFSS software to AutoCAD for printing on a photo laser paper using a laser printer (Ellsworth, 2011). The printed photo laser paper was then placed on the YBCO film of the $LaAlO_3$ substrate and

transferred to a hot-pressed at a temperature of ~80°C. The films were then etched using ferric chloride solution and subsequently annealed at 950°C for 4 h in the presence of flowing oxygen. The device fabrication process is schematically shown in Figure 3.12, describes the representation of the heat-transfer paper of the printed circuit on the thin film step by step. The etching process was applied to remove the unwanted parts of the thin film (leaving only the required designed circuit). The same heat treatment process was conducted to increase the stability of the printed circuit, to increase the oxygen content and to remove the solvent and other impurities that might adhere to the sample during the etching process. The second deposition was then made to produce the thin film of the ground plane for the microwave filter samples. Finally, heat treatment was performed on the samples (in oxygen atmosphere) to increase the oxygen content. High oxygen content would increase the performance of YBCO.

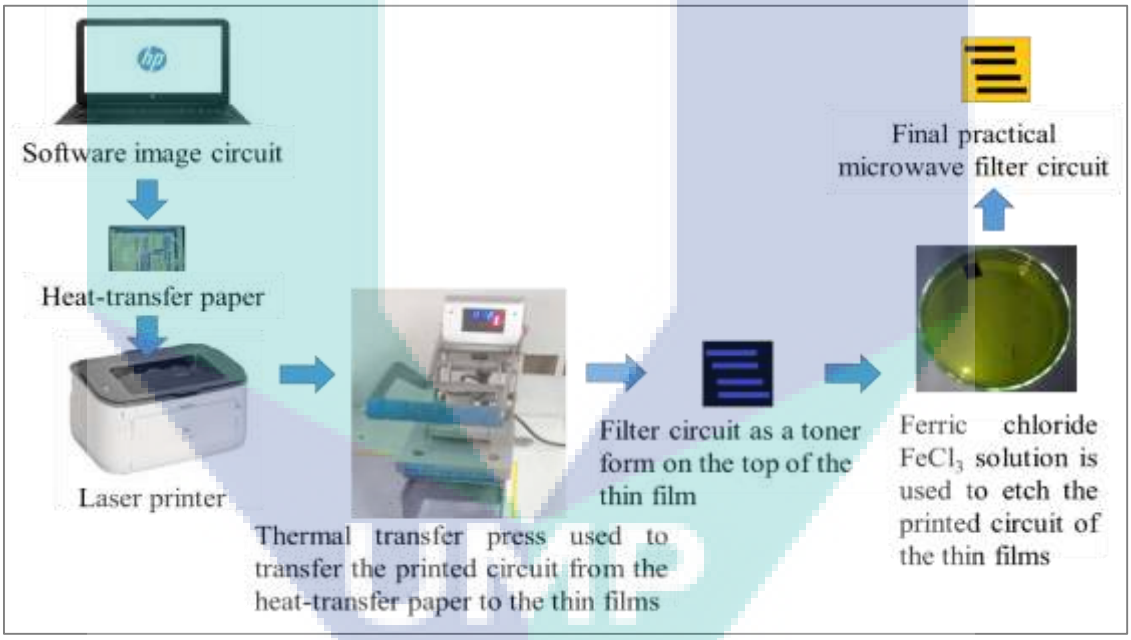

Figure 3.12 The graphic flow chart displays the three steps folowed to transfer the filter circuit from the software to the thin film of the sample using the heated transfer paper and the toner.

3.12 Measurements and Testing of Microwave Device

The performance of the HTS YBCO filters were tested using the Agilent E5071C vector network analyser (VNA). The measurements were carried out at 77 K with liquid nitrogen and at 300 K room temperature (Jing et al., 1994) for the frequency ranging from 5 to 15 GHz. To eliminate all the systematic errors, both of VNA ports were calibrated

before the measurement process. Both the transmission S_{12} and reflection S_{11} coefficients were recorded and will be compared with the simulated data from HFSS software. Figure 3.13 shows the schematic diagram of the device placed in the sample holder. The samples were connected carefully to the SMA connectors using the sample holder. Aluminium plate was used to connect the sample to the ground plane of the filter to provide perfect electrical and thermal conductance and to facilitate the replacement of sample after each test easily. The sample holder was designed to be symmetrical with sample contact pads. It was connected directly to the two VNA ports.

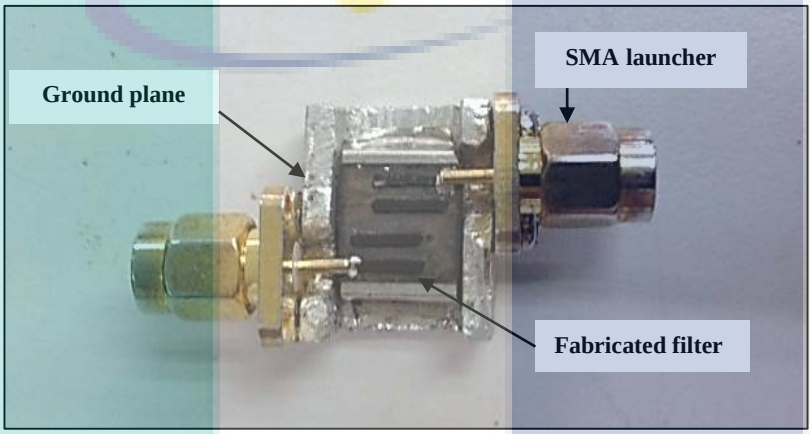

Figure 3.13 The layout of the bandpass filter with four couple parallel line.

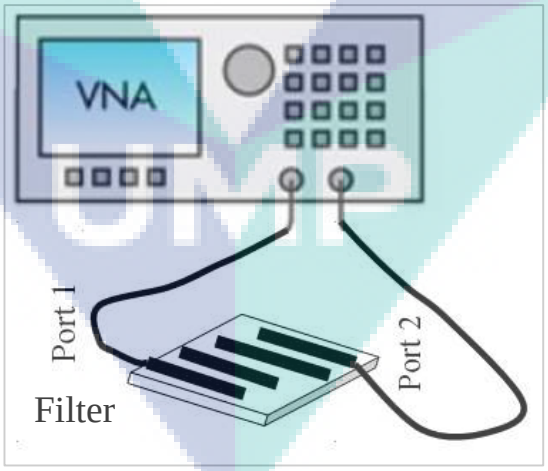

Figure 3.14 The circuit diagram of VNA and Filter

Figure 3.15, shows the experimental setup for transmission and reflection coefficients measurements of HTS YBCO filter, VNA, and liquid nitrogen mini Coolant system.

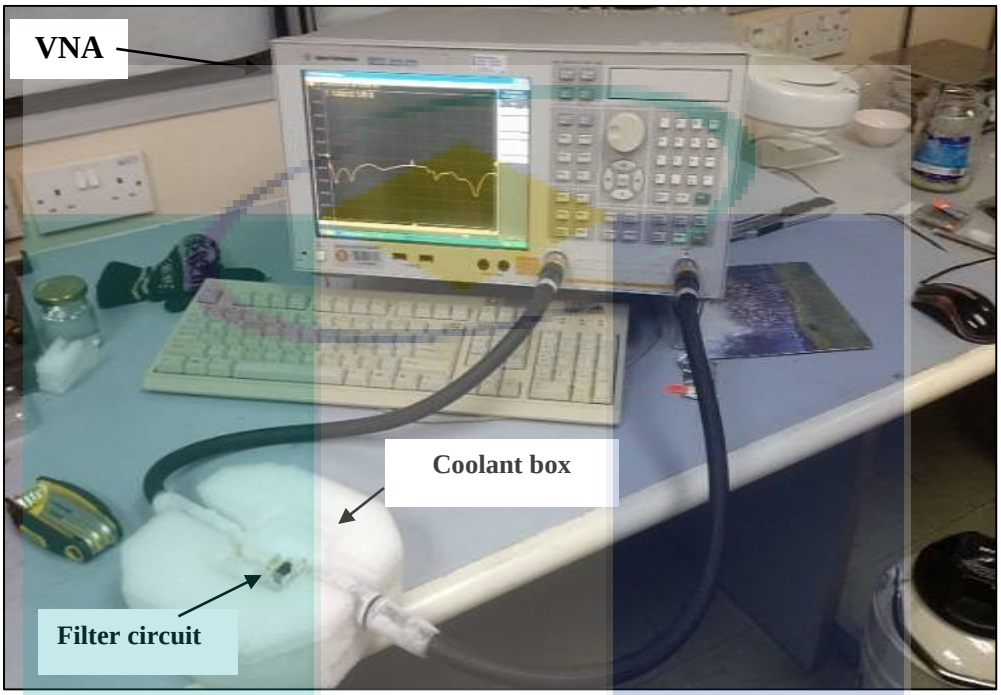

Figure 3.15 Experimental setup for transmission and reflection coefficients measurements of HTS YBCO bandpass filter.

3.13 Summary

This chapter has described the research methodology used to study the potential applications of superconducting YBCO nanostructures on microwave filter circuits. In general, this research consists of the design, simulation and experimental parts. The experimental part involved the preparation of superconducting YBCO in the form of bulk plate and thin film samples. The samples were then characterized. The viscosity and conductivity of the solutions were determined by using high-resolution viscometer and digital conductivity meter at room temperature.

The Thermogravimetric Analyzer was used to perform the thermal analysis of electrospun samples (Y–Ba–Cu Ac). The data of Thermogravimetric Analyzer (TGA) and the Differential Scanning Calorimeter (DSC) curves for YBCO nanostructures mats were obtained. The samples were transformed from the electrospun mats to the final product (powder). The electrospun samples were firstly heated in the box furnaces from room

temperature up to 500 °C for 3 h at a heating rate of 50 °C/h. The second heat treatment was performed in tube furnace, whereby samples were heated and cooled from room temperature up to 900 °C for 4 h at a rate of 250 °C/h, followed by heating up to 950 °C for 3 h in the presence of flowing oxygen (25 °C/h heating rate).

The crystal structure of the samples was analysed from 5° to 85° angle with a count speed of 1° per minute by using X-ray diffractometer operating at 30 kV and 15 mA. The morphology of the samples was observed using Field Emission Scanning Electron Microscope operating at 5.0 kV. The transition temperatures (Tc) of YBCO superconducting bulk and thin film samples were measured via AC Susceptometer and the four-probe technique using a closed cycle of liquid helium refrigeration system. The BET surface areas for both thick and electrospun nanostructured samples were investigated using BET surface area and porosity analyser. The degas temperature was set at 400 °C for 7 h.

The simulation and design part of the current work involves the design and analysis of the microwave filter circuit, followed by circuit layout and simulation. The Ansoft HFSS software was used to design the microwave bandpass filter circuits. The microwave bandpass filter circuit was fabricated from the superconducting YBCO thin films prepared from solid state method and electrospinning process. Thin films of YBCO nanostructures were deposited successfully on $LaAlO_3$ (100) single crystal substrates. The paste method was adopted in this work to produce the desired thin films from the YBCO superconductor. It was used to deposit the thin film by melting the sample powders with the prepared solutions of α-terpinol (α-T, 18 wt. %) and ethyl cellulose (E.C, 10 wt. %).

The designed circuit of microwave filter was transferred from the HFSS software by using laser printer and heat-transfer paper (photo laser paper). The Ferric chloride $FeCl_3$ solution was used to etch the printed circuit of the thin films. The etching process excluded the printed circuit and removed all the thin films outside the desired circuit. The microwave filter devices were analysed to find the transmission and reflection coefficients using the vector network analyser. The HTS YBCO filter was tested at room temperature and after it was cooled down to 77 K using the liquid nitrogen mini coolant system.

CHAPTER 4

RESULTS AND DISCUSSION

4.1 Introduction

This chapter describes the outcomes of the designed microwave filter, structural characterizations, measurements of prepared YBCO samples and analyses. Firstly, the design and simulation results of the microwave bandpass filter circuit are explained. Secondly, the characterization results of HTS YBCO prepared by solid state reaction and electrospinning process, the XRD analysis for the crystal structure of the samples, the FESEM morphology characterizations of the samples, the results of transition temperatures (T_c) and the BET surface area measurements. Finally, the measurement of the microwave bandpass filters response using Vector Network Analyzer (VNA) is presented.

4.2 Design and Simulate Microwave Circuit

As explained in Chapter 3, the passive microwave filter circuit was designed and simulated using Ansoft HFSS software. The microwave filter was designed using the perfect conductors with four parallel couple lines, which were deposited on $LaAlO_3$ substrate (10×10 mm^2). The aim of this work is to develop a microwave filter circuit by using the new superconducting YBCO thin films.

4.3 Simulation Result of Microwave Filter

Figure 4.1 shows the image of the designed circuit result of microwave bandpass filter from the HFSS software. The dimensions of the designed parts of the coupled lines and coax feed of the microwave bandpass filter circuit is listed in Table 4.1. The performance of the designed filter can be summarized in terms of return and insertion losses for the selected frequency; an ideal filter should have high return loss, low insertion loss, broad bandwidth, good impedance matching and high frequency selection.

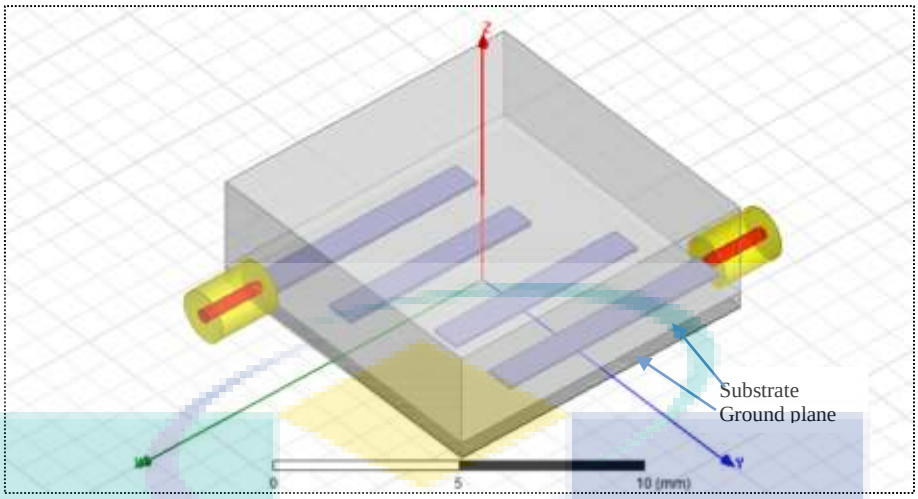

Figure 4.1 The image of the designed circuit of microwave bandpass filter results from the HFSS software

Table 4.1 The dimensions result of the designed part of the proposed microwave bandpass filter

The part	**Dimension (mm^2)**	**Height/Thickness (mm)**
Feed1 (Coax outer diameter)	0.8 (in radius)	2.0
Feedpin1 (Coax inner diameter)	0.2 (in radius)	2.0
Substrate ($LaAlO_3$)	10 × 10 (in Area)	0.5
Ground plane	10 × 10 (in Area)	0.05
L1 Resonator	7.2 × 0.9	0.1
L2 Resonator	6.2 × 0.9	0.1

Figure 4.2 presents the simulated results of the designed device using HFSS software. The simulation results display the response between the scattered S-parameters (S_{11} reflection coefficient and S_{12} transmission coefficient) and the frequency in GHz. Microwave bandpass filter was designed and simulated for the operating frequency of 10.2 GHz with 1.5 GHz broad bandwidth.

However, S_{11} results appear with some details (i.e. several peaks at the bottom of curve). This is due to filtering resonance frequency occurs at specific frequencies. So that, at the mide point of the curve interval frequency band (i.e. 9.5 – 10.9 GHz), the filter has an oscillatory behaviour (i.e. has unconstant refection coefficient S_{11}), while the filter operates well at the frequency bands 9.5 GHz and 10.9 GHz with high return losses. This unstablity is found with all bandpass filters and called the attenuation and transmission

operation and it depend strongly on the filter design. The coupling resonater lenght should be at lest equal to the half of the wavelenght of the resonance frequency or less than by an even number, if not the resonance band will not having high returen losses (as discussed in Chapter 1, page 3).

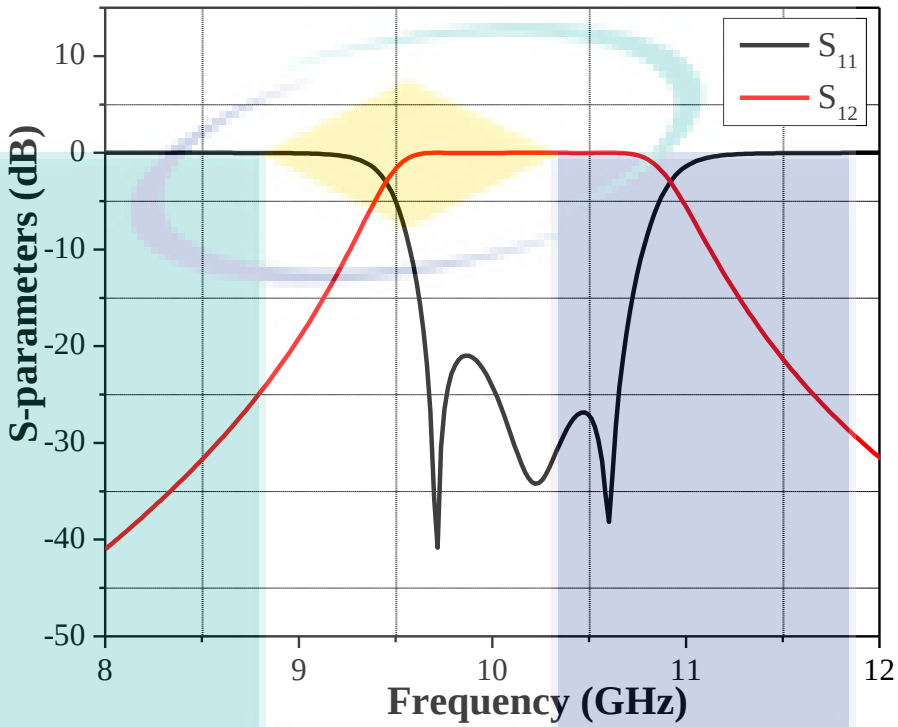

Figure 4.2 Simulation result of the microwave bandpass filter using HFSS, the plot of S-parameters (S_{11} and S_{12}) versus frequency with broad bandwidth 1.5 GHz and the frequency center 10.2 GHz

In general, the performance of a filter depends on line width, line height, coupling length, and distance between the lines (Flanner, 2011; Sun, 2011). As can be seen from Figure 4.2, the optimized filter has an operation frequency of ~10 GHz with a bandwidth of ~1.5 GHz, transmission frequency within 9.5 GHz – 10.9 GHz, return loss of > -30 dB and approximately no insertion losses. On the other hand, other authors (Kumar et al., 2014; Gupta et al., 2015; Gunjal et al., 2016) recently simulated the microwave filter using finite modelling with (5 & 4)-parallel coupled lines with a spacing < 1 mm apart using the HFSS software. These filters were located on the FR4 substrate (i.e. a composite material consisting of flame resistant woven fiberglass cloth with an epoxy resin binder) had dielectric constant of ~4.2 and thickness of ~1.58 mm. Its performance (i.e. operating frequency from 2.4 to 3 GHz, bandwidth between 0.6 and 2 GHz, the higher insertion loss

~-4.0dB, and low return loss ~-8 dB) is lower than the filter developed in the current work using HFSS (i.e. operating frequency ~10.2 GHz, bandwidth ~ 1.5 GHz, insertion loss 0 dB, and return loss ~-30 dB). On the other hand, optimization was conducted in the present work to yield a filter with high performance with wider bandwidth, high return loss for couple line distance >1 mm. In the following, the experimental results on the electrospun YBCO nanostructures and the characteristics of the microwave filter employing the above design will discussed. The properties of the electrospun YBCO particles have been compared with those of the filter fabricated using materials obtained from the conventional solid-state reaction process.

4.4 Comparison between Design Equations and Design HFSS of Filter

Table 4.2 shows a comparison between the microwave filter designed using design equations and the microwave filter designed by HFSS, both filter results are theoretical from the simulation data using HFSS. Kumar *et al* (Kumar et al., 2014) have designed microwave filter using the design equations to find the physical of the filter circuit as explained in chapter 2, the filter presented lower performance for all the given data (i.e. Fc, BW, RL and IL), especially for bandwidth (0.6 GHz) and the insertion loss (-2.2 dB).

However, filters of smallest dimension supposed to be working at high operation frequency, while the presented filter is working for lower frequency (2.48 GHz). On the other hand, Chung (Chung, 2000) designed the microwave bandpass filter with small dimensions of (30 mm^2) at operation frequency ~16 GHz, (see Table 2.1). In addition, the operation frequency is proportional inversely with filter dimensions as explained in chapter 1. "While the strip lines are much smaller than the wavelength (λ, λ/2, λ/4, etc.) at high operating frequencies. Filters based on the short line elements could be physically small"(Ghosh et al., 2014). Therefore, filters designed via the design equations could have lower performance as compared with the current result. In the same way, the researchers (Gupta et al., 2015) and (Gunjal et al., 2016) have been designed microwave bandpass filter using the design equations and simulated the model using HFSS. Table 4.2 shows the difference between the results of these works and the large dimensions used for their design as compared with the current work, (the dimensions are very large, and the performance is not high).

Table 4.2 Comparison between the platform design for bandpass filter using HFSS

Reference	Fc(GHz)	BW(GHz)	RL(dB)	IL(dB)	Platform Filter Design	Dimensions (mm^2)
(Kumar et al., 2014)	2.48	0.6	-12	-2.2	Design equation	71
(Gupta et al., 2015)	3.0	2.0	-8.0	-1.8	Design equation	480
(Gunjal et al., 2016)	2.4	0.14	-10	-4.0	Design equation	2627
This work	10.2	1.5	-30	0	HFSS	100

Figure 4.3 shows the applied magnetic field and their vectors (Ampere per meter unit) for the designed filter circuit from the HFSS software. The waves of the magnetic field are clearly transmitted throughout the whole the filter circuit components area. The vectors clearly transmitted between the lines in three dimensions.

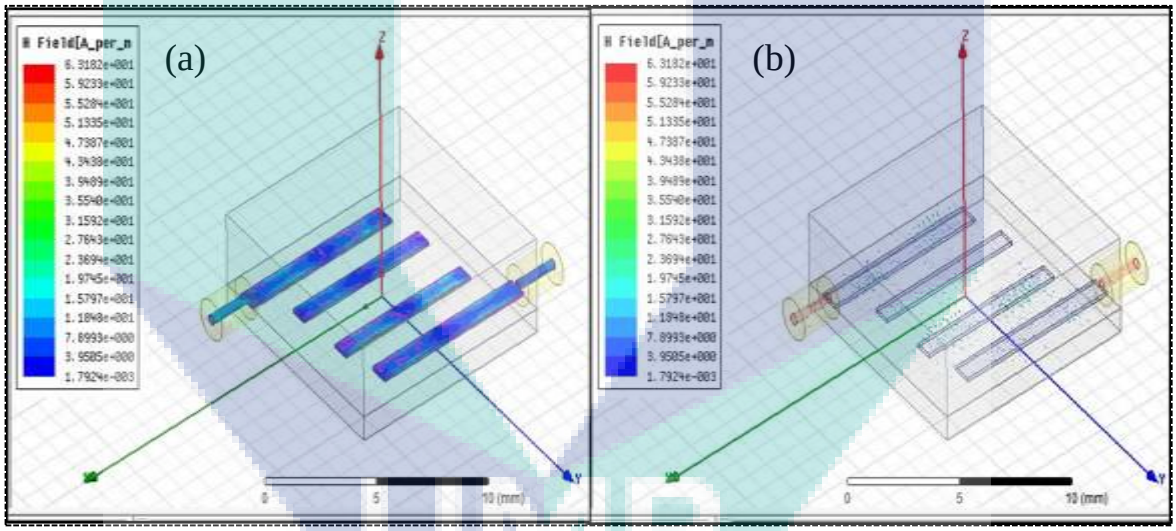

Figure 4.3 (a) The applied magnetic field, (b) The vectors of the applied magnetic field for the designed circuit.

The electric and magnetic fields are entirely dependent on the applied power voltage, while the circuit of the bandpass filter is a parallel line, then they are having an electric field between the lines (like the capacitor). And, if there is any frequently change in the applied voltage the magnetic field will be increased. Therefore, the electric field is affected the magnetic field. As well know the electric and magnetic fields are perpendicular to each other and perpendicular to their direction of propagation. In this section the HFSS software shows the two fields action on the filter circuit and the other component near the

couple lines. Figure 4.4 (a) and (b) shows the images of the components of the designed filter have affected by the electric and magnetic fields were applied at the same time (i.e. complex fields).

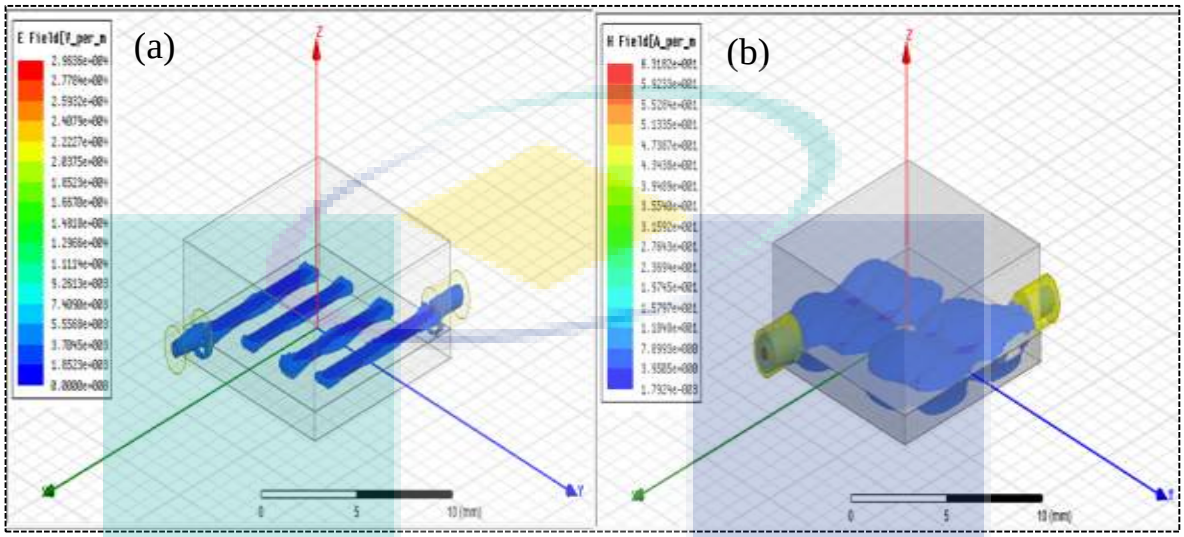

Figure 4.4 (a) The electric field, (b) The electric and magnetic fields are applied together at the same time for the designed circuit.

The image of the transferred electric field vectors throughout the whole filter circuit and the body in x-z axis and x-y axis for the designed filter are obtained in the form of short repeated video using HFSS software. The cross-section view of the filter circuit image shows the vectors of the electric field (Volt per meter unit) distributed around the filter components as shown in Figure 4.5 (a). The view from the top of the filter circuit shows the vectors of the electric filed transmitted from and around the filter components Figure 4.5 (b). The transmitted magnetic and electric fields are perpendicular to each other and they are transmitted between the lines with the resonance frequency upon the coupling resonators conditions. These resonators allow for detected and desired frequency to pass and prevent the other. As the higher frequency, the wavelength will be shorter, and it is possible to detect it using short coupled lines.

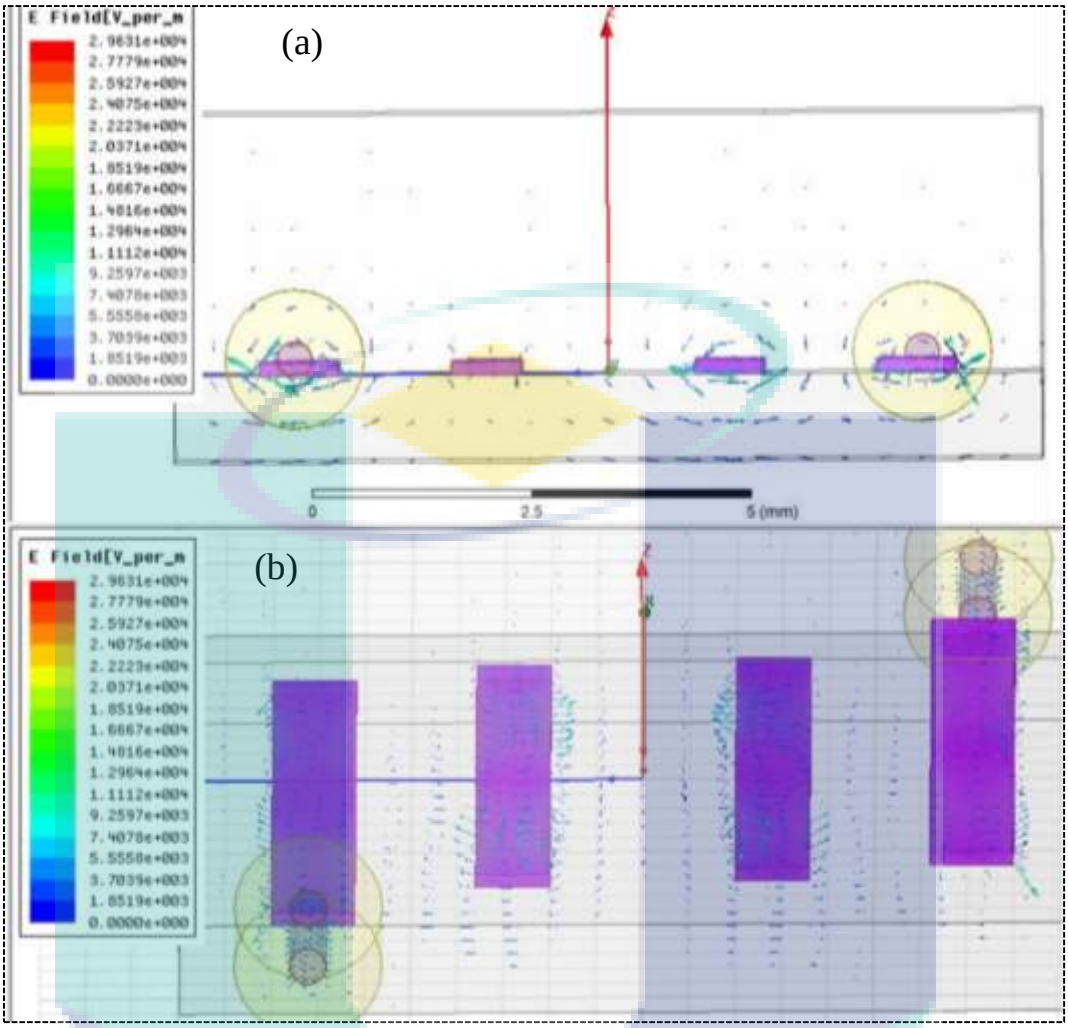

Figure 4.5 The images of the electric field vectors transmitted throughout the filter circuit (a) The cross section of the circuit, (b) The top of the circuit.

Figure 4.6 shows the mesh operation for the microwave filter circuit created by HFSS software. The mesh operation is applied to divide the for the filter circuit in to a finite element area and from these elements the software could calculate the surface resistance, the distributions of the frequency signals and then the response of the filter circuit will be tested and as the mesh operation is applied properly, the filter operation will have high performance (i.e. high return losses and broad bandwidth).

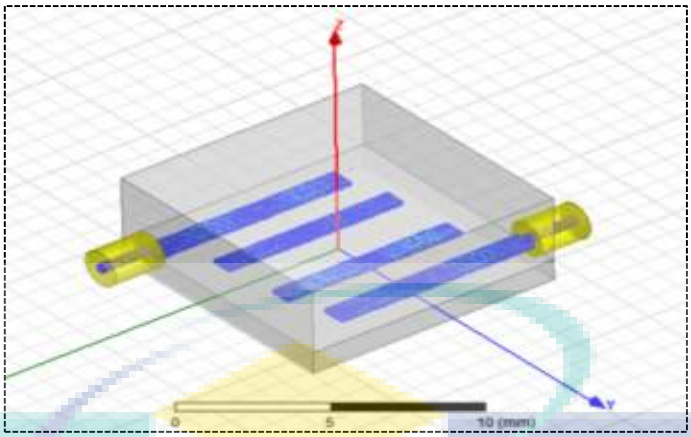

Figure 4.6 The mesh operation for microwave filter using HFSS software.

4.5 Preparation of HTS YBCO

HTS YBCO has been prepared successfully in the form of a bulk plate and thin films using solid state reaction method and electrospinning process as described in Chapter 3. This section deals with the structure, morphology, characterization measurement, and property of each sample fabricated from HTS YBCO. The samples were synthesized with different morphologies by optimizing the molecular weight of the polymer and its ratios with the precursors. Polymer of higher molecular weight and lower precursor to polymer ratio would yield solutions of low viscosity and conductivity and produce NRs and NGs morphology upon annealing. On the other hand, polymer of lower molecular weight and higher precursor to polymer ratio would result in solutions of low viscosity and conductivity. Meanwhile, NH, ANPs and NPs were produced upon annealing see Table 4.3.

Table 4.3 Morphology of the electrospun samples synthesized at different ratio of YBCO and PVP and the respective parameters such as solution viscosity and conductivity (A; Agglomerated).

Sample	**Weight ratio (g) YBCO: PVP**	**Polymer molecular weight (g/mole)**	**Viscosity (cP)**	**Conductivity (mS/cm)**	**Morphology**
1	2:1	1,300,000	100.3	162.8	Nanorod
2	2:2	1,300,000	120.4	174.2	Nanogarlands
3	4:3	160,000	175.2	184.2	Nanoparticle
4	2:3	160,000	150.9	168.5	Nanohierarchical
5	4:5	1,300,000	193.0	155.0	A. Nanoparticle
6	4:0	…	…	…	Bulk

4.5.1 Fabrication of HTS YBCO by Solid State Reaction Method

The bulk samples of HTS YBCO were prepared by solid-state method using sol-gel precursor solution as explained in Chapter 3. The bulk sample plates have been analysed to reveal the superconductivity by Meissner effect. Superconductivity was observed after the sample was cooled down to 77 K by dipping the bulk sample in liquid nitrogen. The sample was then brought outside the liquid nitrogen and placed above the strong neodymium magnets subsequently it levitates for the whole time until the temperature was raised above the critical temperature. The experiment of Meissner effect on YBCO sample above the magnet is not apparent clearly due to the evaporation of liquid nitrogen so, its image has not presented. This observation is consistent with those reported earlier (van Delft, 2012). Additional test results will be given in the next sections.

4.5.2 Optimization of HTS YBCO by Electrospinning Technique

HTS YBCO samples were synthesized by electrospinning process and sol-gel precursor solution. The samples were subjected to the same heat treatment processes as outlined in Chapter 3. Simply by changing the molecular weight of the polymer and modifying the polymers to (Y-Ba-Cu) acetates weight ratios, different morphologies of YBCO nanostructures were obtained. The morphologies such as nanorods (NRs), nanogarlands (NGs), nanoparticles (NPs), hierarchical structures (NH) and agglomerated nanoparticles (ANPs) were optimized and reproduced to fabricate the thin films from HTS YBCO as will be explained in next sections.

4.6 Characterization and Analysis of HTS YBCO

This section describes the characterization results of each polymeric and precursor solution as presented in Chapter 3. The rheological properties of the polymeric solutions at room temperature were used for electrospinning are shown in Table 4.3. The solutions viscosity ranges from 100 to 193 cP while the electrical conductivity ranges from 162 mS/cm to 184 mS/cm, which are the recommended ranges for electrospinning of ceramic samples (Harilal et al., 2017). The electrical conductivity was higher than that reported by Duarte et al (~12.7 µS/cm) (Duarte et al., 2014), which could be due to the differences in chosen polymers, solvents, and amounts of (Y, Ba, and Cu) in the polymeric solution. It is commonly known that large conductivity and viscosity would facilitate the transformation of electrospinning jet from the nozzle tip to the collector surface (Reneker & Yarin, 2008).

The samples were then transformed from the electrospun mats to the final powder, depending on the thermal analysis data. The data of Thermogravimetric Analysis (TGA) and the Differential Scanning Calorimeter (DSC) curves for YBCO nanostructure mats were obtained. Figure 4.7, shows the TGA – DSC data of the as-spun sample after drying for 48 hours. The DSC showed an endothermic event at ~100 °C, i.e. correspondingly ~8% weight loss was observed in the TGA due to the evaporations of water and other low-volatile impurities such as adhered solvent molecules. The DSC showed a major endothermic event cantered at ~230 °C with ~15% weight loss due to melting and evaporation of polymer. Two additional endothermic events were observed in the DSC, cantered at 300 °C, 400 °C and 450 °C with a total weight loss of ~30%, signifying complete removal of polymers. An exothermic event (a slight change in weight of the sample) was observed at ~750 °C, which is assigned to the crystallization of YBCO and oxygenation of the samples. These observations were consistent with the previous reports (Duarte et al., 2014; Shen et al., 2013; Uslu et al., 2010). Therefore, both DSC and TGA results suggest that crystalline nanostructured samples of YBCO can be obtained from electrospinning by combining two heat treatment processes. The first heat treatment was performed to fully evaporate the polymers and the second one was performed to attain the required crystallized phase of YBCO. The samples were subjected to the double heat treatments in oxygen pressure for facilitating necessary in order to promote chemical reactions for creating the single-phase samples and necessary for the fully oxygenated samples (Howe, 2014).

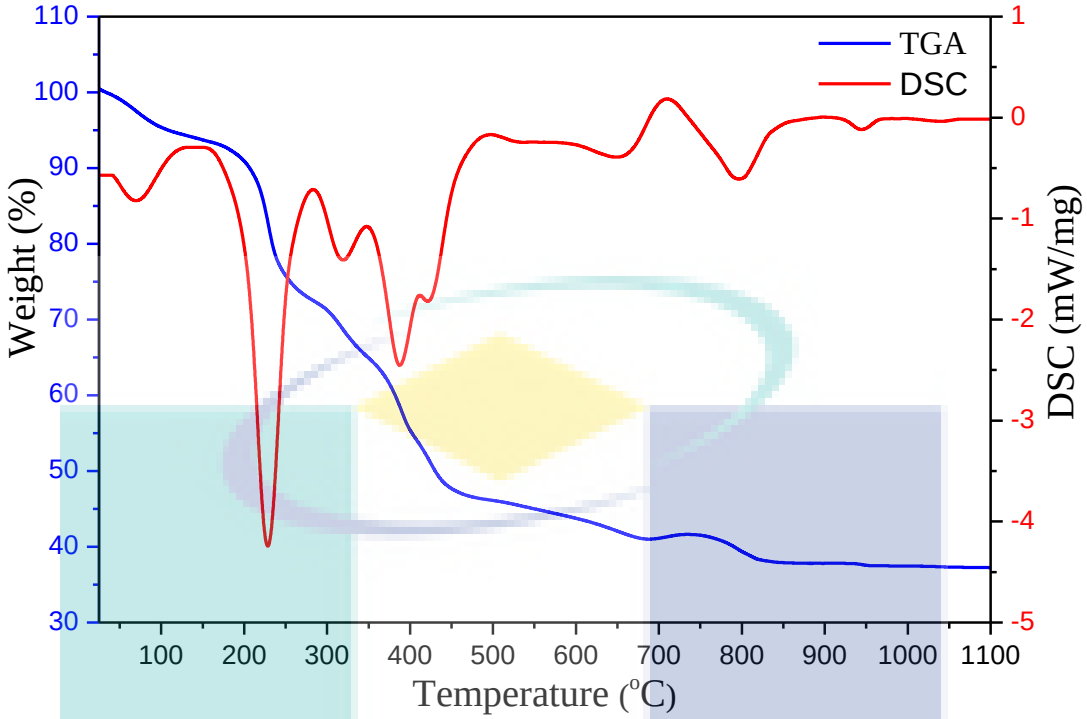

Figure 4.7 Simultaneous thermogravimetric analysis (TGA / DSC) curves vs. temperature for YBCO nanostructure mats

4.6.1 X-Rays Diffraction Analysis

The crystal phase and the purity of structure for all optimized HTS YBCO samples have been determined by X-ray diffractometer. The samples were tested (after the heat treatments) using the angle 2θ ranging from 5° to 80° and the count speed of 1° per minute. Figure 4.8, shows the Miller indices corresponding to the d-spacing of optimum powder XRD patterns of various synthesized YBCO nanostructures and normal structure by electrospinning and solid-state techniques. The fabricated samples were labelled from 1 – 6 as presented in Table 4.3, in order to refer their results for each one by using the sample labels. The XRD patterns of all optimized HTS YBCO were obviously quite similar. However, there were some samples contain unknown peaks maybe refer to some of Aluminium oxides atoms. Because they are probably fails during the collecting and heating processes of the electrospun samples. The aluminium foils were used to collect the electrospun fibres of YBCO samples and burnout the polymers then contained the pure YBCO nanostructures.

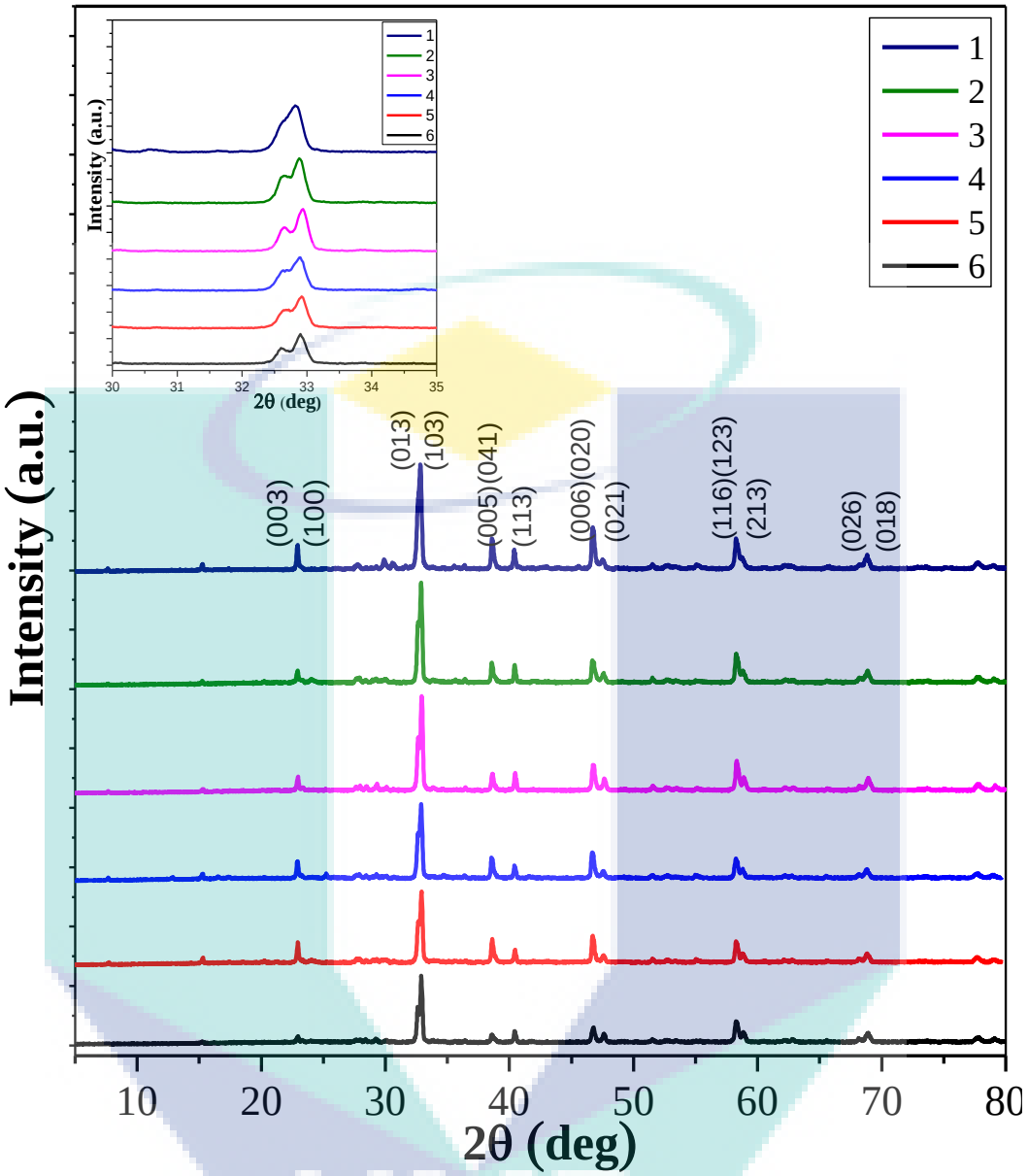

Figure 4.8 XRD pattern of HTS YBCO prepared by solid-state and electrospinning process, (1) Nanorods, (2) Nanogarlands, (3) Nanoparticle, (4) Nanohierarchical, (5) Agglomerated Nanoparticle, (6) Bulk Sample.

Most of XRD peaks can be indicated to YBCO and matched to the d-spacing at the corresponding 2θ. The highest peaks of the XRD patterns for all samples are almost same and can be noticed from the magnified figure of the XRD data "Figure 4.8"; the two common high peaks are centred at 2θ ~32.5 and 2θ ~32.8 corresponded to planes (013) and (103), respectively. However, there were extra planes for some peaks, these planes are expected due to the high crystalline structures of the samples.

Table 4.4 shows the results of the average crystallite size L (nm) for all YBCO samples were calculated from XRD data (for all common peaks corresponding to 2θ) using Scherrer formula equation ($L = K\lambda / \beta \cos\theta$) (Salama et al., 2015), where K, is the constant of crystallite shapes, λ, the wavelength of x-ray, β = (FHWM), is the full width of the dominant diffraction peak at the half of the maximum heights peak and θ, is the Braggs angle.

Table 4.4 The average d-spacing and crystallite size of YBCO samples using XRD data

Sample	Structure	d-spacing (nm)	FWHM (deg)	Average Crystallite (nm)
1	NRs	2.13	0.27	36.40
2	NGs	2.14	0.18	50.56
3	NPs	2.32	0.21	45.01
4	NH	2.14	0.19	51.22
5	ANPs	2.15	0.26	37.33
6	Bulk	2.14	0.25	39.12

Clearly, the average crystal size for all YBCO samples is lies in nanoscale and ranged from 36.40 to 51.22 nm. However, the YBCO nanostructures such as NRs and ANPs showed the smallest crystal size, while the NH and NGs, showed the largest crystallite size. On the other hand, NPs sample has the intermediate average crystallite size. Meanwhile, the NS YBCO sample prepared by solid-state crystallite size presents average crystal size larger than the size of NRs and ANPs with few nanometres compared to the other the crystallite size is being so small. The reason behind this issue is related to the various synthesis process, heat treatment process, oxygen contents, crystalline structure, porosity and the surface area values.

XRD diffraction patterns of YBCO samples are intensive in open literature (Duarte et al., 2014; Shen et al., 2013). The structure of sample was single phase, pure, orthorhombic and symmetric which was better known as the perovskite like structure. The dimensions of the lattice parameters were calculated using Braggs Law ($n\lambda = 2d \sin\theta$) and the miller indices (hkl) from XRD data. Table 4.5 shows the lattice parameters were unequal ($a \neq b \neq c$), and the volume of the unit cell for all YBCO samples (1 - 6). The values of the calculated lattice parameters were quite similar and consistent with the standard data of XRD in literature (Alikhanzadeh-Arani et al., 2013; Shen et al., 2013; Uslu et al., 2010).

Salama et al work have explained the better superconducting properties of YBCO samples are results from the high value of orthorhombicity (δ) (i.e. the oxygen content), which can be found from the difference between the calculated lattice parameters (a and b). Table 4.5 shows the calculated difference from the equation $\delta = (b - a)/(b + a)$ and the oxygen content ($O_{7-\delta}$). In this work the calculated orthorhombicity (δ) values for all the samples are in between 0.002 to 0.008, i.e. the average of $\delta = 0.005$, from which the calculated oxygen contents is around $7- \delta = 6.995$. Hence, according to the above information, all YBCO samples having full oxygen saturation stoichiometry, which is unacceptable, because they are having different transition temperature T_c.

Table 4.5 The dimensions of the lattice parameters calculated for YBCO samples

Sample	Structure	a (Å)	b (Å)	c (Å)	Volume (Å^3)	$O_{7-\delta}$
1	NRs	3.8152	3.8812	11.6125	171.9527	6.992
2	NGs	3.8137	3.8783	11.6239	171.9253	6.994
3	NPs	3.8140	3.8464	11.6135	170.3720	6.993
4	NH	3.8112	3.8749	11.6598	172.1921	9.997
5	ANPs	3.8161	3.8332	11.7053	171.2236	6.996
6	Bulk	3.8227	3.8760	11.6609	172.7770	6.998

4.6.2 Morphology study (FESEM)

The morphology and surface analysis for all HTS YBCO samples have been performed via Field Emission Scanning Electron Microscope (FESEM). The effect of the solution parameters such as the viscosity on the electrospun fibres diameter have been discussed in Chapter 2. Figure 4.9 shows the FESEM images of the electrospun YBCO nanofibers morphology before burnout the polymers for different solution viscosity. The high viscous solution will yield YBCO fibres having larger diameter and vice versa. Whereas the electrospun YBCO morphologies cannot being seen without removing the polymers. Therefore, the electrospun samples were subjected to a heat treatment up to 500 °C to burnout the polymers. To explore the morphology of YBCO samples using FESEM images, the samples were grinded into a fine powder and placed on a tape with systematic scattering at regular distribution on the testing unit and dried. The FESEM image of samples for various areas, directions and enlargement were obtained. The detailed morphology results of YBCO samples prepared by electrospinning process are listed in Table 4.3.

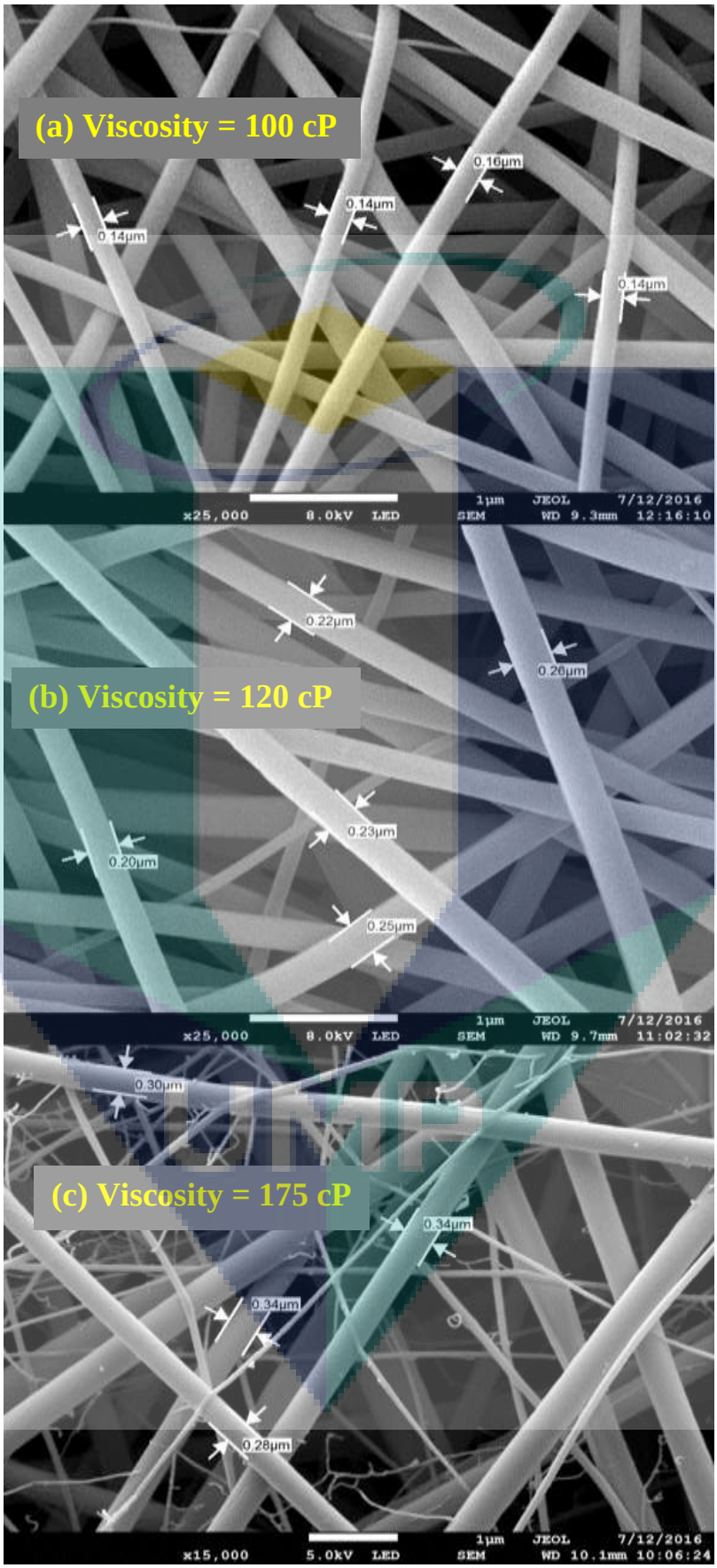

Figure 4.9 FESEM images of YBCO nanofibers for different solution viscosity.

Figure 4.10 shows the FESEM images of the synthesized electrospun YBCO samples of different stoichiometric ratios fabricated by electrospinning process. At first, YBCO:PVP (Mw = 1,300,000 g/m) in the ratio 2:1 termed Sample 1 shows nanorod (NRs) morphology, having average diameter of ~75 nm and length of ~900 nm, (see image 1 at the top of the Figure 4.10). The NRs were having arbitrary direction and dense with a non-uniform diameter especially at the end their cross section is looked as a circular shape. On the other hand, sample with similar YBCO:PVP ratio (with lower polymer molecular weight) does not have similar morphology and it contains undesired electrospun mats. By lowering the YBCO concentration (Sample 2), i.e. YBCO:PVP (Mw = 1,300,000 g/mol) ratio of 2:2, (image 2) shows a nanogarland (NGs) morphology with diameter ranging from 250 nm to 400 nm is obtained. Like Sample 1, a similar YBCO:PVP ratio of Sample 2 has polymer of lower molecular weight and it does not contain any electrospun mats. Obviously, the third solution with a slightly different concentration of YBCO:PVP (Mw = 160,000 g/mol) in the ratio 4:3, termed Sample 3 (image 3) shows uniform nanoparticle (NPs) morphology with diameter ranging from 40 nm to 50 nm.

The electrospun NRs and NGs Samples have been fabricated by dissolving the polymers PVP of high molecular weight 1,300,000 g/mol with acetates to prepare the sol-gel solutions, while Sample NPs was prepared by dissolving the polymer PVP of lower molecular weight 160,000 g/mol. From the FESEM images, it is obvious that the solution parameters would affect the nanostructures of YBCO morphology. This result verified that, in electrospinning process, the solution parameters play an important role and can be manipulating to produce several types of morphologies. This work presents a new morphology results for YBCO, which is not obtained before using electrospinning technique and sol-gel solution parameters.

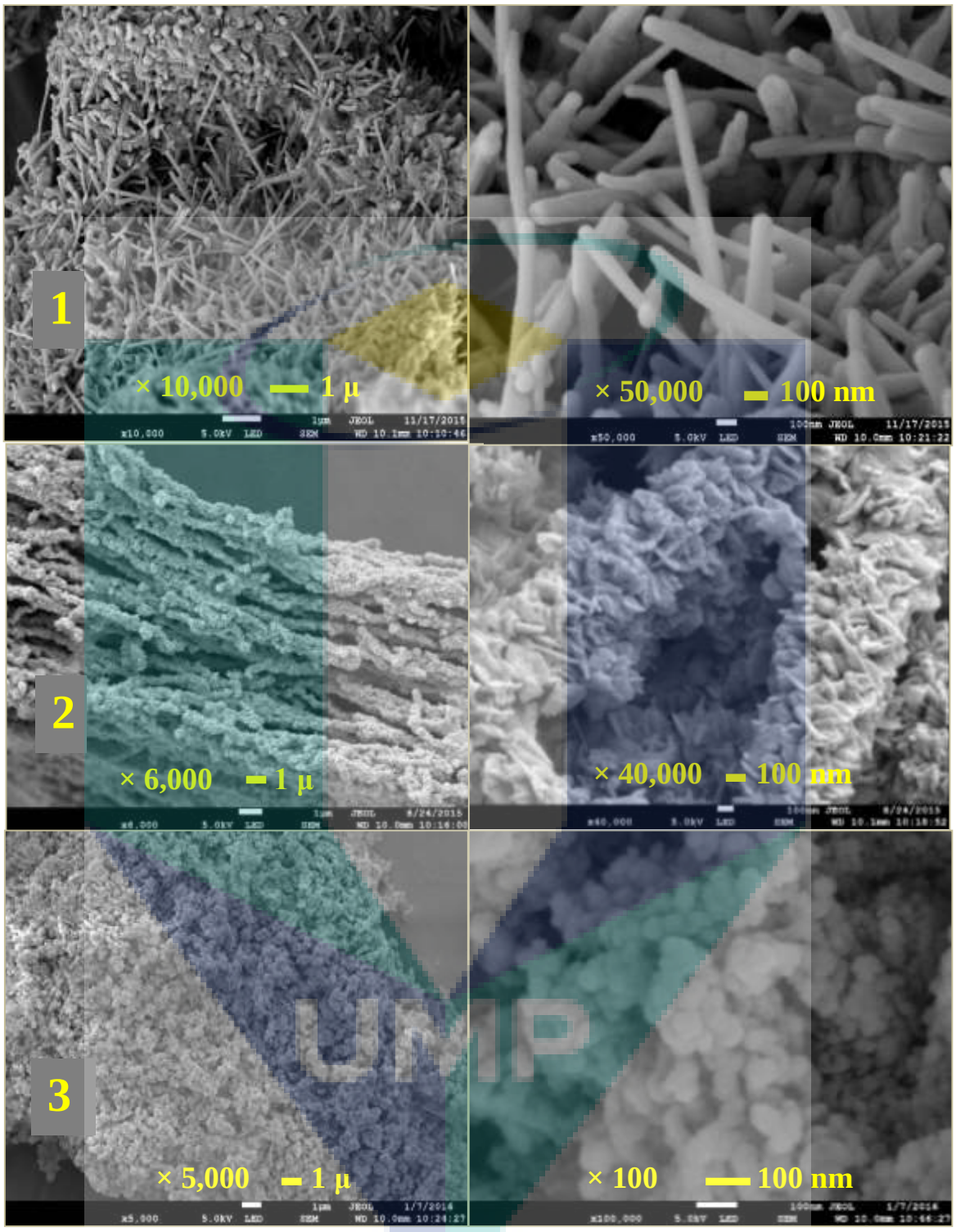

Figure 4.10 FESEM images of the optimized HTS YBCO samples labelled from 1 to 3 displays various morphologies, (1) NRs, (2) NGs and (3) NPs samples

Similarly, with slightly different solution and concentration of YBCO:PVP (Mw = 160,000 g/mol), in the ratio of 2:3, results Sample nanohierarchical (NH) morphology is obtained. Its average diameter is ~70 nm and its length is ~ 400 nm. These structures can be seen grown on flat large sheets throughout the sample as depicted in Figure 4.11, image 4. Interestingly, another sample of similar YBCO:PVP ratio (but with higher polymer molecular weight) does not exhibit any electrospun mats with clear morphology. The rest of FESEM images for HTS YBCO Sample 5, where produced by another electrospinning instrument setup (Figure in the last page of appendix B).

By increasing the YBCO concentration i.e., YBCO:PVP (Mw = 1,300,000 g/mol) in the ratio 4:5, solution termed Sample 5 (Figure 4.11, image 5) shows agglomerated nanoparticles (ANPs) morphology of size ranging in between 200 nm and 400 nm. This agglomeration may occur due to the elevated temperature at heat treatment process. A closer examination reveals that these agglomerates contain finer particles of size ~50 nm. In the case of using similar YBCO: PVP ratio (lower polymer molecular weight), Sample 5 does not contain any electrospun mats with homogeneous morphology. The samples are labelled from 1 to 5 represent the FESEM images of HTS YBCO prepared by electrospinning process, while Sample 6 (image 6) refers to the HTS YBCO sample prepared by the solid-state method, which is called the normal structure (NS) of HTS YBCO see Table 4.3. Even the sample 6 was treated with elevated temperature for long time in presence of oxygen. The sample morphology, looks like a group of diverse stones and welded together and created looks like a large agglomerated stone.

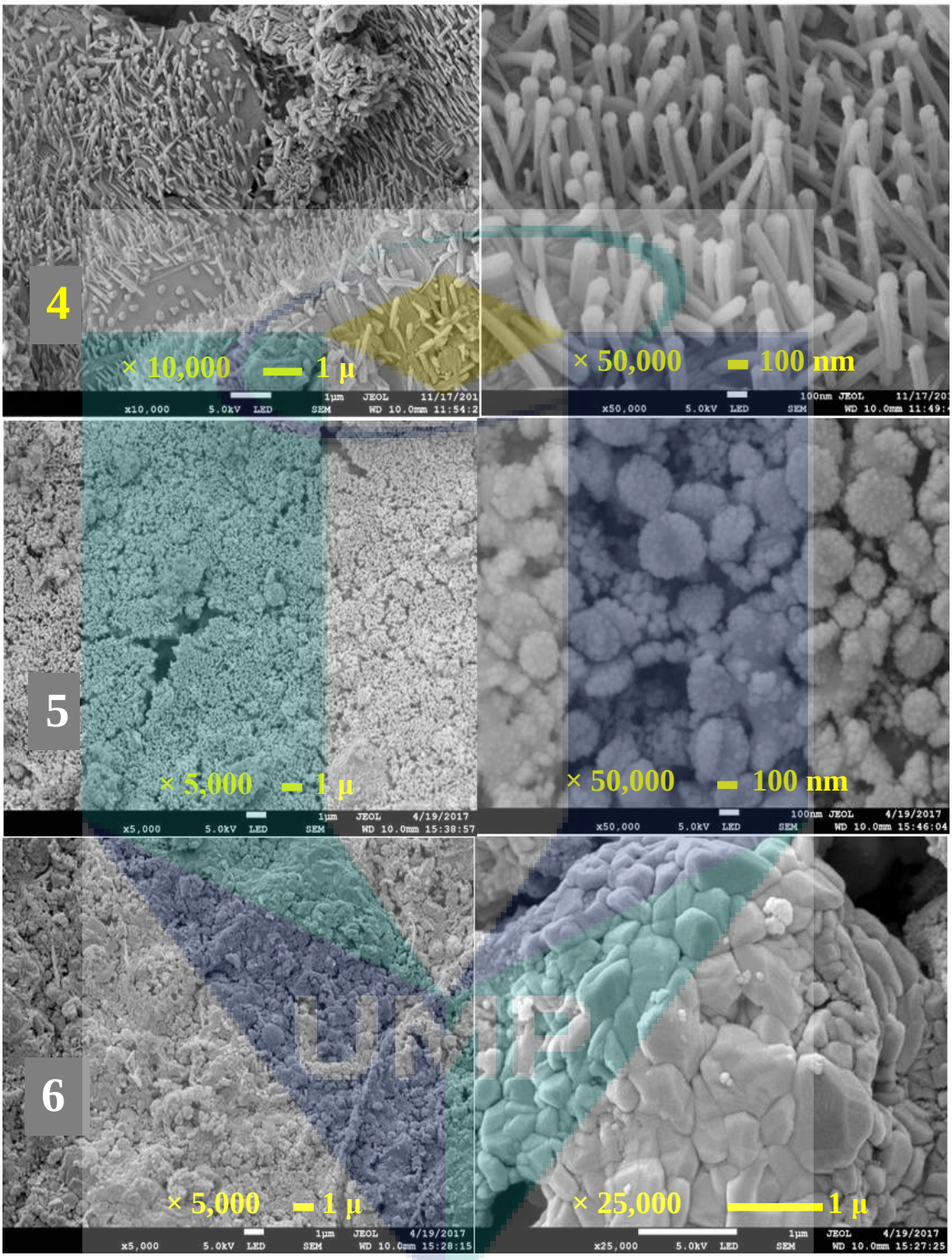

Figure 4.11 FESEM images of HTS YBCO morphology samples labelled from 4 to 6, (4) NH, (5) ANPs and (6) Normal structure samples

4.6.3 T_c Measurements

The transition temperature $T_{c\chi'}$ was measured using Alternating Current Susceptibility (ACS) that consists of closed cycle liquid helium refrigeration system. It is considered as an effective route to find the transition temperature. In general, the AC susceptibility technique is consistent with the conventional four-probe technique (Mohajeri et al., 2016; Nur-Akasyah et al., 2017). The complex susceptibility (χ) consists of real and imaginary parts ($\chi = \chi' + i\chi''$). The $T_{c\chi'}$ values measured for YBCO samples were ranging from 82 K to 92 K. The data of the AC susceptibility as a function of temperature for all samples shows the transition to the superconducting state. The AC susceptibility of the sample decreased as the sample temperature decreased below the transition temperature. By this time the samples turned to a perfect diamagnetic material and does not allow magnetic flux line to pass through. The T_c values of YBCO samples can be estimated from these curves, which were taken at the part of the midpoint between the temperatures of 10 and 90% of the superconducting transition curve. Figure 4.12, shows the AC susceptibility as function of temperature for all YBCO samples. Table 4.6 summarizes the structure and the critical transition temperature of the HTS YBCO samples.

Table 4.6 The critical transition temperature for all the HTS YBCO samples

Sample	**Structures**	$T_{c\chi'}$ **(K)**
1	Nanorods	82
2	Nanogarlands	88
3	Nanoparticles	84
4	Nanohierarchical	90
5	Agglomerated Nanoparticles	90
6	Bulk	92

Figure 4.12 clearly shows that the real part of susceptibility decreases suddenly as the temperature is below the transition temperature. The imaginary part of susceptibility, however, increases gradually as the temperature is below the transition temperature. The decrease in real part (χ') is attributed to the diamagnetic properties of the samples at temperature below the transition temperature. On the other hand, the increase in imaginary part (χ'') of susceptibility indicates AC losses after the transition of YBCO samples (Nur-Akasyah et al., 2017). The superconducting transition temperatures of the samples ranged from 82 K to 92 K.

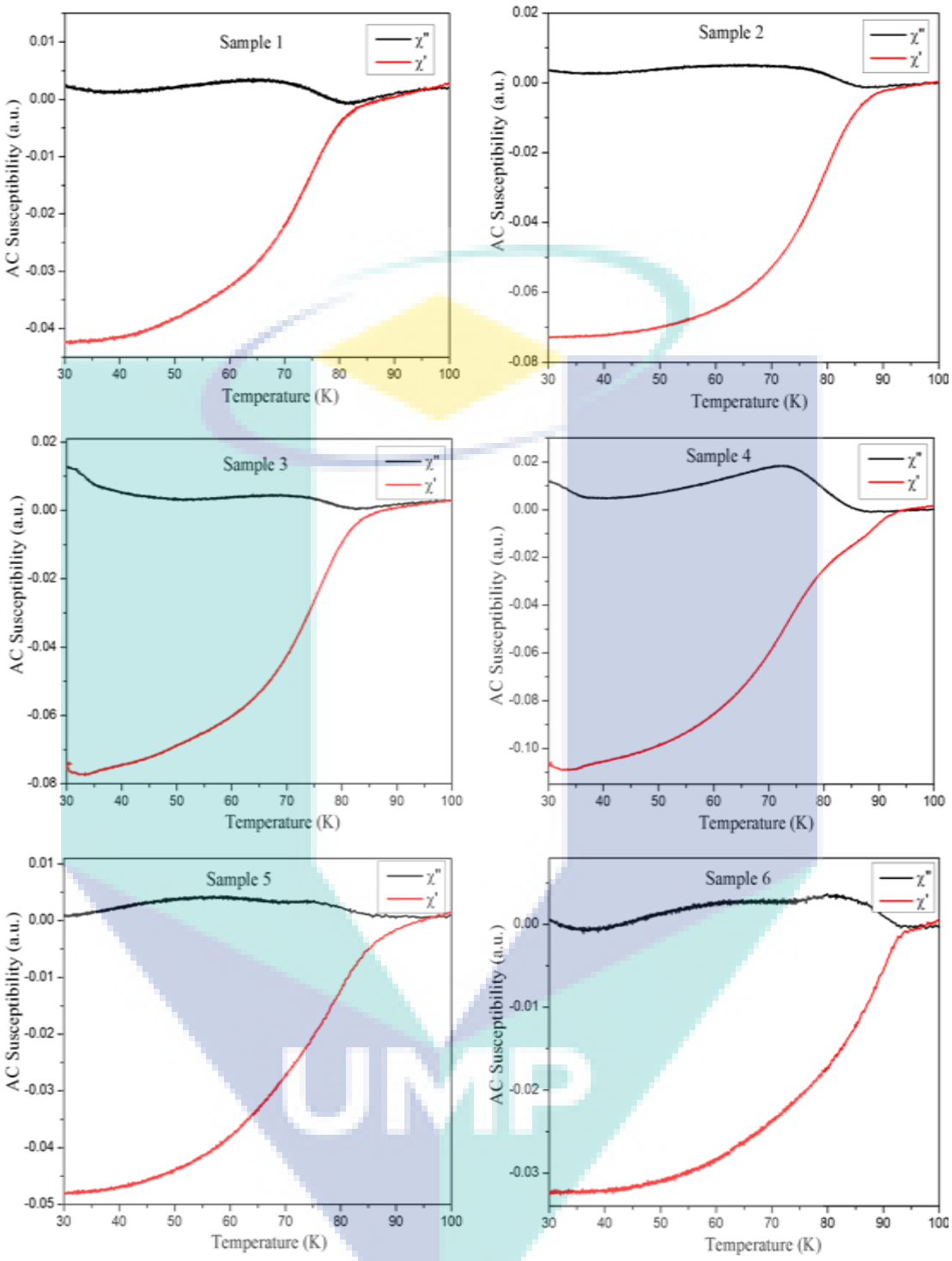

Figure 4.12 AC Susceptibility ($\chi = \chi' + i\chi''$) measurements versus temperature of YBCO nanostructure samples, (1) Nanorods, (2) Nanogarlands, (3) Nanoparticle, (4) Nanohierarchical, (5) Agglomerated Nanoparticle, (6) Bulk Sample.

It was proven that the transition temperature of superconducting YBCO is dependent strongly on the oxygen content (Howe, 2014). The transition temperature decreased as the oxygen concentration increased from 6.7 to 6.96.

Moreover, the broad transition of diamagnetic responses of the samples is strongly dependent on the oxygen content. This observation is consistent with the other work (Amado & Sarmago, 2015). The superconductivity of YBCO sample were found with high transition temperatures (between 83 K and 92 K) with relatively 10 K different, this case is attributed to the structural properties at nanoscale and oxygen contents. However, the samples were collected with single crystal orthorhombic structure, Samples of high stability and high transition temperature were obtained upon annealing process for a long time in the presence of flowing oxygen, consequently yielding high stability and high transition temperature due to the high oxygen content.

4.6.4 BET Surface Area Results

The surface area measurements of HTS YBCO samples prepared by solid state reaction method and electrospinning process were studied using the adsorption-desorption test performed in nitrogen atmosphere using the BET surface area technique. Figure 4.13 shows the adsorption-desorption isotherm linear plots of YBCO six samples, which are corresponding to type IV isotherm. It is clearly show that the gas adsorption-desorption isotherm linear plot curves are presented with closed-loop of nitrogen gas adsorption-desorption process. The surface area was calculated from the adsorption data of the first five points (Klobes et al., 2006). Therefore, the amount of surface area is proportional with the gas adsorption data as it illustrated in the isotherm relation for all samples.

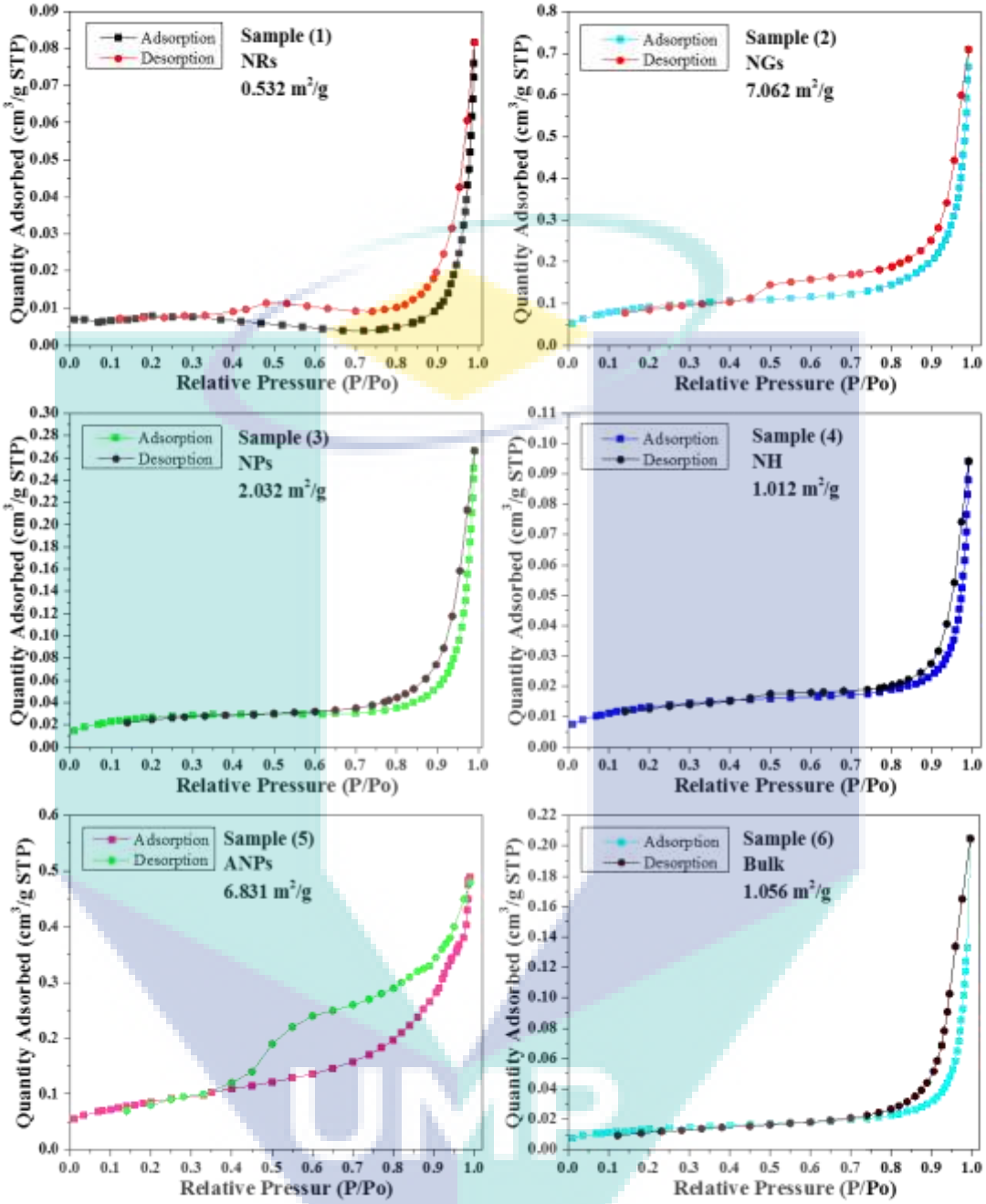

Figure 4.13 Gas adsorption-desorption isotherm linear plot of HTS YBCO samples (from 1 to 6).

Table 4.7 shows the samples morphology, the BET surface area, the pore size and the pore volume measurements. Although, the YBCO sample consists of heavy elements such as Yttrium (Y), Barium (Ba) and Copper (Cu), in addition the fabrication process parameters used to prepare the samples via electrospinning technique, YBCO porous samples still exhibit high surface area.

Table 4.7 Morphology, BET surface area, pore size and pore volume measurements of YBCO samples

Sample Label	Morphology	Surface area (m^2/g)	Pore size (nm)	Pore volume (cm^3/g)
1	Nanorods	0.532	16.087	0.0021
2	Nanogarlands	7.062	10.924	0.0193
3	Nanoparticles	2.032	14.364	0.0073
4	Nanohierarchical	1.012	10.162	0.0024
5	Agglomerated Nanoparticles	6.831	9.626	0.0164
6	Bulk	1.056	15.435	0.0040

Clearly, the surface areas measurements of YBCO samples ranged from 0.532 m^2/g to 7.062 m^2/g. The surface area represents the number of monolayers and multilayers formed through the pores morphology in the YBCO structure. Sample 2 and Sample 5 had high surface area (i.e. 7.062 m^2/g and 6.831 m^2/g, respectively) due to the formation of monolayer over multilayer during the synthesis process. Generally, the values of pore diameter and pore volume of a sample are dependent on the internal structural morphology. Sample 1 has the highest pore diameter (16.087 nm), while Sample 5 has the lowest pore diameter. As explained in Chapter 2, the fabrication process of YBCO depends on several parameters such as solution properties, electrospinning parameters and ambient parameters.

Although, the sample has different weight of starting material and ratio of polymer with different polymer molecular weight. In addition, the electrospinning process has several parameters by which an electrospun solution will produce new morphology for the material. Therefore, the YBCO superconductor of different morphologies have been produced since the past ten years (Duarte et al., 2014; Shen et al., 2013). It is important to note that preparing YBCO from different precursors by electrospinning technique will yield various structural morphologies and properties such as transition temperature and surface area (Alikhanzadeh-Arani et al., 2013).

The interrelation between the surface area and the calcination temperature of YBCO was studied by Shter et al. (Shter et al., 1995). When the temperature increased from 750 ºC to 910 ºC, the surface area shrank from 2.36 m^2/g to 0.46 m^2/g. In another study, Shter and Grader (Shter & Grader, 1994) developed YBCO powder with surface area of ~1.7 m^2/g. Heat treatment was performed at 780 °C for 12 h. However, calcining at 920 °C would lower the surface area to 0.3 m^2/g due to particle coarsening. In contrast, the current work shows that increased calcination temperature does not influence the surface area of YBCO

nanostructures, which is primarily due to the one-dimensional morphology where particles can be grown without increasing the diameter of the fibres (Archana et al., 2009).

4.7 Deposition of HTS YBCO Thin Films

The thin films of YBCO were deposited via two methods, i.e. the electrospinning process and spin coating procedure. Experimentally, these techniques are relativity not applicable 100% for depositing a finite and limited structures of thin films such as YBCO nanostructures on $LaAlO_3$ substrates.

4.7.1 Deposition of HTS YBCO Thin Films by electrospinning process

However, the superconductivities of the thin film samples deposited by electrospinning process on the $LaAlO_3$ substrate could not be verified yet. This occurred due to the high surface area, which leads to increase the band gap (Dadras & Ghavamipour, 2016). High surface area, high porosity and irregular grain boundary distribution can be realized by electrospinning technique. This resulting property can be attributed to the experiment process as follow; the sample was prepared as precursor solutions (dissolved with a polymer) and the solutions were injected into the syringe and transferred by applying the high voltage (refer to the section of electrospinning process in Chapter 3). Then, the collected fibres were deposited on the substrate and the polymer was removed in a furnace (via burning). In this case, substantial number of holes would be created in the thin films. After removing the polymer particles, the mismatches between other grain boundaries in thin film would increase. Furthermore, the thin film was unstable and hence it might be detached from the substrate. Shen *et. al*. have deposited the HTS YBCO by electrospinning process and the detail of deposition was not mentioned. Moreover, there is no detected propertied for the YBCO thin film in detail. In this work the samples of YBCO thin films prepared successfully. Importunely, like the previous work by Shen *et. al.* (Shen et al., 2013) the prepare thin film not shows any superconducting transition properties T_c. The result of the sample showed semiconducting properties. For more details the sample results are presented in appendix B.

4.7.2 Deposition of HTS YBCO Thin Films by Spin Coating Technique

In this section, the YBCO thin films were deposited properly by using the spin coating procedure as explained in Chapter 3. Spin coating technique was used to deposit

YBCO for all samples labelled from 1 to 5 using the nanostructure powder prepared by the electrospinning process. The deposition was performed on Sample 6 as well using the powder of YBCO prepared by the solid-state reaction method. However, the important things need to explain is; only two kinds from YBCO nanostructure (i.e., nanoparticle and nanorod morphology) thin films are stable on the substrate and have a smooth faced surface area to be useful for the next step of experiment process.

4.8 Analysis and Testing of Microwave Device

The Vector Network Analyzer (VNA, Model E5071C, 300 kHz- 20 GHz, Agilent Technology) was used to test the performance of the devices. The experimental setup used to test the performance of the filters consisted of VNA, coolant box, sample holder and fabricated bandpass filter. The sample was connected to SMA connectors using the sample holder. This holder was designed to connect the ground plane of the filter with the aluminium plate in order to produce a perfect electric/thermal conductor. The two conductive terminals of VNA were calibrated using the full two port SOLT method to eliminate all instrumentation errors. The measurements were carried out at frequency ranging from 8 GHz to 12 GHz for both temperatures, i.e. 300 K (room temperature) and 77 K.

Here, the variations of S-parameter at different frequencies are presented. For each sample, both reflection coefficient (S_{11}) and transmission coefficient (S_{12}) are discussed. For clarity purpose, a framework explaining the presentation of filter results is illustrated in Figure 4.14. The bandpass filter was fabricated from two types of YBCO thin films prepared by electrospinning and solid-state processes. Via electrospinning, two kinds of morphologies (i.e. nanorod and nanoparticle) were formed. The details of the designed filters such as morphology and synthesis process are listed in Table 4.8.

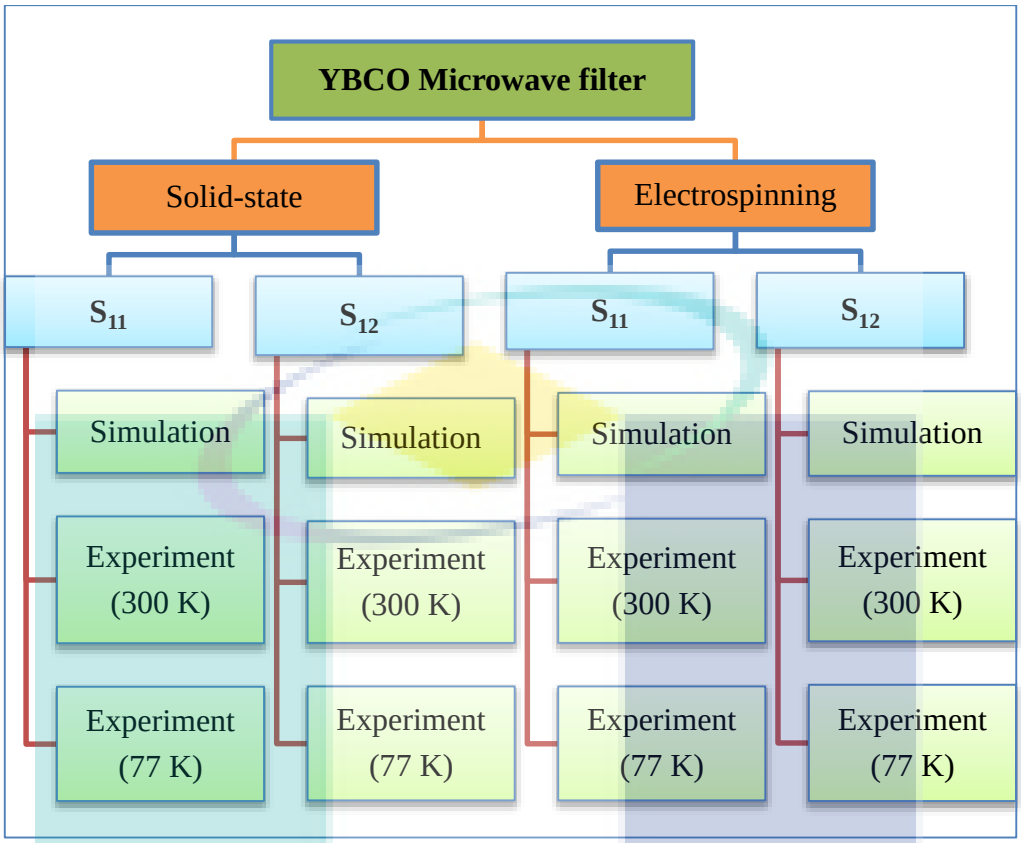

Figure 4.14 Framework to display the simulation and experiment results of the designed and fabricated filters.

Table 4.8 The samples morphology and synthesis process of the designed filters.

Filter Name	Morphology	Synthesis process
A	Bulk	Solid state
B	Nanoparticle	Electrospinning
C	Nanorod	Electrospinning

4.8.1 Microwave Filter YBCO Results

Figure 4.15 summarizes the simulation and experimental results of the frequency response characteristics of the microwave filter using YBCO thin film prepared from the solid-state reaction. The reflection coefficient (S_{11}) differ from the transmission coefficient (S_{12}) considerably at 300 K and 77 K as illustrated in panel (a) by the left (S_{11}) and the right (S_{12}) panel (b) of the Figure 4.15. Thus, revealing the role of superconductivity on the microwave characteristics. The return loss was calculated from S_{11} (left panels) and insertion loss was calculated from S_{12} (right panels). The filter made from the solid-state reaction (77 K) showed return losses of -22 dB and -15 dB at frequencies ~9.7 GHz and 10.8 GHz, respectively. Therefore, the return loss is lower as compared to the simulated

response of S_{11}. No response was observed at 300 K. It is interesting to note that the experimental response is very similar to the simulated one. Filter (A) showed lower return loss than the simulated one, which was mainly due to the mismatches and resistance between the contact pads and the electrical contact, which probably affected by dipping the filter into the liquid nitrogen).

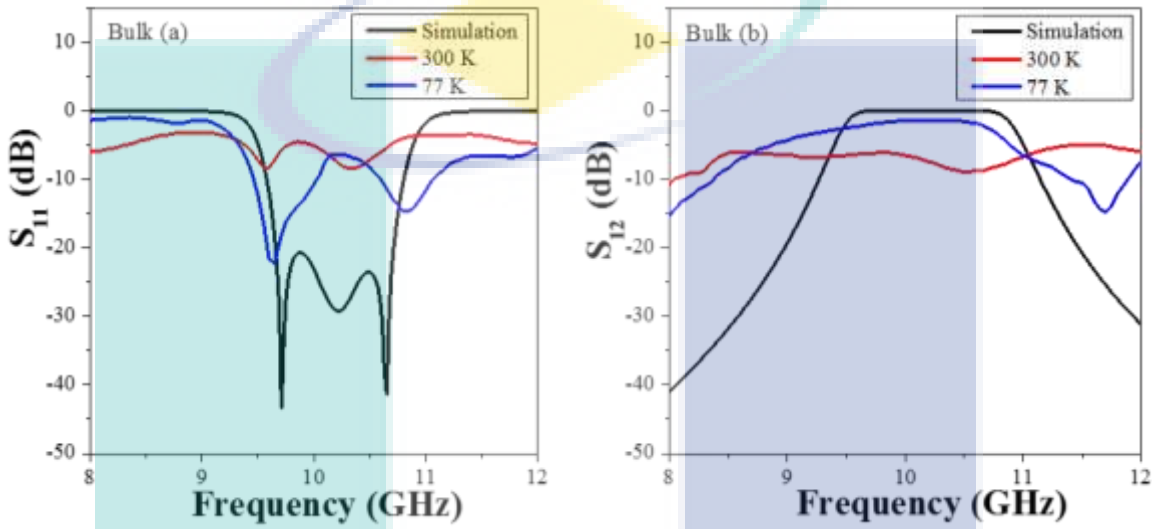

Figure 4.15 Simulation and experiment results of (Sample A) YBCO microwave bandpass filter prepared by solid-state reaction method, measured using VNA at temperature 300 and 77 K, (a) S_{11} response, (b) S_{12} response.

On the other hand, the S_{11} responses in the spectrums of microwave Filters B and C made from the thin film of the electrospun YBCO nanostructures are shown in the left panels. The average return losses are -15 dB at ~10.2 GHz and -12 dB at 10.3 GHz, which showed lower return loss as compared to the simulated responses of S_{11} shown in Figure 4.16 and Figure 4.17 (left panel (a) and right panel (b)). This result is consistent with that work reported by Zhang *et al.* (Zhang et al., 2012), the authors have synthesized the filter using YBCO thin film, where an Au thin film was deposited on the top of YBCO thin film. Their measured return loss results of the S_{11} response was also less than the simulation result. However, this could be attributed to the sample structure, for YBCO at nanoscale (high surface area, increased the band gap), which was lastly improved by (Dadras & Ghavamipour, 2016). The authors have investigated the effect of doping nanomaterial in pure YBCO as well. Besides, the study of (Croitoru et al., 2007), the authors investigated the superconducting properties at nanoscale. These properties were dependent on confining

geometry and shapes. The oscillatory behaviour of superconducting property is consistent with the current finding. The current results are consistent with those reported in the literature (Croitoru et al., 2007; Dadras & Ghavamipour, 2016). It is important to mention here that perfect insulator (with homogeneous property) was adopted in the simulation. Moreover, different properties of the material used in simulation and it is quite perfect conductors as compared to measured results. It is also because of the simulation process did not consider the structure of the material and it is only considering the perfect conductor and homogeneous material.

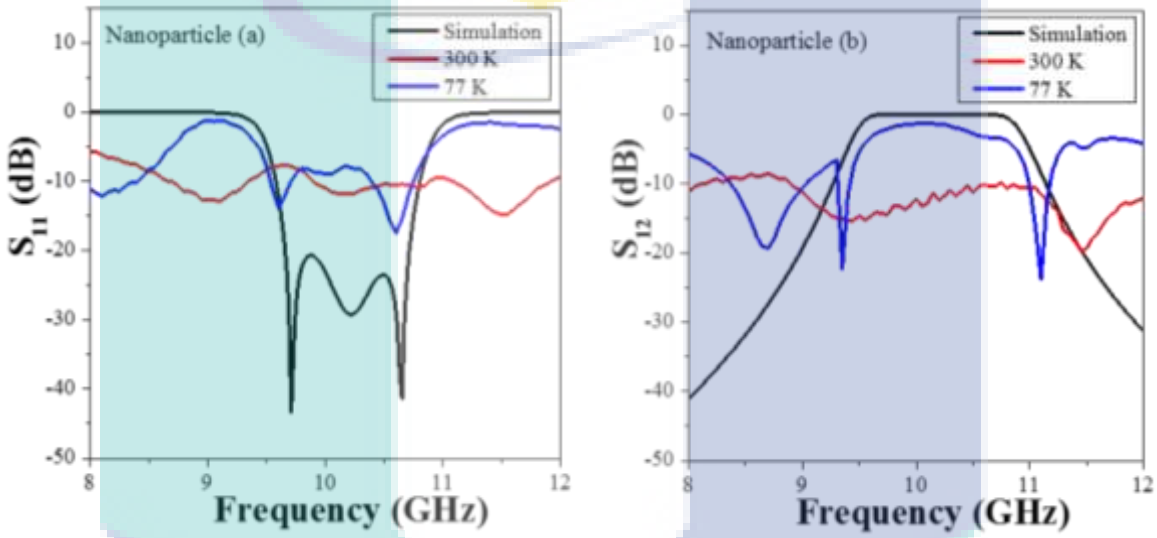

Figure 4.16 Simulation and experiment results of (Sample B) YBCO microwave bandpass filter prepared by electrospinning process, measured using VNA at temperature 300 and 77 K, (a) S_{11} response, (b) S_{12} response.

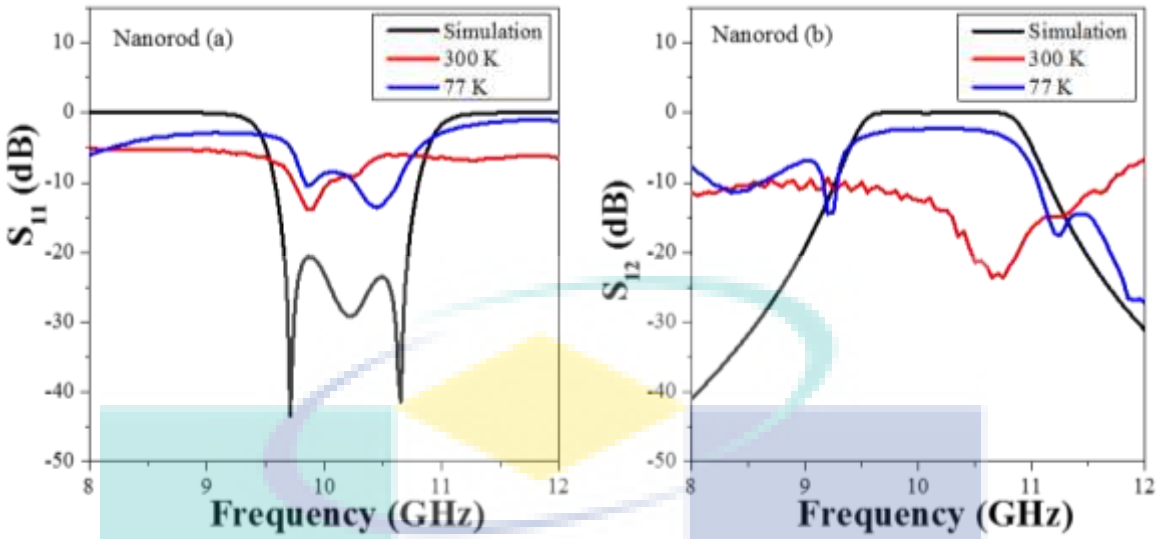

Figure 4.17 Simulation and experiment results of (Sample C) YBCO microwave bandpass filter prepared by electrospinning process, measured using VNA at temperature 300 and 77 K, (a) S_{11} response, (b) S_{12} response.

The insertion losses for YBCO filters calculated from S_{12} (in right panels), are ~-2, ~-1.5 and ~-3 dB for the normal, nanoparticle and nanorod respectively. The electrospun YBCO nanoparticles show much lower insertion loss as compared to that of Lu *et al.* work (Lu et al., 2015). The resulted bandwidth of the bulk filter shows more than 1.5 GHz, while the nanostructured YBCO filters bandwidths are almost similar at 1.5 GHz, which is consistent to the simulated result. The agreement is due to the low losses of YBCO sample at high frequency. Hence, the broad bandwidth of YBCO filters can be produced. Table 4.9 summarizes the characteristic results of each filter made from the three kinds of YBCO thin films prepared by solid-state reaction and electrospinning process.

Table 4.9 Response of the YBCO microwave bandpass filter samples.

Filter	**Morphology**	**Bandwidth (GHz)**	**Return loss (dB)**	**Insertion loss (dB)**
A	Bulk	2.0	-22	-2.0
B	Nanoparticle	1.5	-15	-1.5
C	Nanorod	1.5	-12	-3.0

4.9 Result Analysis of the Designed Filters

The response of the electrospun YBCO filters are consistent with the simulation result. The experimental results of nanostructured YBCO filters display lowest return losses than the normal YBCO filter prepared from solid-state thin film. The relative regression performance of the electrospun filters reflect some of their properties of YBCO at nanoscale, high resistance, and high surface area. The observed insertion losses could be related to the mismatches and resistance between the contact pads and the electrical contact, which probably affected by dipping the filter inside the liquid nitrogen (Jing et al., 1994). Although, the dimension of the filter is smaller as compared to other previous work reported in open literatures (Bhattacharjee et al., 2013; Zhang et al., 2015) were larger than the current ones, and the circuits were fabricated from the conventional YBCO prepared by solid-state and electrospun YBCO. Furthermore, the coupled parallel lines were relatively far apart from each other, and the substrate thickness was very thin, i.e. ~ 0.5 mm.

Table 4.10 presents the simulation and experimental results for the designed, simulated and measured filters using HTS YBCO thin films deposited by different techniques. The proposed technique and fabricated filters were have been compared to the ones reported in open literature (Bhattacharjee et al., 2013; Zhang, et al., 2015), which were designed using parallel coupled line and pole. These filters of different substrates, dimensions and YBCO structures (due to various deposition techniques) were simulated with different software (Chung, 2000; Shang et al., 2013; Shivhare et al., 2008; Wang et al., 2005). Both simulated and measured results in terms of bandwidth, return loss and insertion loss are consistent. The filter developed in the current work has lower performance, although its dimensions are smaller. This result indicates the filter design is reliable and it can be adopted in the industry. As the purchase of each 1 g of YBCO powder costs less than 5 $ (Rm21), by which at least five of the designed microwave bandpass filter in present work can be produced. However, the commercial microwave bandpass filter now available and costs around 300 $ (Rm1260) from the Mini-Circuits company, detailed information about the costs required to synthesize the current microwave bandpass filter using HTS YBCO is included in the appendix B (A-19).

Table 4.10 Evaluation summary of the microwave filters designed, simulated and fabricated with different model, Software and synthesize process respectively using superconducting YBCO.

Reference	Characterization				Performance Evolution							
					Simulation				Experiment			
	Platform for simulation	Filter Design	Substrate	Dimensions (mm^2)	Fc (GHz)	BW	RL (dB)	IL (dB)	Fc (GHz)	BW	RL (dB)	IL (dB)
(Chung, 2000)	EM Sonnet	Three parallel coupled H-type	MgO	30	16.65	1.0 GHz	-22.0	0	16.5	1.35 GHz	-22.0	-0.5
(Wang et al., 2005)	IE3D	Four-pole cross-coupled	$LaAlO_3$	225	2.152	12.0 MHz	-23.3	0	2.18	9.8 MHz	-5.0	-1.48
(Shivhareet al., 2008)	E6	Four parallel-coupled poles	$LaAlO_3$	254	4.035	80.0 MHz	-20.0	-0.5	3.7	3.6 GHz	-5.8	-3.5
(Zhang et al., 2012)	HFSS	Five-parallel pole hairpin	MgO	200	8.0	2.0 GHz	-45.0	-0.5	7.8	2.0 GHz	-20.0	-1.2
(Shang et al., 2013)	EM Sonnet	Ten poles	MgO	218	10.0	4.0 GHz	-20.0	0	10.0	2.5 GHz	-14.0	-0.31
(Bai et al., 2013)	EM Sonnet	Ten poles	$LaAlO_3$	5898	2.15	0.1 GHz	-20.0	0	2.15	0.1 GHz	-15.0	-3.0
(Bai et al., 2013)	EM Sonnet	compact eight-pole	MgO	200	11.0	2.0 GHz	-40.0	0	11.0	2.0 GHz	-40.0	-0.8
(Kumar et al., 2014)	HFSS	Five parallel-coupled lines	FR4	71	2.48	0.6 GHz	-12.5	-2.2	…..	…..	…	….
(Zhang et al., 2015)	EM Sonnet	Parallel-connected network	$LaAlO_3$	666	2.0	30.0 MHz	-25.0	0	2.0	30.0 MHz	-12.5	-0.3

Continue

(Gupta et al., 2015)	HFSS	Five parallel-coupled lines	FR4	480	3.0	2.0 GHz	-8.0	-1.8	…..	…..	….	……
(Zhang et al., 2015)	EM Sonnet	linear phase filter.	$LaAlO_3$	425	0.83	10.0 MHz	-20.0	0	0.83	10.0 MHz	-13.0	-0.3
(Gunjal et al., 2016)	HFSS	4- parallel line coupled	FR4	2627	2.4	140 MHz	-10.0	-4.0	2.35	140 MHz	-10.0	-5.0
(Liu et al., 2017)	EM Sonnet	multi-loop resonators	MgO	335	1.8	1GHz	-20.0	0	1.5	1.0 GHz	-19.0	-0.2
This work	HFSS	Parallel-coupled line	$LaAlO_3$	100	10.2	1.5 GHZ	-30.0	0	10.2	2.0 GH	-22.0	-2.0
This work	HFSS	Parallel-coupled line	$LaAlO_3$	100	10.2	1.5 GHZ	-30.0	0	10.2	1.5 GHz	-15.0	-1.5

Where,

Fc, center of frequency

BW, Bandwidth

RL, return loss

IL, insertion loss

4.10 Summary

This work presents new devices in a new design of microwave bandpass filter circuits developed by finite element method employing the Ansoft HFSS software. The designed model of the filter circuits used the perfect conductors consisting of four parallel couple lines deposited on $LaAlO_3$ substrate. The HTS YBCO samples were prepared in combining sol-gel and solid-state techniques. The YBCO superconductor has been prepared by optimization the solution parameters employing the electrospinning process. Electrospinning process is an effective and inexpensive technique to generate numerous nanostructured morphologies of high porosity, high surface area to volume ratio and high critical transition temperature. The electrospinning technique uses a sol-gel of polymer and precursor of metal acetate solutions of different ratios, followed by a complicated heat treatment procedure. The diameter and morphology of the YBCO nanostructured samples are influenced by the viscosity of electrospun solution. From the FESEM measurement, the morphologies of YBCO nanostructured samples such as nanorods (NRs), nanogarlands (NGs), nanoparticle (NPs), nanohierarchical structure (NH) and Agglomerated nanoparticle (ANPs) have been obtained. Via conducting the XRD test, the YBCO samples show orthorhombic structure upon conducting the annealing process in the presence of flowing oxygen. High oxygen content increases the stability and the transition temperature (Duarte et al., 2014; Herbstritt, Kemen, Marx, & Gross, 2002). The critical temperatures of YBCO nanostructures and bulk samples range from 82 K to 92 K. The surface area of YBCO is greater than other nanostructure samples previously developed, and it is not dependent on calcination temperature.

Finally, the perfect conductors of the designed microwave filter circuits have been replaced by the superconductor YBCO thin films prepared by electrospinning and solid-state techniques using etching process. The YBCO thin films have been deposited on both sides of $LaAlO_3$ substrates (10×10 mm^2) using spin coating procedure. The microwave properties of YBCO filter have been determined using VNA (8 GHz– 12 GHz) at 300 K (room temperature) and 77 K. At 77 K, The YBCO filter made from the solid-state reaction has shown high return losses of -22 dB and -15 dB at frequencies of ~9.7 GHz and 10.8 GHz, respectively. These losses are lower than those simulated, while there is no response at 300 K. The electrospun YBCO filters have shown average return loss of -15 dB at ~10.2 GHz and -12 dB at 10.3 GHz. Again, these losses are lower than the simulated result. The

insertion losses are ~-2dB, ~-1.5 dB and ~-3 dB for the bulk and nanostructured YBCO filters, respectively, which are much lower than those of the electrospun YBCO filter and those of Lu *et al.* (Lu et al., 2015).

The bandwidth of the bulk filter is more than 1.5 GHz, while the bandwidths of nanostructured YBCO filters are almost similar (i.e. ~1.5 GHz) which are consistent with the simulated results. The small losses of YBCO sample at high frequency could produce the broad bandwidth of YBCO filters. Both simulation and experiment results of the frequency response characteristics of the microwave filters are consistent. However, the electrospun YBCO microwave filters exhibited lower performance than conventional YBCO powders derived through solid state reaction, due to the nano-structural properties of the former which leads to high surface resistance. Nevertheless, the best result has been achieved using the solid state reacted YBCO and the novel design. The results embodied in this thesis is promising directions to develop next-generation microwave filters.

CHAPTER 5

CONCLUSIONS AND RECOMMENDATIONS

5.1 Conclusions

This chapter summarizes the results of this work. The miniaturized microwave filter circuits of low losses and broad bandwidth has been developed. The superconducting YBCO nanostructures have been prepared via the electrospinning process. The YBCO thin films have been deposited using spin coating technique. The adopted microwave bandpass filter simulation model has been developed using the computer-aided design (CAD) software, namely the high frequency structural simulator (HFSS). A cascade design of four parallel-coupled lines deposited on high dielectric material $LaAlO_3$ substrate has been implemented to produce the miniaturized microwave bandpass filter operating at high frequency. The designed microwave bandpass filter has been synthesized from the thin films of YBCO superconductor nanoparticle, nanorod and normal structures prepared by the solid-state reaction method and the electrospinning process. The prepared YBCO nanostructures have been optimized using the electrospinning process, by forming precursors of (Y, Ba, Cu) acetates of different weight ratio solutions as well as with addition two types of polymer (PVP) having different molecular weights. The synthesized HTS YBCO samples have been characterized and measured using thermogravimetric analysis (TGA/DSC), X-ray diffraction (XRD) and field emission scanning electron microscopy (FESEM). The transition temperature (T_c) and the surface area have been determined via gas adsorption techniques (BET). Finally, the response of the microwave bandpass filter YBCO has been determined using VNA at different temperatures (i.e. 300 K and 77 K). Following are the conclusions will be made based on the research objectives in addition to aspects identified for the extension of this work and some future works will be recommended.

i. The physical dimensions of the microwave filter circuit components (i.e. the length, width (space between the lines) and thickness) are obtained based on the return loss method employing HFSS. Therefore, this procedure could save time, cost and reduce the number of experimentations. The surface resistance of YBCO is smaller than that for the normal conductors at high microwave frequencies and due to the lower losses of YBCO. Therefore, up on using four parallel couple line model it is possible to produce the miniaturized bandpass filter, while maintaining its excellent performance.

ii. By controlling the molecular weight of polymer and polymer to precursor weight ratio, various YBCO morphologies such as nanorods (NRs), nanogarlands (NGs), nanohierarchical (NH), nanoparticles (NPs) and agglomerated nanoparticles (ANPs) with relatively high surface area and porosity can be synthesized by employing the electrospinning process. The orthorhombic crystal structure in the electrospun YBCO samples can be produced by applying appropriate heat treatment procedure (annealing process) at elevated temperature in the presence of flowing oxygen. The T_c value of YBCO sample is dependent on surface area and oxygen contents. NH structures synthesized using low polymer molecular weight exhibit high critical temperature (T_c ~90 K) and small pore diameter (10 nm). Meanwhile, NRs synthesized using high polymer molecular weight exhibit lower T_c (T_c ~82 K) and large pore diameter (16 nm). NGs, however, contain the highest surface area (7.5 m^2/g) with intermediate Tc (Tc ~ 88 K). The surface area of ANPs is 6.8 m^2/g with T_c ~84 K. The current results are useful for designing advanced superconducting YBCO nanostructures for various superconducting electronic applications.

iii. The thin films of YBCO were deposited via two methods, i.e. the electrospinning process and spin coating techniques. Experimentally, these techniques are relativity not applicable 100% for depositing of the thin films structures such as YBCO nanostructures on $LaAlO_3$ substrates. However, the superconductivities of the thin film samples deposited by electrospinning process did not verified yet. This occurred due to the high surface area, which leads to increase the band gap. High surface area, high porosity and irregular grain boundary distribution can be realized by electrospinning technique.

iv. The superconducting properties of YBCO samples at nanoscale are dependent on their confining geometry and morphology shape. The oscillatory behaviour of YBCO nanostructures could be due to the change of band gap. The measured return loss is less than the simulated one, which is consistent with other works. This occurs due to the nanostructure of YBCO (high surface area), leading to increased band gaps, which is consistent with the literature. Therefore, the research question on how the superconducting properties in one-dimensional morphology differ from those of the three-dimensional counterpart has been answered. Moreover, both simulation and experiment results of the frequency response characteristics of the microwave filters are consistent, indicating that the filter design is reliable, and it can be applied in industry.

5.2 Future Recommendation

The following future works can be considered:

a) Fabrication of the microwave filter using YBCO nanostructured thin films deposited on MgO substrate. The same design of parallel microstrip lines can be used.

b) Deposit a thin layer (gold) on the top of YBCO nanostructured thin films of the filter. The measured performance can then be studied and compared with the current design.

c) Design and analyse a microwave bandpass filter with different software designer and compare the result with the current designed filter.

REFERENCES

Alikhanzadeh-Arani, S., Salavati-Niasari, M., & Almasi-Kashi, M. (2013). Influence of the utilized precursors on the morphology and properties of $YBa_2Cu_3O_{7-y}$ superconducting nanostructures. *Physica C: Superconductivity, 488*, 30-34.

Amado, J., & Sarmago, R. (2015). AC Magnetic Susceptibility and Morphological Development of YBCO HTS Formed from Y: Ba: Cu= 1: 2: 3 and 3: 5: 8. *Journal of Superconductivity and Novel Magnetism, 28*, 3455-3461.

Archana, P., Jose, R., Vijila, C., & Ramakrishna, S. (2009). Improved electron diffusion coefficient in electrospun TiO_2 nanowires. *The Journal of Physical Chemistry C, 113*(52), 21538-21542.

Arpaia, R. (2016). YBa2Cu3O7-[delta] Nanowires to Study Nanoscale Ordering in High-T_c Superconductors: *Thesis For The Degree of Doctor of Philosophy*, Department of Microtechnology and Nanoscience, Chalmers University of Technology.

Arpaia, R., Arzeo, M., Nawaz, S., Charpentier, S., Lombardi, F., & Bauch, T. (2014). Ultra low noise $YBa_2Cu_3O_{7-\delta}$ nano superconducting quantum interference devices implementing nanowires. *Applied Physics Letters*, 104, 072603.

Arpaia, R., Ejrnaes, M., Parlato, L., Tafuri, F., Cristiano, R., Golubev, D., Pepe, G. (2015). High-temperature superconducting nanowires for photon detection. *Physica C: Superconductivity and its Applications*, 509, 16-21.

Arpaia R., Nawaz S., Lombardi F.,Bauch T. (2013). Improved nanopatterning for YBCO nanowires approaching the depairing current. *IEEE transactions on applied superconductivity*, 23, 1101505-1101505.

Attwood, D., & Sakdinawat, A. (2017). X-rays and Extreme Ultraviolet Radiation: Principles and Applications: *books.google.com*. Cambridge university press.

Bai, D., Du, J., Zhang, T., & He, Y. (2013). A compact high temperature superconducting bandpass filter for integration with a Josephson mixer. *Journal of Applied Physics*, 114, 133906-133911.

Bai, D., He, X., Zhang, X., Li, H., Zhang, Q., Li, C., & He, Y. (2013). Design of an s-band HTS filter with high power capability. *IEEE transactions on applied superconductivity*, 23, 14-18.

Baji, A., Mai, Y.-W., Wong, S.-C., Abtahi, M., & Chen, P. (2010). Electrospinning of polymer nanofibers: effects on oriented morphology, structures and tensile properties. *Composites science and technology*, 70, 703-718.

Baquero, R. (2005). Brief Introduction to Superconductivity. *Section Book.* Departamento de Física, Cinvestav. 69.

Barnes, P. N., Murray, P. T., Haugan, T., Rogow, R., & Perram, G. P. (2002). In situ creation of nanoparticles from YBCO by pulsed laser deposition. *Physica C: Superconductivity*, 377, 578-584.

Barnes, P. N., Sumption, M. D., & Rhoads, G. L. (2005). Review of high power density superconducting generators: Present state and prospects for incorporating YBCO windings. *Cryogenics*, 45, 670-686.

Benzi, P., Bottizzo, E., & Rizzi, N. (2004). Oxygen determination from cell dimensions in YBCO superconductors. *Journal of Crystal Growth*, 269, 625-629.

Bezryadin, A., Lau, C., & Tinkham, M. (2000). Quantum suppression of superconductivity in ultrathin nanowires. *Nature*, 404, 971-974.

Bhardwaj, N., & Kundu, S. C. (2010). Electrospinning: a fascinating fiber fabrication technique. *Biotechnology advances*, 28, 325-347.

Bhattacharjee, S., Poddar, D., Mukherjee, S., Saurabh, S., & Das, S. (2013). Design of microstrip parallel coupled band pass filter for global positioning system. *Journal of Engineering, Computers & Applied Sciences (JEC&AS)*, 2, 28-32.

Callister Jr, William D, Rethwisch, David G (2012). Fundamentals of materials science and engineering: an integrated approach: *Book*. John Wiley & Sons NY.

Choi, J., Bhalodia, M., Samph, S., Snowden, P., Yahner, P., & Scoles, K. (1989). Processing and Diagnostics for Thick Film Superconductors Produced from Y-Ba-Cu-O Materials. *Microelectronics International, 6*, 17-22.

Chowdhury, N. T., & Chowdhury, D. (2014). Design and optimization of an UWB microstrip patch antenna using dielectric substrates Duroid 5880 And FR4. *Thesis for the degree of Bachelor of Science*. Department of Electrical and Electronic Engineering, BRAC University.

Chung, D.-C. (2000). HTS bandpass filters using parallel coupled microstrip-stepped impedance resonator. *Physica C: Superconductivity, 341*, 2659-2660.

Croitoru, MD Shanenko, AA Peeters, FM, (2007). Dependence of superconducting properties on the size and shape of a nanoscale superconductor: From nanowire to film. *Physical Review B*, 024511.

Cui, X. M., Lyoo, W. S., Son, W. K., Park, D. H., Choy, J. H., Lee, T. S., & Park, W. H. (2006). Fabrication of $YBa_2Cu_3O_{7-\delta}$ superconducting nanofibres by electrospinning. *Superconductor Science and Technology*, 19, 1264.

Curtz, N., Koller, E., Zbinden, H., Decroux, M., Antognazza, L., Fischer, Ø., & Gisin, N. (2010). Patterning of ultrathin YBCO nanowires using a new focused-ion-beam process. *Superconductor Science and Technology*, 23, 045015.

Dadras, S., & Ghavamipour, M. (2016). Investigation of the properties of carbon-base nanostructures doped $YBa_2Cu_3O_{7-\delta}$ high temperature superconductor. *Physica B: Condensed Matter*, 13-17. doi: https://doi.org/10.1016/j.physb.2015.12.025

Davidson, D. B. (2010). Computational electromagnetics for RF and microwave engineering: *Books.google.com.* Cambridge University Press.

DiNardo, A., Smith, J., & Arams, F. (1971). Superconducting Microstrip High-Q Microwave Resonators. *Journal of Applied Physics*, 42, 186-189.

Doshi, J., & Reneker, D. H. (1993). Electrospinning process and applications of electrospun fibers. Paper presented at the Industry Applications Society Annual Meeting, 1993., *Conference Record of the 1993 IEEE*.

Duarte, E. A., Rudawski, N. G., Quintero, P. A., Meisel, M. W., & Nino, J. C. (2014). Electrospinning of superconducting YBCO nanowires. *Superconductor Science and Technology*, 28, 015006.

Durrell, J. H., & Rutter, N. A. (2008). Importance of low-angle grain boundaries in $YBa_2Cu_3O_{7-\delta}$ coated conductors. *Superconductor Science and Technology*, 22, 013001.

Ellsworth, J. (2011). Graphics hot spot: Technology review printing digital heat transfers. *Printwear*, 24, 38-41.

Emeakaroha, T. M. (2016). Enhancement of Critical Current Density of Yttrium Barium Copper Oxide (YBCO) Thin Films by Introducing Nano dimensional Cerium oxide (CeO_2) Defects. *Thesis for the degree of Master of Science*. Department: Physics, North Carolina Agricultural and Technical State University.

Eom, C., Marshall, A., Suzuki, Y., Geballe, T., Boyer, B., Pease, R., Phillips, J. M. (1992). Growth mechanisms and properties of 90° grain boundaries in $YBa_2Cu_3O_{7-\delta}$ thin films. *Physical Review B*, 46, 11902.

Flanner, M. S. (2011). Microwave Filter Design: Coupled Line Filter. *Thesis for Master of Science*. California State University, Chico.

Frenot, A., & Chronakis, I. S. (2003). Polymer nanofibers assembled by electrospinning. *Current opinion in colloid & interface science*, 8, 64-75.

Garg, K., & Bowlin, G. L. (2011). Electrospinning jets and nanofibrous structures. *Biomicrofluidics*, 5, 013403.

Ghosh, A., Thomas, T. A., Cudak, M. C., Ratasuk, R., Moorut, P., Vook, F. W., Nie, S. (2014). Millimeter-wave enhanced local area systems: A high-data-rate approach for future wireless networks. *IEEE Journal on Selected Areas in Communications*, 32(6), 1152-1163. doi: 10.1109/JSAC.2014.2328111

Goldstein, J., Newbury, D. E., Echlin, P., Joy, D. C., Romig Jr, A. D., Lyman, C. E., Lifshin, E. (2012). Scanning electron microscopy and X-ray microanalysis: a text for biologists, materials scientists, and geologists: *Books.google.com*. Springer Science & Business Media.

Golubev, D., Lombardi, F., & Bauch, T. (2014). Effect of heating on critical current of YBCO nanowires. *Physica C: Superconductivity and its Applications, 506*, 174-177.

Greenberg, Y., Lumelsky, Y., Silverstein, M., & Zussman, E. (2008). YBCO nanofibers synthesized by electrospinning a solution of poly (acrylic acid) and metal nitrates. *Journal of Materials Science,* 43, 1664-1668.

Gunjal, S. R., Pawase, R., & Labade, R. (2016). Design And Implementation Of Microstrip Bandpass Filter Using Parallel Coupled Line For ISM Band. *International Journal of Advance Research and Innovative Ideas in Education,* 2, 3056 - 3036.

Gupta, A. G. V. (2015). Design of bpf using interdigital bandpass filter on center frequency 3ghz. *International journal of research review in engineering science & technology,* 4, 135 - 139.

Harilal, M., Krishnan, S. G., Vijayan, B. L., Reddy, M. V., Adams, S., Barron, A. R., Jose, R. (2017). Continuous nanobelts of nickel oxide–cobalt oxide hybrid with improved capacitive charge storage properties. *Materials & Design,* 122, 376-384.

Hein, M. A. (2011). Microwave properties of superconductors. Microwave Superconductivity. *Book section.* (pp. 21-53): Springer.

Herbstritt, F., Kemen, T., Marx, A., & Gross, R. (2002). Ultraviolet light assisted oxygenation process for submicron $YBa_2Cu_3O_{7-\delta}$ thin film devices. *Journal of Applied Physics,* 91, 5411-5418.

Higuchi, T., Sakai, N., Murakami, M., & Hashimoto, M. (1995). Critical Current Density Estimation of YBCO by Trapped Field Measurement Using a Hall Probe *Advances in Superconductivity. Book section. VII* (pp. 423-426): Springer.

Howe, B. A. (2014). Crystal structure and superconductivity of $YBa_2Cu_3O_{7-x}$. Thesis for Master of Science. Physics Department, Minnesota State University.

Huebener, R. P. (2015). The Big Surprise: High-Temperature Superconductivity *Conductors, Semiconductors, Superconductors. Book section.* (pp. 131-144): Springer.

Izumi, T., & Shiohara, Y. (2010). R&D of coated conductors for applications in Japan. *Physica C: Superconductivity*, 470, 967-970.

Jin Yu, Yang Dayong, Kang Dongyang, Jiang Xingyu (2009). Fabrication of necklace-like structures via electrospinning. *Langmuir,* 26, 1186-1190.

Jing, D., Shao, K., Cao, C., Zhang, L., Jiao, G., Zhang, Z., Wang, X. (1994). 10 GHz bandpass YBCO superconducting microstrip filter. *Superconductor Science and Technology,* 7, 792-799.

Khalil, K. A., Sherif, E.-S. M., Nabawy, A., Abdo, H. S., Marzouk, W. W., & Alharbi, H. F. (2016). Titanium Carbide Nanofibers-Reinforced Aluminum Compacts, a New Strategy to Enhance Mechanical Properties. *Materials,* 9, 399-402.

Klobes, P., Meyer, K., & Munro, R. G. (2006). Porosity and specific surface area measurements for solid materials. *Book.* Special Publication 960-17. Materials Science and Engineering Laboratory,National Institute of Standards and Technology.

Kolodziej, C. M., & Maynard, H. D. (2012). Electron-beam lithography for patterning biomolecules at the micron and nanometer scale. *Chemistry of materials*, 24, 774-780.

Kullberg, M., Lanagan, M., Wu, W., & Poeppel, R. (1991). A sol-gel method for preparing oriented $YBa_2Cu_3O_{7-delta}$ films on silver substrates. *Superconductor Science and Technology*, 4, 337-341.

Lancaster, M. J., Huang, F., Porch, A., Avenhaus, B., Hong, J.-S., & Hung, D. (1996). Miniature superconducting filters. *IEEE transactions on microwave theory and techniques*, 44, 1339-1346.

Jing Yu Lao, Jian Guo Wen, and Zhi Feng Ren (2002). Hierarchical ZnO nanostructures. *Nano Letters*, 2, 1287-1291.

Lawrence, K. L. (2012). ANSYS Tutorial*: Book. Release 14*: SDC publications.

Lee, H.-H. (2015). Finite element simulations with ANSYS workbench 16: *Book.* SDC publications.

Lee, J. S. (2009). Microwave resonator filters for advanced wireless systems.*Thesis for degree of Doctor of Philosophy*. Electrical Engineering, University of Michigan.

Lee, J. S., Choi, K. H., Ghim, H. D., Kim, S. S., Chun, D. H., Kim, H. Y., & Lyoo, W. S. (2004). Role of molecular weight of atactic poly (vinyl alcohol)(PVA) in the structure and properties of PVA nanofabric prepared by electrospinning. *Journal of Applied Polymer Science*, 93, 1638-1646.

Lee, K., Mazare, A., & Schmuki, P. (2014). One-dimensional titanium dioxide nanomaterials: nanotubes. *Chemical Reviews*, 114, 9385-9454.

Li, D., & Xia, Y. (2004). Electrospinning of nanofibers: reinventing the wheel? *Advanced materials*, 16, 1151-1170.

Liu, A., Yu, A., & Zhang, Q. (2006). Broad-band band-pass and band-stop filters with sharp cut-off frequencies based on series CPW stubs. *Paper presented at the Microwave Symposium Digest*, 2006. IEEE MTT-S International.

Liu, H., Rao, L., Xu, Y., Wen, P., Ren, B., Guan, X., Ma, J. (2017). Design of High-Temperature Superconducting Wideband Bandpass Filter With Narrow-Band Notch Resonators for Radio Telescope Application. *IEEE transactions on applied superconductivity*, 27, 1-4.

Lu, X., Wei, B., Xu, Z., Cao, B., Guo, X., Zhang, X., Song, F. (2015). Superconducting Ultra-Wideband (UWB) Bandpass Filter Design Based on Quintuple/Quadruple/ Triple-Mode Resonator. *IEEE transactions on microwave theory and techniques*, *63*(4), 1281-1293. doi: 10.1109/TMTT.2015.2402152

Lu, X., Wei, B., Xu, Z., Cao, B., Guo, X., Zhang, X., Song, F. (2015). Superconducting Ultra-Wideband (UWB) Bandpass Filter Design Based on Quintuple/Quadruple/Triple-Mode Resonator. *IEEE transactions on microwave theory and techniques*, 63, 1281-1293.

Luo, Q.-w., Li, Y.-n., Li, F.-h., & Fan, Z.-g. (2014). Preparation of $YBa_2Cu_3O_{7-\delta}$ superconducting thick film on Ni-W tapes via electrophoretic deposition. *Transactions of Nonferrous Metals Society of China*, 24, 120-125.

Ma, B., Koritala, R., Fisher, B., Uprety, K., Baurceanu, R., Dorris, S., Balachandran, U. (2004). High critical current density of YBCO coated conductors fabricated by inclined substrate deposition. *Physica C: Superconductivity*, 403, 183-190.

Mansour, R. R. (2002). Microwave superconductivity. *Microwave Theory and Techniques, IEEE Transactions on*, 50, 750-759.

Marimuthu, J. (2004). Design of Microwave Bandpass Filter with Novel Parallel Coupled Grooved Microstrip Structure. *Master's Thesis, unpublished dissertation, Universiti Technologi Malaysia*.

Mohajeri, R., Opata, Y. A., Wulff, A. C., Grivel, J.-C., & Fardmanesh, M. (2016). All Metal Organic Deposited High-Tc Superconducting Transition Edge Bolometer on Yttria-Stabilized Zirconia Substrate. *Journal of Superconductivity and Novel Magnetism*, 1-6.

Montemurro, D., Massarotti, D., Lucignano, P., Roddaro, S., Stornaiuolo, D., Ercolani, D., Tafuri, F. (2015). Towards a Hybrid High Critical Temperature Superconductor Junction With a Semiconducting InAs Nanowire Barrier. *Journal of Superconductivity and Novel Magnetism*, 28, 3429-3437.

Mukesh Kumar, S. K. (2014). Designing of Half Wavelength Parallel- Edge Coupled Line Bandpass Filter Using HFSS. *International Journal of Advanced Research in Computer Science and Software Engineering*, 4, 876-882.

Muralidhar, M., Sakai, N., Machi, T., Hirabayashi, I., & Tanaka, S. (2007). Potentials of RE- $YBa_2Cu_3O_6$ in the silver base technology. *Physica C: Superconductivity and its Applications*, 463, 314-319.

Nawaz, S., Arpaia, R., Bauch, T., & Lombardi, F. (2013). Approaching the theoretical depairing current in $YBa_2Cu_3O_{7-x}$ nanowires. *Physica C: Superconductivity*, 495, 33-38.

Newman, N., & Lyons, W. G. (1993). High-temperature superconducting microwave devices: fundamental issues in materials, physics, and engineering. *Journal of Superconductivity*, 6, 119-160.

Nirmala, R., Navamathavan, R., Park, S.-J., & Kim, H. Y. (2014). Recent progress on the fabrication of ultrafine polyamide-6 based nanofibers via electrospinning: a topical review. *Nano-Micro Letters*, 6, 89-107.

Nisenoff, M. (2011). Microwave superconductivity part 1: History, properties and early applications. *Paper presented at the Microwave Symposium Digest (MTT)*, 2011 IEEE MTT-S International.

Nur-Akasyah, J., Nur-Shamimie, N., & Abd-Shukor, R. (2017). Effect of CdTe Addition on the Electrical Properties and AC Susceptibility of $YBa_2Cu_3O_{7-\delta}$ Superconductor. *Journal of Superconductivity and Novel Magnetism*, 1-5.

Pal, Shreyasi Maiti, Soumen Maiti, Uday Narayan Chattopadhyay, Kalyan Kumar (2014). Scalable approach for the realization of garland shaped 3D assembly of CuTCNQ nanorods: an efficient electron emitter. *Journal of Materials Chemistry C*, 2, 4005-4011.

Papari, G., Carillo, F., Stornaiuolo, D., Longobardi, L., Beltram, F., & Tafuri, F. (2012). High critical current density and scaling of phase-slip processes in $YBa_2Cu_3O_{7-\delta}$ nanowires. *Superconductor Science and Technology*, 25, 035011.

Paranthaman, M. P., & Izumi, T. (2004). High-performance YBCO-coated superconductor wires. *MRS bulletin*, 29, 533-541.

Park, J. Y., Lee, I. H., & Bea, G. N. (2008). Optimization of the electrospinning conditions for preparation of nanofibers from polyvinylacetate (PVAc) in ethanol solvent. *Journal of Industrial and Engineering Chemistry*, 14, 707-713.

Pashkin, A., Porer, M., Beyer, M., Kim, K. W., Dubroka, A., Bernhard, C., Erb, A. (2010). Femtosecond response of quasiparticles and phonons in superconducting $YBa_2Cu_3O_{7-\delta}$ studied by wideband terahertz spectroscopy. *Physical review letters*, 105, 067001.

Poole, C. K., Farach, H. A., & Creswick, R. J. (1999). *Handbook of superconductivity*: Elsevier.

Ramaseshan, R., Sundarrajan, S., Jose, R., & Ramakrishna, S. (2007). Nanostructured ceramics by electrospinning. *Journal of Applied Physics*, 102, 111101-111109.

Reneker, D. H., & Yarin, A. L. (2008). Electrospinning jets and polymer nanofibers. *Polymer*, 49, 2387-2425.

Ribadeneira-Ramírez, J., Martínez, G., Gomez-Barquero, D., & Cardona, N. (2016). Interference analysis between digital terrestrial television (DTT) and 4G LTE mobile networks in the digital dividend bands. *IEEE Transactions on Broadcasting*, 62, 24-34.

Rius Suñé, G., Pérez Murano, F., & Bausells Roige, J. (2008). Electron beam lithography for nanofabrication: *Book*. Facultat de Ciències, Departament de Física. Bellaterra : Universitat Autònoma de Barcelona, 2008.

Romanenko, A., & Grassellino, A. (2013). Dependence of the microwave surface resistance of superconducting niobium on the magnitude of the rf field. *Applied Physics Letters*, 102, 252603.

Salama, A., El-Hofy, M., Rammah, Y., & Elkhatib, M. (2015). Effect of magnetic and nonmagnetic nano metal oxides doping on the critical temperature of a YBCO superconductor. *Advances in Natural Sciences: Nanoscience and Nanotechnology*, 6, 045013.

Salama, K., Selvamanickam, V., Gao, L., & Sun, K. (1989). High current density in bulk YBa2Cu3Ox superconductor. *Applied Physics Letters*, 54, 2352-2354.

Sawicka, K. M., & Gouma, P. (2006). Electrospun composite nanofibers for functional applications. *Journal of Nanoparticle Research*, 8, 769-781.

Schlosser, R., Schmidt, H., Leghissa, M., & Meinert, M. (2003). Development of high-temperature superconducting transformers for railway applications. *Applied Superconductivity, IEEE Transactions on*, 13, 2325-2330.

Shang, Z., Guo, X., Cao, B., Zhang, X., Wei, B., Heng, Y., Li, Q. (2013). Design and performance of an HTS wideband microstrip bandpass filter at X-band. *Microwave and Optical Technology Letters*, 55, 1027-1029.

Sharma, G., Navin, P. S., Bhati, Y., & Walia, Y. (2013). Half-wavelength parallel edge coupled filter simulation using Matlab. *International Journal of Innovative Research in Computer and Communication Engineering*, 1, 248-253.

Shen, Z., Hu, Y., Fei, L., Li, K., Chen, W., Gu, H., & Wang, Y. (2015). Photocatalytically Active $YBa_2Cu_3O_{7-x}$ Nanoparticles Synthesized via a Soft Chemical Route. *Journal of Nanomaterials*. Hindawi Publishing Corporation. 2015, 1-5.

Shen, Z., Wang, Y., Chen, W., Fei, L., Li, K., Chan, H. L. W., & Bing, L. (2013). Electrospinning preparation and high-temperature superconductivity of $YBa_2Cu_3O_{7-x}$ nanotubes. *Journal of Materials Science*, 48, 3985-3990.

Shen, Z. Y. (1994). High-temperature superconducting microwave circuits. *Google Books.* Artech House microwave library. 272.

Shivhare, J. (2008). Design and development of low loss microstrip band pass filters by using YBCO-high temperature superconducting thin film. *International Conference on Recent Advances in Microwave Theory and Applications, Microwave 2008.*, IEEE. 382-383.

Shter, G., Schwartzman, A., & Grader, G. (1995). Interrelation of calcination temperature, surface area and densification of oxalate-derived YBCO. *Applied superconductivity*, 3, 543-550.

Shter, G. E., & Grader, G. S. (1994). YBCO oxalate coprecipitation in alcoholic solutions. *Journal of the American Ceramic Society*, 77, 1436-1440.

Sigmund, W., Yuh, J., Park, H., Maneeratana, V., Pyrgiotakis, G., Daga, A., . . . Nino, J. C. (2006). Processing and structure relationships in electrospinning of ceramic fiber systems. *Journal of the American Ceramic Society*, 89, 395-407.

Sing, K. S. (1985). Reporting physisorption data for gas/solid systems with special reference to the determination of surface area and porosity (Recommendations 1984). *Pure and applied chemistry*, 57, 603-619.

Singh, M., Wang, J., & Sun, Y. (2012). Superconductivity in nanoscale systems: *Section Book*. Center for Nanoscale Science & Department of Physics, The Pennsylvania State University, University Park,USA. INTECH Open Access Publisher.

Sun, L. P. (2011). Dual-Mode Dual-Band Microstrip Bandpass Filter. *A project report for the award of Bachelor of Engineering*. Faculty of Engineering and Science, Universiti Tunku Abdul Rahman.

Suzuki, M. (2012). Comprehensive study of lanthanum aluminate high-dielectric-constant gate oxides for advanced CMOS devices. *Materials*, 5, 443-477.

Tan, A. W., Pingguan-Murphy, B., Ahmad, R., & Akbar, S. A. (2013). Advances in fabrication of TiO_2 nanofiber/nanowire arrays toward the cellular response in biomedical implantations: a review. *Journal of Materials Science*, 48, 8337-8353.

Tekmen, C., Suslu, A., & Cocen, U. (2008). Titania nanofibers prepared by electrospinning. *Materials Letters*, 62, 4470-4472.

Thommes, M., Kaneko, K., Neimark, A. V., Olivier, J. P., Rodriguez-Reinoso, F., Rouquerol, J., & Sing, K. S. (2015). Physisorption of gases, with special reference to the evaluation of surface area and pore size distribution (IUPAC Technical Report). *Pure and applied chemistry*, 87, 1051-1069.

Thompson, M., Ellison, S. L., & Wood, R. (2006). The international harmonized protocol for the proficiency testing of analytical chemistry laboratories (IUPAC Technical Report). *Pure and applied chemistry*, 78, 145-196.

Toossi, A., Moghadas, H., Daneshmand, M., & Sameoto, D. (2015). Bonding PMMA microfluidics using commercial microwave ovens. *Journal of Micromechanics and Microengineering*, 25, 085008.

Ushakov, S. V., & Navrotsky, A. (2014). Direct Measurement of Fusion Enthalpy of LaAlO3 and Comparison of Energetics of Melt, Glass, and Amorphous Thin Films. *Journal of the American Ceramic Society*, 97, 1589-1594.

Uslu, I., Kemal Ozturk, M., Levent Aksu, M., & Gokmese, F. (2010). Fabrication and characterization of boron supported YBCO superconductive nanofibers by electrospinning. *Current Nanoscience*, 6, 408-412.

Valizadeh, A., & Farkhani, S. M. (2014). Electrospinning and electrospun nanofibres. *Nanobiotechnology, IET*, 8, 83-92.

Van Delft Dirk. (2012). History and significance of the discovery of superconductivity by Kamerlingh Onnes in 1911. *Physica C: Superconductivity*, 479, 30-35.

Wali, Q. (2016). Nanostructured tin oxide materials as photoanode for dye sensitized solar cells. *Thesis for degree of doctor pholosiphy*. Faculty of Industrial Scince & Technology, Universiti malaysia pahang.

Wali, Q., Fakharuddin, A., Ahmed, I., Ab Rahim, M. H., Ismail, J., & Jose, R. (2014). Multiporous nanofibers of SnO2 by electrospinning for high efficiency dye-sensitized solar cells. *Journal of Materials Chemistry A*, 2, 17427-17434.

Walliman, D. C. (2010). Fabrication and measurement of superconducting nanowires. *Thesis for degree of doctor pholosiphy*. College of Engineering & Physical Sciences, University of Birmingham.

Wang, L., Hsieh, C.-H., & Chang, C.-C. (2005). Cross-coupled narrow-band filter for the frequency range of 2.1 GHz using YBCO resonators with artificial magnetic pinning lattices. *IEEE transactions on applied superconductivity*, 15, 1040-1043.

Wei, X., Peng, E., Xie, Y., Xue, J., Wang, J., & Ding, J. (2017). Extrusion printing of a designed three-dimensional $YBa_2Cu_3O_{7-x}$ superconductor with milled precursor powder. *Journal of Materials Chemistry C*. 5, 3382-3389

Weigel, R., Valenzuela, A., & Russer, P. (1993). YBCO superconducting microwave components. *Applied Superconductivity*, 1, 1595-1604.

Weinstock, H., & Nisenoff, M. (2012). Microwave superconductivity. *Books.google.com* (Vol. 375): Springer Science & Business Media.

Wijeyesekera, D., Ho, M., Bai, X., & Bakar, I. (2016). Strength and Stiffness Development in Soft Soils: A FESEM aided Soil Microstructure Viewpoint. *Paper presented at the IOP Conference Series*: Materials Science and Engineering.

Wu, H., Pan, W., Lin, D., & Li, H. (2012). Electrospinning of ceramic nanofibers: fabrication, assembly and applications. *Journal of Advanced Ceramics*, 1, 2-23.

Xu, K., & Heath, J. R. (2008). Long, highly-ordered high-temperature superconductor nanowire arrays. *Nano Letters*, 8, 3845-3849.

Yao, P.-J., Wang, J., Qiao, Q., & Du, H.-y. (2015). Direct fabrication of $La_{0.7}Sr_{0.3}FeO_3$ nanofibers with tunable hollow structures by electrospinning and their gas sensing properties. *Journal of Materials Science*, 50, 1338-1349.

Zaleski, T., & Kopeć, T. (2006). Possible origin of 60− K plateau in the $YBa_2Cu_3O_{6+y}$ phase diagram. *Physical Review B*, 74, 014504-014509.

Zayer, M. Q. (2016). The improvement of the physical properties of indium tin oxide thin film through annealing process. *Thesis for the degree of Doctor of Philosophy*. Faculty of Industrail Scince & Technology, Universiti malaysia pahang.

Zhan, S., Chen, D., Jiao, X., & Tao, C. (2006). Long TiO_2 hollow fibers with mesoporous walls: sol-gel combined electrospun fabrication and photocatalytic properties. *The Journal of Physical Chemistry B*, 110, 11199-11204.

Zhang, G., Lu, X., Zhang, T., Qu, J., Wang, W., Li, X., & Yu, S. (2006). Microstructure and superconductivity of highly ordered $YBa_2Cu_3O_{7-\delta}$ nanowire arrays. *Nanotechnology*, 17, 4252-4259.

Zhang, T., Du, J., Guo, Y. J., & Sun, X.-W. (2012). On-chip integration of HTS bandpass and lowpass filters with Josephson mixer. *Electronics letters*, 48, 729-731.

Zhang, T., Du, J., Guo, Y. J., & Sun, X. (2013). A compact HTS bandpass microstrip filter with novel coupling structure for on-chip integration. *Physica C: Superconductivity*, 495, 69-73.

Zhang, T., Yang, K., Zhu, H., Zhou, L., Jiang, M., Dang, W., Hou, F. (2015). Miniaturized HTS linear phase filter based on neighboring CQ units sharing resonators. *Superconductor Science and Technology*, 28, 105012-105016.

Zhang, T., Zhou, L., Yang, K., Luo, C., Jiang, M., Dang, W., & Ren, X. (2015). The research of parallel-coupled linear-phase superconducting filter. *Physica C: Superconductivity and its Applications*, 519, 153-158.

Zhang, Y. (2006). Modeling and design of microwave-millimeterwave filters and multiplexers. *Thesis for the degree of Doctor of Philosophy*. Faculty of the Graduate School, University of Maryland, College Park.

Zhao, Z., Chen, L., Yang, Q., Huang, Y., Chen, G., Tang, R., Wang, L. (1987). Superconductivity above liquid-nitrogen temperature in Ba-Y-Cu oxides. *Kexue Tongbao*, 32, 661-664.

Zueger, H. (1998). 630kVA high temperature superconducting transformer. *Cryogenics*, 38, 1169-1172.

APPENDIX A
PUBLICATIONS

Paper submitted to Scopus and ISI journals

1. In brief the superconducting YBCO nanowires review (Indian Journal of Pure & Applied Physics_ 17-05-2017).
2. Effect of processing parameters on the morphology, particulate, and superconducting properties of electrospun YBCO nanostructures (Materials Chemistry and Physics_31-08-2017).
3. Fabrication of superconducting YBCO agglomerated particles by electrospinning (Journal of experimental and theoretical nanotechnology specialise research_27-09-2017).

Journals and conference paper (published Scopus index)

1. Finding the Best Feeding Point Location of Patch Antenna using HFSS, ARPN Journal of Engineering and Applied Sciences, 2015.
2. Fabrication of Superconducting YBCO Nanoparticles by Electrospinning, Procedia Engineering, 2016.
3. A Review of Process Parameters and Morphology of HTS YBCO by Electrospinning, 3rd National Conference for Postgraduate Research (NCON-PGR 2016).
4. Design Broad Bandwidth Microwave Bandpass Filter of 10 GHz Operating Frequency Using HFSS, International Conference on Science, Innovation and Management (ICSIM), Putrajaya, Malaysia, 4th-5th September 2017.
5. Low loss microwave Bandpass Filter using Superconducting Electrospun YBCO Nanostructures (Progress in Electromagnetics Research Letters_January_2018).

6. Design of 2.5 GHz Broad Bandwidth Microwave Bandpass Filter at Operating Frequency of 10 GHz Using HFSS (ICITES 2018 – International Conference on Innovative Technology, Engineering and Sciences_1-3_March_2018).

APPENDIX B

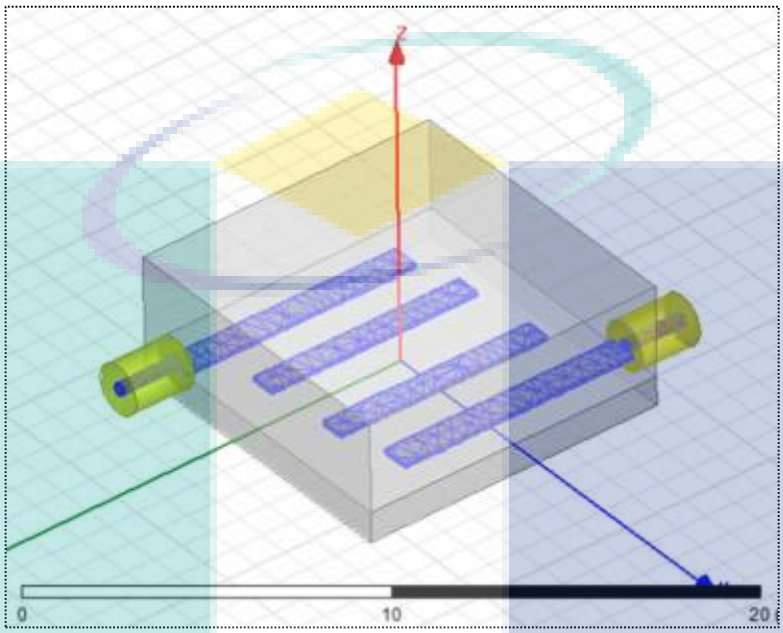

Figure B-1 The image of mesh operation for bandpass filter from the software HFSS.

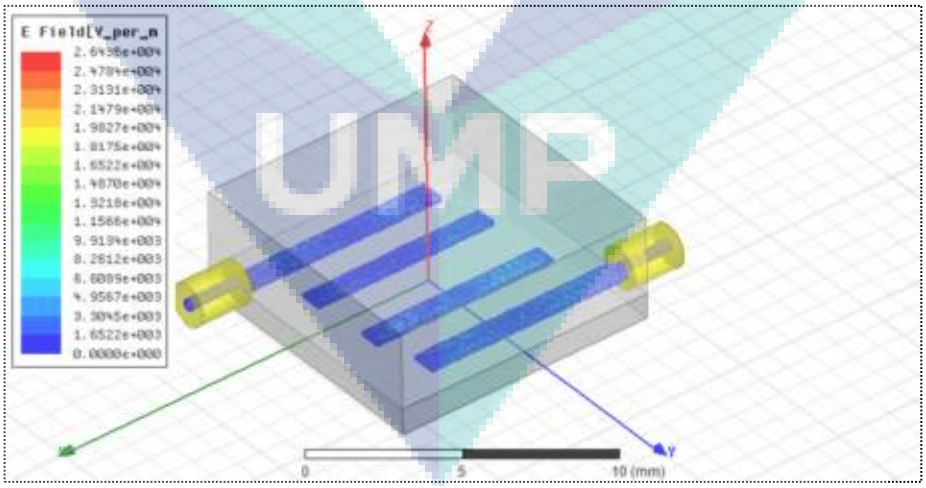

Figure B-2 The image of mesh operation and electric field for bandpass filter from the software HFSS.

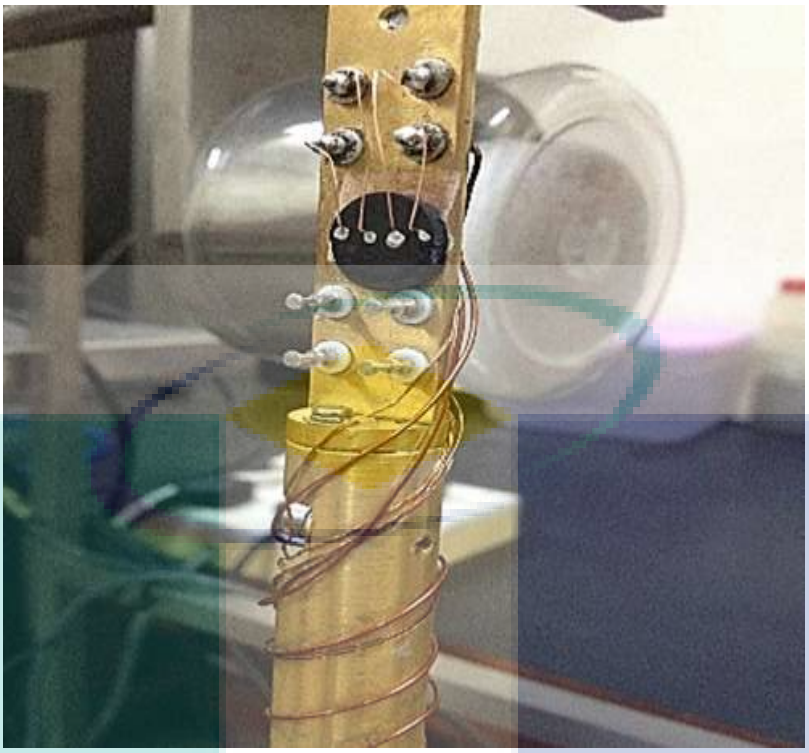

Figure B-3 Four-point probe used to measure the transition temperature of YBCO bulk sample.

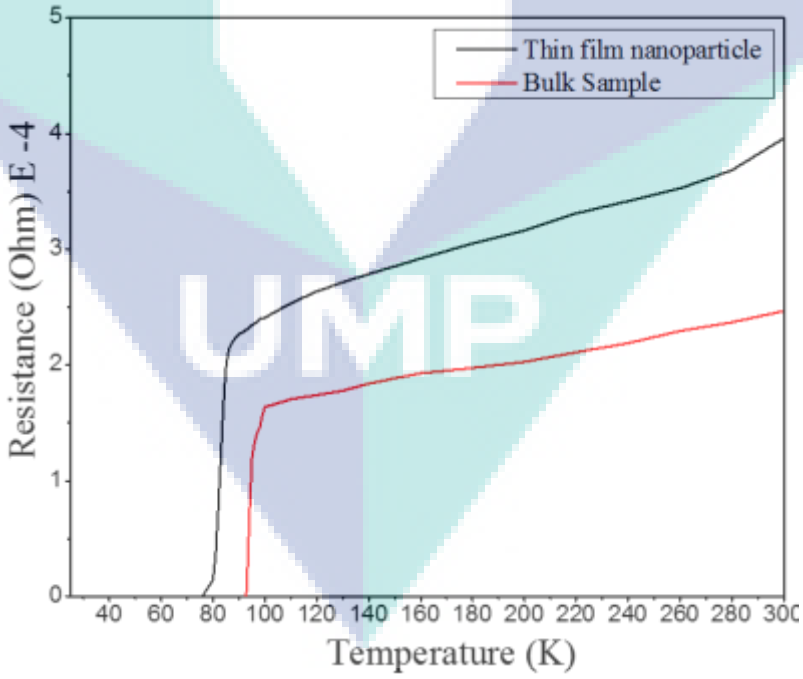

Figure B-4 The Tc measurements of the thick film nanoparticles and bulk palette of YBCO samples.

Table B-1 The calculated average crystallite size of YBCO samples corresponding to their structures and the two theta angles of diffraction of the highest peaks.

Sample	Structure	2θ (deg)	hkl	d-spacing	FWHM (deg)	Crystallite (nm)
1	NRs	23.05	100	3.85	0.24	35.30
		32.75	013	2.73	0.25	34.61
		33.04	103	2.70	0.16	52.16
		38.67	041	2.32	0.35	25.13
		40.59	113	2.22	0.14	63.22
		46.81	020	1.93	0.30	30.15
		47.76	021	1.90	0.25	36.31
		58.41	123	1.57	0.26	36.58
		58.96	213	1.56	0.31	30.76
		68.28	026	1.37	0.39	25.72
		69.04	018	1.35	0.33	30.53
2	NGs	22.90	003	3.87	0.14	57.61
		32.64	013	2.74	0.19	45.52
		32.92	103	2.71	0.17	50.03
		38.62	005	2.32	0.17	49.41
		40.45	113	2.22	0.14	61.01
		46.71	020	1.94	0.19	46.85
		47.64	200	1.90	0.2	45.37
		58.29	123	1.58	0.2	47.52
		58.9	213	1.58	0.2	47.67
		68.18	026	1.37	0.14	71.60
		68.94	018	1.36	0.30	33.57
3	NPs	22.82	101	3.89	0.18	47.04
		32.55	013	2.74	0.27	32.03
		32.79	103	2.72	0.15	57.30
		38.51	104	2.33	0.17	49.96
		40.33	113	2.23	0.11	74.31
		46.58	015	1.94	0.25	36.15
		47.47	201	1.91	0.30	30.23
		58.17	024	1.58	0.21	45.23
		58.17	116	1.57	0.29	32.85
4	NH	22.8	003	3.88	0.19	44.57
		32.61	013	2.74	0.28	30.45
		32.88	103	2.72	0.13	62.53
		38.57	005	2.33	0.13	67.65
		40.4	113	2.23	0.12	73.71
		46.60	020	1.94	0.16	56.49
		47.55	200	1.91	0.22	40.86
		58.24	123	1.58	0.22	43.19
		58.81	213	1.56	0.28	33.44
		68.17	026	1.37	0.13	77.11
		68.84	018	1.36	0.23	42.46
5	ANPs	22.74	003	3.90	0.26	32.56
		32.48	013	2.75	0.29	29.81
		32.71	111	2.73	0.16	51.19
		38.38	005	2.34	0.36	23.88
		40.24	113	2.23	0.15	57.41
		46.91	020	1.93	0.30	30.16
		47.38	200	1.91	0.31	29.24

		58.08	116	1.58	0.32	29.67
		58.59	213	1.57	0.23	41.39
		68.02	220	1.37	0.17	58.91
		68.70	018	1.36	0.38	26.46
6	Bulk	22.84	003	3.89	0.20	42.34
		32.55	013	2.74	0.21	41.18
		32.80	103	2.72	0.17	49.16
		38.51	005	2.33	0.40	21.98
		40.32	113	2.23	0.14	63.16
		46.63	006	1.94	0.27	33.48
		47.38	200	1.91	0.27	33.57
		58.17	116	1.58	0.25	38.00
		58.66	213	1.57	0.28	34.01
		68.08	026	1.37	0.22	45.54
		68.72	018	1.36	0.36	27.94

Table B-2 The component of the designed microwave bandpass filter system.

NO.	The designed part	The Number	Assigned material
1	Air body (enclosure contains the filter)	1	Vacuum
2	Feed1 (Coax outer diameter)	2	Vacuum
3	Feedpin1 (Coax inner diameter)	2	Perfect conductor
4	Substrate ($LaAlO_3$)	1	Dielectric material
5	Ground plane	1	Perfect conductor
6	Resonators (lines)	4	Perfect conductor

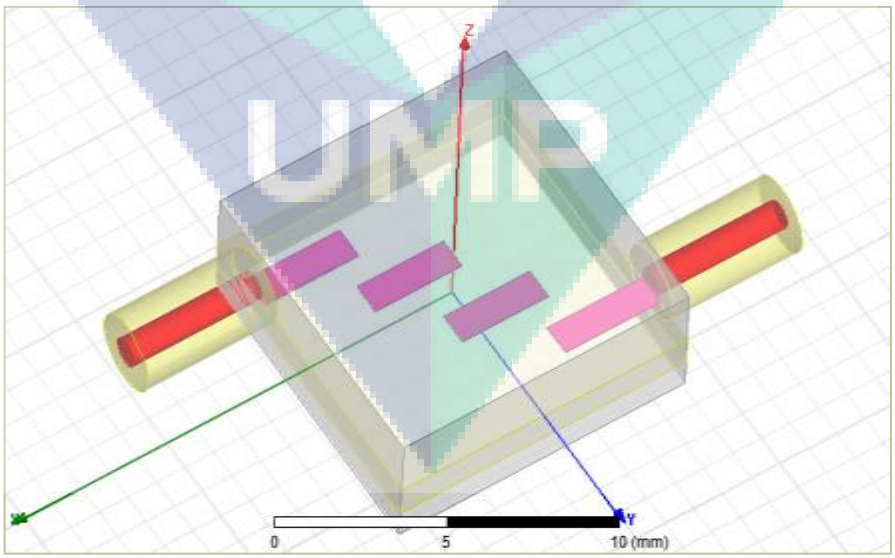

Figure B-5 The image of the designed microwave bandpass filter circuit from the HFSS software.

Table B-3 Adaptive solution in the HFSS software.

Sweep type	Maximum number of pass	Maximum Delta
fast	15	0.01

Table B-4 The frequency setup details in the HFSS software

Start frequency	Stop frequency	Step Size
8.0 GHz	12.0 GHz	0.001

Table B-5 The designed part dimensions of the bandpass filter.

The designed part	The Dimension (mm^2)	The high (mm)
Feed1 (Coax Outer Diameter)	1.2 (in Radius)	4.5
Feedpin1 (Coax Inner Diameter)	0.45 (in Radius)	4.5
Substrate ($LaAlO_3$)	10 × 10 (in Area)	1.0
L1 Resonator	3.3 × 1.0	0.05
L2 Resonator	3.0 × 1.0	0.05

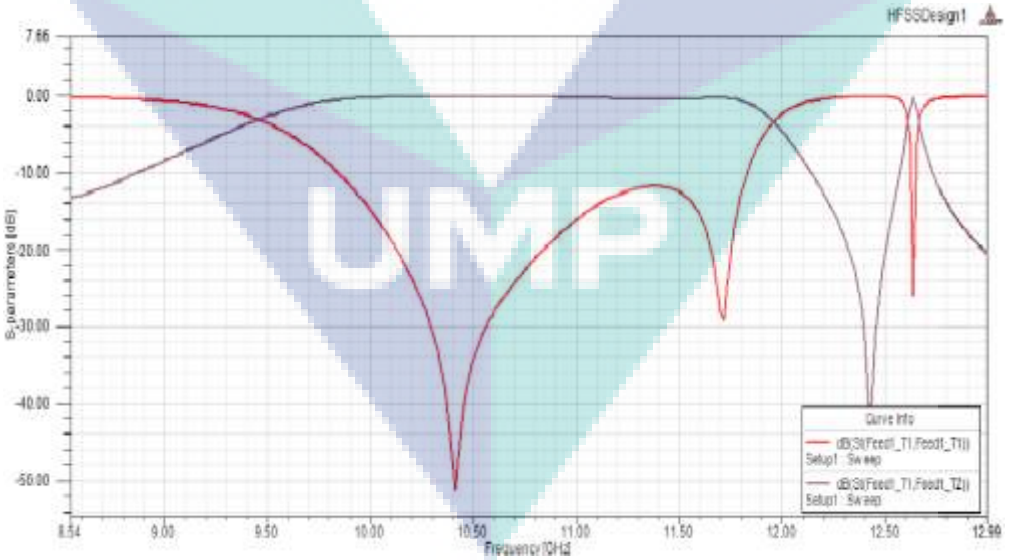

Figure B-6 HFSS plot of the S-parameters versus frequency with broad bandwidth 2.5 GHz and the frequency centre 10 GHz.

Table B-6 The samples morphology and synthesis process of the designed filters.

NO.	Filter Sample	Morphology	Synthesis process
1	(1a)	Nanoparticle	Electrospinning
2	(1b)	Nanoparticle	Electrospinning
3	(2a)	Nanorod	Electrospinning
4	(2b)	Nanorod	Electrospinning
5	(3)	Bulk	Solid state

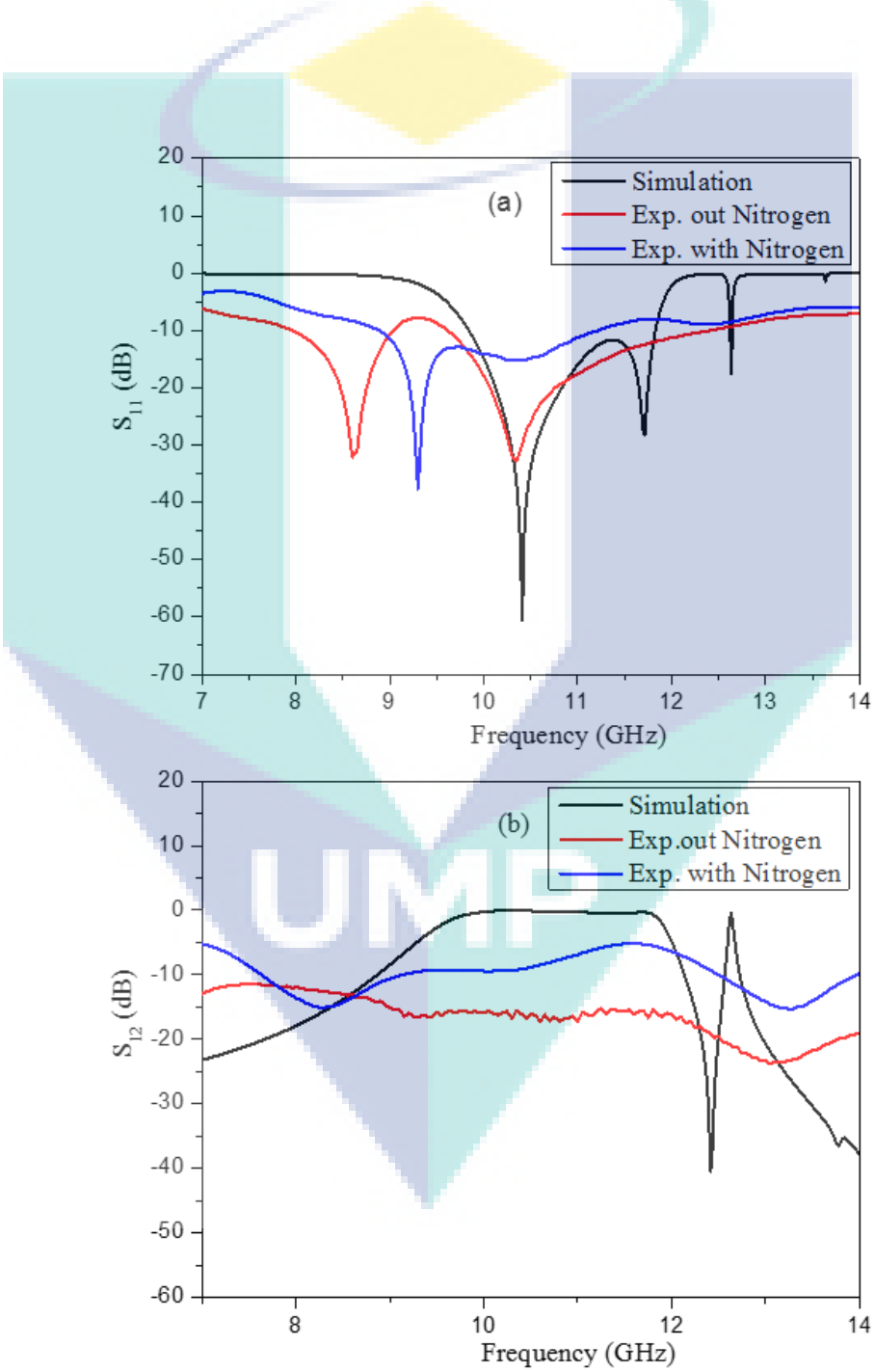

Figure B-7 Simulation and experiment results for the HTS YBCO sample 1a.

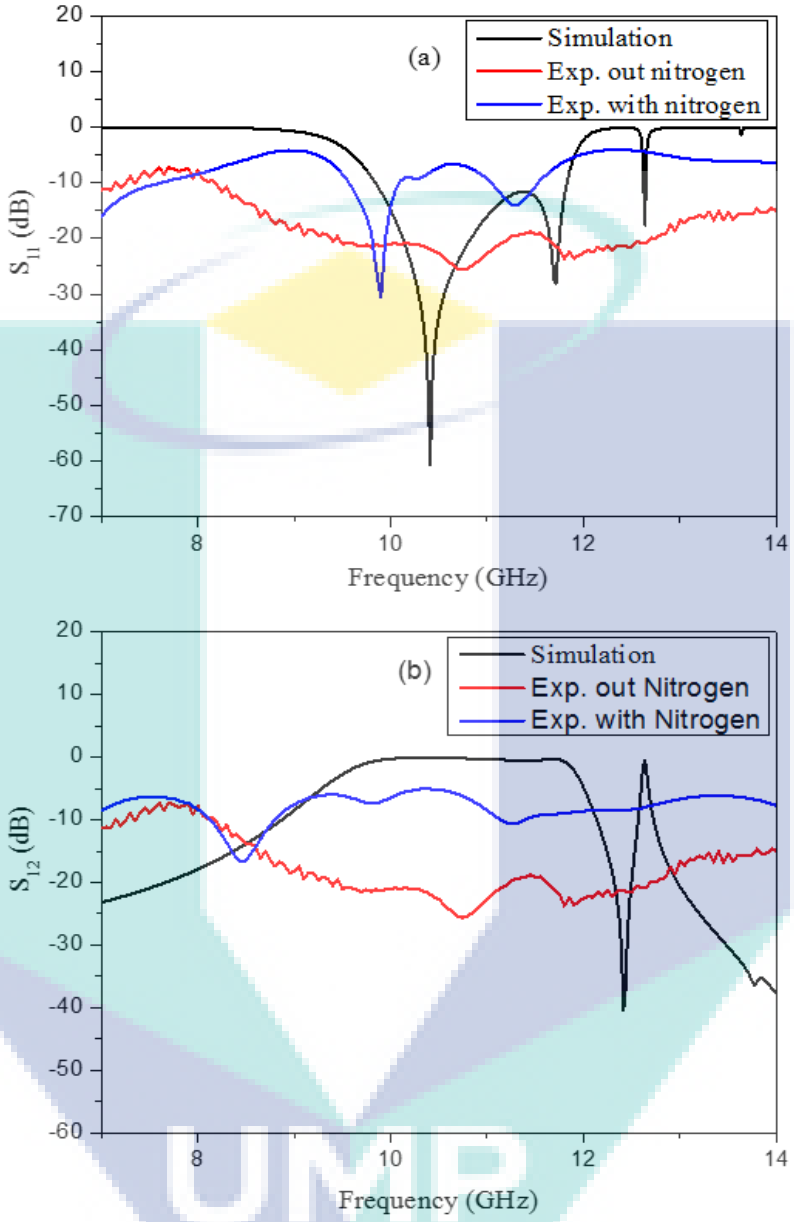

Figure B-8 Simulation and experiment results for the HTS YBCO sample 1 b.

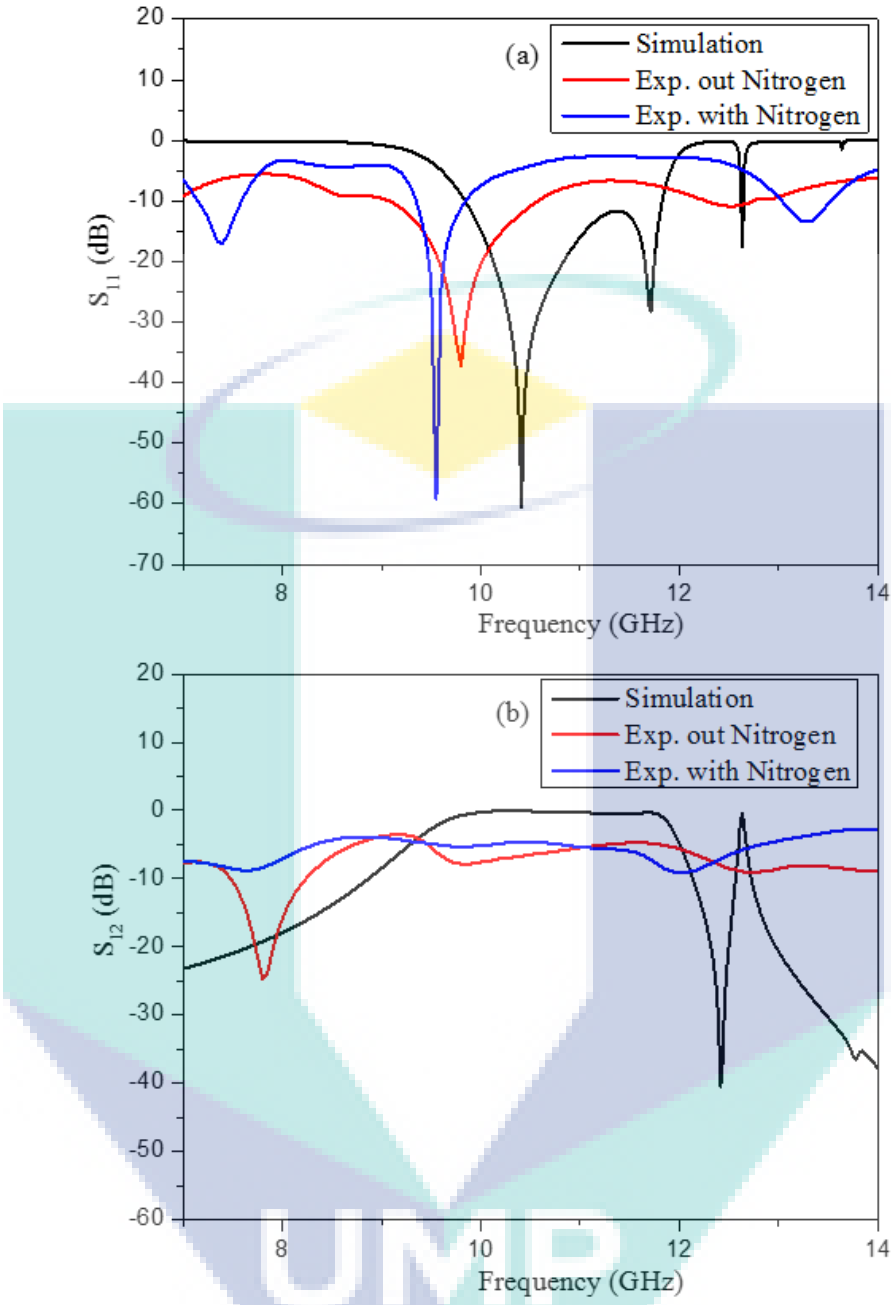

Figure B-9 Simulation and experiment results for the HTS YBCO Filter 2 a.

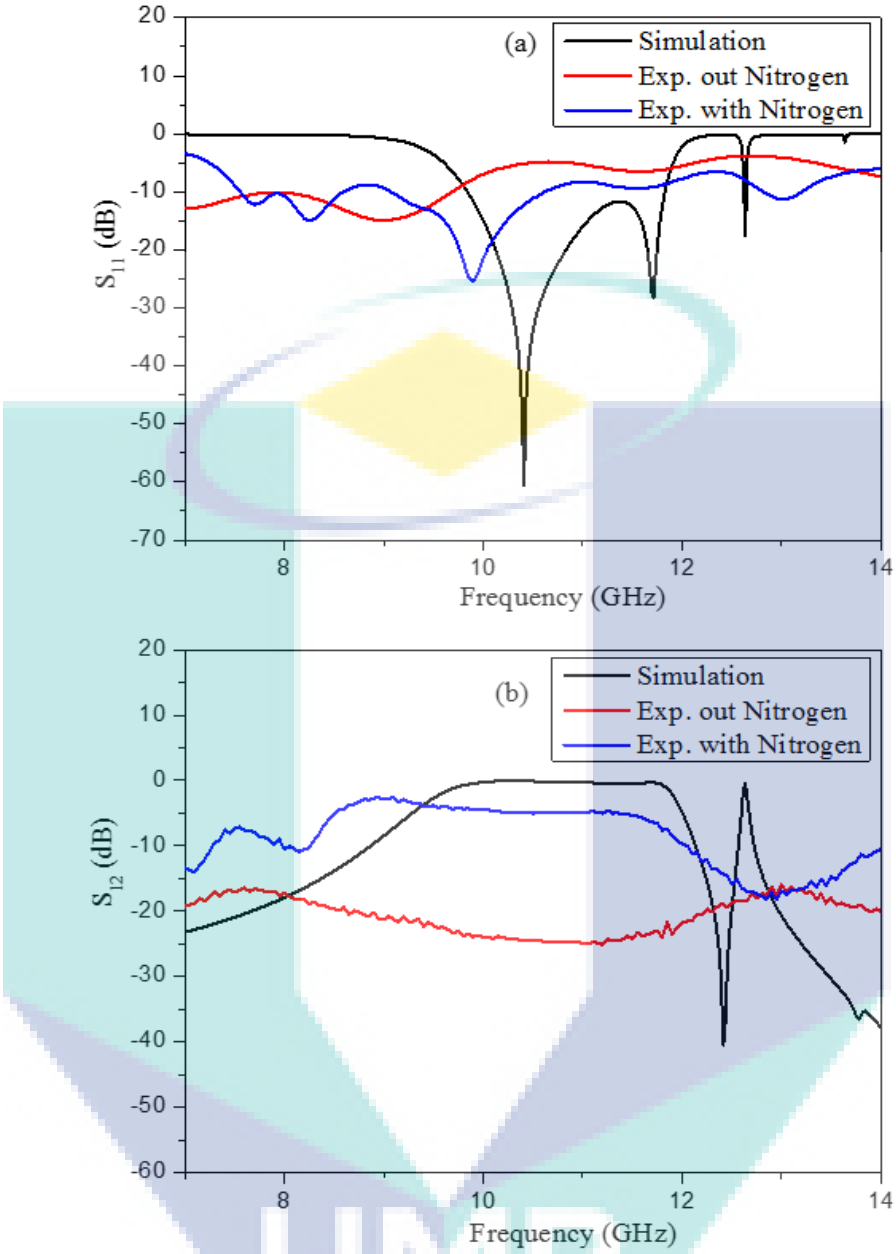

Figure B-10 Simulation and experiment results for the HTS YBCO sample 2 b.

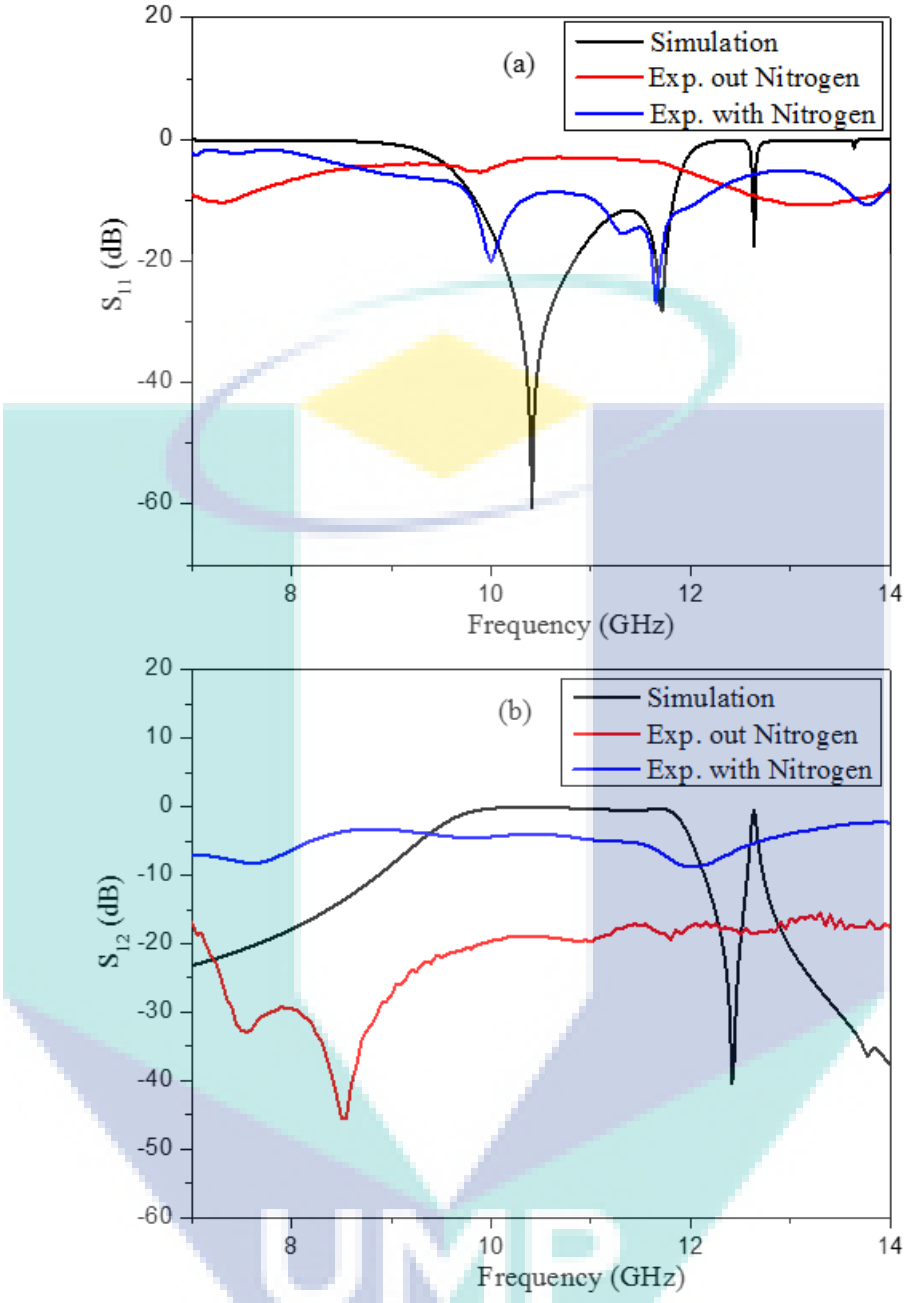

Figure B-11 Simulation and experiment results for the HTS YBCO sample 3.

Table B-7 Result summary of the designed filters.

NO.	Sample	Bandwidth (GHz)	Return loss (dB)	Insertion loss (dB)
1	(1a)	3.5	-37	-4
2	(1b)	3	-30	-6
3	(2a)	4	-60	-4
4	(2b)	3.5	-25	-3
5	(3)	4	-25	-3

The Cost of YBCO Microwave Bandpass Filter

Table B-8 presents the potential cost to synthesis the microwave bandpass filter for the current work.

The Material	The Quantity	Price (Rm)	Total Price (Rm)
YBCO	0.2	4.2	4.2
$LaAlO_3$ Substrate	1	120	120
SMA	2	13	26
			Rm150.2 Total price

Figure B-12 The images of the electrospinning units were used in this work to synthesize the HTS YBCO with different morphologies.